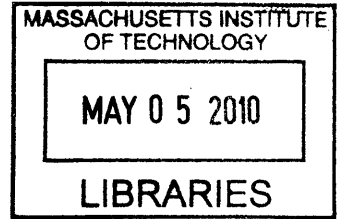


Energy Saving Potential of Various Roof Technologies

by

Stephen Douglas Ray

B.S., Mechanical Engineering
Massachusetts Institute of Technology, 2008



ARCHIVES

Submitted to the Department of Mechanical Engineering
in partial fulfillment of the requirements for the degree of

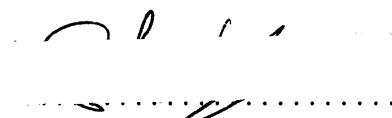
Master of Science in Mechanical Engineering

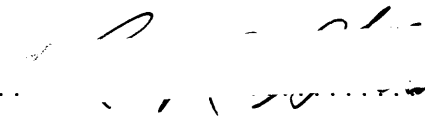
at the

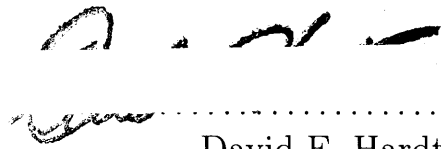
MASSACHUSETTS INSTITUTE OF TECHNOLOGY

Feb 2010

© Massachusetts Institute of Technology 2010. All rights reserved.

Author 
Department of Mechanical Engineering
October 14, 2009

Certified by 
Leon R. Glicksman
Professor of Building Technology and Mechanical Engineering
Thesis Supervisor

Accepted by 
David E. Hardt
Chairman, Department Committee on Graduate Students

Energy Saving Potential of Various Roof Technologies

by

Stephen Douglas Ray

Submitted to the Department of Mechanical Engineering
on October 14, 2009, in partial fulfillment of the
requirements for the degree of
Master of Science in Mechanical Engineering

Abstract

Unconventional roof technologies such as cool roofs and green roofs have been shown to reduce building heating and cooling load. Although previous studies suggest potential for energy savings through such technologies, many factors affect potential savings. To further investigate these factors, a tool has been developed to allow architects and designers the ability to quickly assess the energy saving potential of different roof technologies and roof constructions for various sites around the world. A first principles heat transfer model is developed for each of the roof technologies, with particular care for green roof heat and mass transfer. Two sets of experimental data from Japan and Florida validate the models by predicting roof surface temperature. The predicted roof surface temperatures in Japan agree with measured values within 10 and 26% of peak roof temperature fluctuations for the cool and green roof respectively, while the same models in Florida agree with measured values there within 7.2 and 14% for the cool and green roof respectively.

The models have been integrated into a free online building simulation tool, MIT's Design Advisor, available at <http://designadvisor.mit.edu>. Numerous simulations are run, showing that potential energy savings are found to strongly vary with many parameters, particularly roof type, climate, and amount of insulation. For example, a one-story building in Boston with an uninsulated modified-bitumen roof can save 82% in cooling and heating energy by adding $3 \text{ m}^2\text{K}/\text{W}$ of roof insulation, whereas only 34% if an uninsulated green roof is installed instead. However, in Lisbon, the same addition of roof insulation to the same building results in 54% savings, while the installation of an uninsulated green roof results in a 67% reduction. Such findings and their implications are discussed for other locations and design parameters.

Thesis Supervisor: Leon R. Glicksman

Title: Professor of Building Technology and Mechanical Engineering

Acknowledgments

I am extremely grateful for the encouragement, challenges, and all other forms of guidance with which Professor Leon Glicksman aided my writing this thesis. I also extend gratitude to Professor Daniel Roos and the MIT-Portugal Program for its funding this thesis, and for the invaluable intercultural exchanges.

I also must thank Jeff Sonne of the Florida Solar Energy Center and Professor Hideki Takebayashi of the University of Kobe for their collaboration in this work, and for their extraordinary generosity in sharing experimental results with me.

My many colleagues in the MIT Building Technology group and Mechanical Engineering department deserve thanks as well, but Bryan Urban and all other contributors to the MIT Design Advisor deserve a special thanks.

Lastly, my wife Allison receives more gratitude than I can express for her limitless support and encouragement. Your blessing my life truly is a God-given gift.

Contents

Nomenclature	19
1 Roof Technologies	25
1.1 Potential Impact of Roofs	26
1.2 Cool Roofs	27
1.2.1 General Overview of Cool Roofs	27
1.2.2 Benefits of Cool Roofs	30
1.2.3 Areas for Research - Cool Roofs	35
1.3 Modified-Bitumen Roofs	36
1.3.1 General Overview of Modified-Bitumen Roofs	36
1.4 Green Roofs	37
1.4.1 General Overview of Green Roofs	38
1.4.2 Benefits of Green Roofs	41
1.4.3 Areas for Research - Green Roofs	47
1.5 Roof Construction	47
1.5.1 Roof Insulation - Amount	48
1.5.2 Roof Insulation - Location	51
1.5.3 Number of Floors in Building	52
1.5.4 Areas for Research - Roof Construction	53
1.6 Motivation for Thesis	53
1.7 Outline of Thesis	54

2	Energy Modeling	55
2.1	Cool and Modified-Bitumen Roof Model	55
2.1.1	Cool and Modified-Bitumen Roof Energy Balance	55
2.1.2	Cool and Modified-Bitumen Roof Numerical Modeling	61
2.1.3	Differences between Cool and Modified-Bitumen Roofs	70
2.2	Green Roof	70
2.2.1	Modeling Vegetation and Growing Media	70
2.2.2	Green Roof Energy Balance	77
2.2.3	Green Roof Numerical Modeling	83
2.3	Validation of Models	90
2.3.1	Experimental Setups	91
2.3.2	Model Validation	96
3	Model Integration to Building Simulator: MIT's Design Advisor	107
3.1	Overview of Design Advisor	107
3.1.1	High Level Overview	107
3.1.2	Daylight Model	109
3.1.3	HVAC - Ventilation	111
3.1.4	HVAC - Envelope Loads	115
3.1.5	HVAC - Thermal Mass	117
3.1.6	HVAC - Combination of Components	118
3.2	New Roof Parameters in Design Advisor	120
3.2.1	Type of Roof	122
3.2.2	Roof Insulation R-Value	122
3.2.3	Roof Insulation Location	123
3.2.4	Number of Floors in the Building	123
3.3	Integration of Roof Model into Design Advisor	123
3.3.1	Accounting for Heat Flux through Roof	124
3.3.2	Accounting for Multiple Building Floors	125

4 Results	127
4.1 Roof Type	127
4.2 Roof Insulation	131
4.2.1 Roof Insulation - Amount	131
4.2.2 Roof Insulation - Location	134
4.3 Number of Floors	136
4.4 Considerations for Natural Ventilation	142
4.5 Conclusions	145
4.6 Next Steps	147
A Altered Design Advisor Java Source Files and HTML Code	149
B Building Simulation Parameters	153

List of Figures

1-1	Numerous kinds of roofs used in today’s building stock	25
1-2	2006 U.S. buildings energy end-use split	26
1-3	Example of cool roof and comparative plot of roof surface temperature for cool and conventional roof	28
1-4	Impact of reflectivity and emissivity on effectiveness of cool roof	28
1-5	“Cool” color pigments developed by LBNL that allow colored cool roofs	29
1-6	Effectiveness of colored cool roofs	29
1-7	Hashem Akbari’s summary of documented field studies of measured sum- mertime air-conditioning daily energy savings and demand from cool roofs.	31
1-8	Average summertime cooling load shapes for a 170 m^2 one-story home in Sacramento, CA with roof insulation 1.94 m^2C/W	32
1-9	Daily summertime cooling energy use at an 89 m^2 one-story school in Sacra- mento, CA with roof insulation 3.34 m^2C/W	33
1-10	Simulated annual heating load in MJ for a one-story home in Bismark, ND with various roof reflectivities and insulation levels	34
1-11	Modified-bitumen roofs in Boston	36
1-12	Cross section of a modified-bitumen roof	37
1-13	An extensive green roof in New York, New York	38
1-14	Typical construction schematic of a green roof	39
1-15	An extensive and intensive green roof	40
1-16	Comparative chart between extensive and intensive green roofs	40
1-17	Experimental data supporting green roof’s ability to reduce storm watre runoff	42

1-18	Additional experimental data supporting green roof's ability to reduce storm watre runoff	43
1-19	Average summertime surface temperature on a 307 m^2 building in Orlando, FL for a green and conventional roof	43
1-20	Meausred roof surface temperatures showing ability of green roof to reduce thermal stress on roof	44
1-21	Average daily energy requirement due to the heat flow through the roof surfaces from Nov 22, 2000 - Sep 31, 2001 in Ottawa, Canada	45
1-22	Two examples of additional useable space green roofs provide	47
1-23	Soffit temperature on small-scale buildings in Sri Lanaka as a function of roof insulation	48
1-24	Heat flux into small-scale buildings in Sri Lanka as a function of roof insulation	49
1-25	Heat flux into a full-scale building in Kobe, JP for a conventional and green roof	50
1-26	Simulated annual total energy savings from installing an extensive green roof on a building in Greece and a cool roof in Miami, FL as a function of roof insulation	51
1-27	Analytical model of heat flux through a concrete roof as insulation location is varied	52
2-1	Cool roof energy balance	56
2-2	Average wind speed at 10 m aroundn the world from 1976-1995	59
2-3	Ratio of measured $\frac{Re^2}{Gr}$ for a concrete roof at the University of Kobe	60
2-4	Nodal diagram of cool and modified-bitumen roof model with insulation beneath roof slab	64
2-5	Diagram of nodes 1 and 2 in cool roof model that shows the additional half length through which heat must conduct from node 2 to the surface	65
2-6	Nodal diagram of cool and modified-bitumen roof model with insulation above roof slab	67
2-7	Thermal resistance of various components in green roof system	72

2-8	Green roof energy balance	78
2-9	Exploded view of interaction between vegetation and soil layers	79
2-10	Saturation vapor pressure of water vapor in air as a function of temperature	82
2-11	Nodal diagram of green roof model with roof insulation beneath roof slab .	86
2-12	Relative crop transpiration and soil evaporation as percentages of the overall evapotranspiration	87
2-13	Nodal diagram of green roof model with insulation above roof slab	89
2-14	Image of extensive green roof in Florida used to validate roof models . . .	92
2-15	Section of the green and conventional roofs in the FSEC green roof study .	93
2-16	Roof diagram showing symmetric thermocouple placement on both green and conventional roofs in FSEC study	93
2-17	Experimental layout of roofs used in University of Kobe study used to vali- date roof models	95
2-18	Simulated and experimental roof surface temperatures of cool roof in Japan during August	98
2-19	Variation in surface temperatures show importance of material properties in Japanese study	99
2-20	Simulated and experimental roof surface temperatures of a cool roof in Florida during February	100
2-21	Simulated and experimental roof surface temperatures of a cool roof in Florida during July and August	102
2-22	[Simulated and experimental roof surface temperatures of a green roof in Japan during August	103
2-23	Simulated and experimental roof surface temperatures of a green roof in Florida during February	104
2-24	Simulated and experimental roof surface temperatures of a green roof in Florida during July and August	105
3-1	Logic diagram of the DA simulation tool	108
3-2	A portion of the single-page MIT Design Advisor interface	109

3-3	Two-dimensional workplane grid used in DA to determine the lighting level in each subarea	110
3-4	Illustration of the heat transfer through the windows and walls in DA . . .	117
3-5	Schematic of heat transfer involving the thermal mass stored in the floor of a building in DA	118
3-6	Model used for heat exchange with air in a room in DA	120
3-7	Hourly logic used for the DA software	121
3-8	User interface for roof module in DA	122
3-9	Screen shot of the types of insulation that can be chosen in DA	122
4-1	Annual heating and cooling load for a single-story residential building with no roof insulation	128
4-2	Average total annual heating and cooling load for a four-story building . .	129
4-3	Average total annual heating and cooling load for a single-story building with $3\text{ m}^2\text{K}/\text{W}$ roof insulation	130
4-4	Average total annual heating and cooling load for a one-story building with moderate plug loads as a function of roof insulation in Minneapolis, MN .	132
4-5	Average total annual heating and cooling load for a one-story building with moderate plug loads as a function of roof insulation in Sacramento, CA . .	132
4-6	Average total annual heating and cooling load for a one-story building with moderate plug loads as a function of roof insulation in St.Louis, MO . . .	133
4-7	Average total annual heating and cooling load for a one-story building with moderate plug loads as a function of roof insulation in Boston, MA	133
4-8	Average total annual heating and cooling load for a one-story building with moderate plug loads as a function of roof insulation above and below roof slab in Lisbon, PT	135
4-9	Average total annual heating and cooling load for multi-story buildings with no roof insulation as a function of number of floors in Boston, MA	137
4-10	Average total annual heating and cooling load for multi-story buildings with no roof insulation as a function of number of floors in Lisbon, Portugal . .	137

4-11	Average total annual heating and cooling load for multi-story buildings with $3 \text{ m}^2 K/W$ roof insulation as a function of number of floors in Boston, MA	138
4-12	Average total annual heating and cooling load for multi-story buildings with $3 \text{ m}^2 K/W$ roof insulation as a function of number of floors in Lisbon, Portugal	138
4-13	Hourly heating load for the interior floors (with adiabatic ceilings) and top floor with a green and cool roof for a multi-story building in Lisbon, PT	139
4-14	Hourly heating load for the interior floors (with adiabatic ceilings) and top floor with a green and cool roof for a multi-story building in Boston, MA	141
4-15	Indoor temperatures for a naturally ventilated building with $0 \text{ m}^2 K/W$ roof insulation in Boston, MA	143
4-16	Indoor temperatures for a naturally ventilated building with $3 \text{ m}^2 K/W$ roof insulation in Boston, MA	144
4-17	Indoor temperatures for a naturally ventilated building with $0 \text{ m}^2 K/W$ roof insulation in Lisbon, Portugal	144
4-18	Indoor temperatures for a naturally ventilated building with $0 \text{ m}^2 K/W$ roof insulation in Lisbon, Portugal	145

List of Tables

2.1	Variation of average heat transfer coefficient over a flat roof with wind speed	58
2.2	Thermal properties of roof used in model	61
2.3	Physical Vegetation Parameters	75
2.4	Thermal properties of green roof used in model	84
2.5	Summary of FSEC Experimental Roof Construction	94
2.6	Summary of University of Kobe Experimental Roof Construction	96
2.7	Variation of concrete properties	97
3.1	Variables used in the DA room Energy Balance	119
B.1	Simulation Input Parameters for Fig. 4-1	154
B.2	Simulation Input Parameters for Figs. 4-4 through 4-7	155
B.3	Simulation Input Parameters for Fig. 4-8	156
B.4	Simulation Input Parameters for Figs. 4-9 through 4-12	157
B.5	Simulation Input Parameters for naturally ventilated building in Figs. 4-15 through 4-18	158

Nomenclature

$(mC)_{slab}$ [J/m^2K] product of concrete slab mass and heat capacity per square meter

$(mC)_{soil}$ [J/m^2K] product of soil mass and heat capacity per square meter

α_{soil} [*none*] absorptivity of soil

α_l [*none*] longwave absorptivity of individual leaf

α_s [*none*] shortwave absorptivity of individual leaf

α_{soil} [*none*] absorptivity of soil

Δt_{max} [s] maximum allowable time step in roof model

Δ [kPa/C] saturation slope vapour pressure curve at T_{hr}

\dot{m} [kg/s] mass flow rate into room

\dot{Q}_{in} [W/s] net energy entering node

\dot{Q}_{out} [W/s] net energy leaving node

$\frac{dE_{internal}}{dt}$ [W/s] change in internal energy over small time

γ [kPa/C] psychrometric constant

λ_v [MJ/kg] latent heat of water vaporization

ν [m^2/s] kinematic viscosity of air

\bar{h}	[W/m^2K] average convective heat transfer coefficient between roof and environment
\bar{T}_i	[K] averaged temperature of i th node at current and next time step
\overline{Nu}	[<i>none</i>] average Nusselt number
\vec{Q}	[<i>none</i>] matrix containing all constants in numerical model
ρ	[<i>none</i>] roof surface reflectivity
ρ_{board}	[kg/m^3] density of coverboard
ρ_{veg}	[<i>none</i>] collective vegetation reflectivity
B	[$1/K$] volumetric thermal expansion coefficient
σ	[J/sm^2K^4] Stefan-Boltzman coefficient
τ_l	[<i>none</i>] longwave transmittance of grass
τ_s	[<i>none</i>] shortwave transmittance of vegetation
ε	[<i>none</i>] emissivity of roof
A_{roof}	[m^2] area of roof
B	[<i>none</i>] matrix containing all coefficients for T' terms
Bi	[<i>none</i>] Biot number
C	[J/kgK] heat capacity of single concrete node in cool roof model
$C_{p_{air}}$	[J/kgK] specific heat capacity of air
$C_{p_{board}}$	[J/kgK] specific heat capacity of coverboard
ET_0	[mm/hr] reference evapotranspiration
Fo	[<i>none</i>] Fourier number

G [MJ/m²hr] soil heat flux density
 g [m/2²] acceleration due to gravity
 Gr [none] Grashof number
 h [W/m²K] convective heat transfer coefficient
 h_{blinds} [W/m²K] convective heat transfer coefficient between window glass and blinds
 h_{rad} [W/m²K] linearized radiation heat transfer coefficient between roof and sky
 H_{roof} [W/m²] convective heat exchange between roof and outside environment
 h_{room} [W/m²K] effective heat transfer coefficient from the ceiling to the room
 H_{veg} [W/m²] convective heat transfer between vegetation and environment
 $height_{grass}$ [m] green roof grass height
 I_s [W/m²] incident short-wave radiation to roof from the sun
 k [W/mK] conductivity of medium
 k_{board} [W/mK] conductivity of coverboard
 $k_{concrete}$ [W/mK] conductivity of concrete
 $k_{ext,l}$ [none] longwave vegetation extinction coefficient
 $k_{ext,s}$ [none] shortwave vegetation extinction coefficient
 k_{fluid} [W/mK] conductivity of fluid
 k_{slab} [W/mK] conductivity of concrete slab
 k_{soil} [W/mK] conductivity of soil
 L [m] length of roof over which wind flows
 l [m] characteristic length

l_{max} [m] maximum nodal thickness
 l_{slab} [m] thickness of concrete slab node
 l_{soil} [m] thickness of soil node
 L_{veg} [W/m²] latent heat transfer between vegetation and environment
 LAI [none] leaf area index
 m [kg] mass of single concrete node in cool roof model
 $m_{air,room}$ [kg] mass of air in room
 MW_a [g/mol] molecular weight of air
 MW_v [g/mol] molecular weight of water vapor
 P_{act} [kPa] average hourly actual vapour pressure
 P_{sat} [kPa] saturation vapour pressure at specified temperature
 Pr [none] Prandtl number
 $q_{conduct}$ [W/m²] heat conduction through roof
 $Q_{internal}$ [W] sum of internal plug and lighting loads
 $q_{ir,roof}$ [W/m²] long-wave radiation exchange between roof and sky
 $q_{ir,soil-veg}$ [W/m²] longwave radiation between soil and vegetation
 $q_{ir,soil}$ [W/m²] longwave radiation between sky and soil
 Q_{roof} [W] heat flux into room through roof
 $Q_{thermalmass}$ [W] heat flux from thermal mass
 R_n [MJ/m²hr] net radiation at grass surface

R_{eff} [m^2K/W] R value of effective resistance to heat transfer between ceiling and room
 R_{ins} [m^2K/W] R value of roof insulation
 Re [*none*] Reynolds number
 Re_L [*none*] Reynolds number based on total length
 Re_{tr} [*none*] Reynolds number at transition
 RH [*none*] outdoor relative humidity
 S [*none*] matrix containing all coefficients for T terms
 T_i [K] temperature of i th node at current time step
 T_m [K] averaged temperature of roof surface and sky
 T_{amb} [K] temperature of ambient outdoor environment
 T_{hr} [C] mean hourly air temperature
 T_{room} [K] temperature of room
 T_{sky} [K] temperature of sky
 $T_{slab,n}$ [K] temperature of final node of roof slab
 T_{st} [K] steam-point temperature
 $T_{surface}$ [K] temperature of roof surface
 T_{veg} [K] temperature of vegetation
 u_2 [m/s] average hourly wind speed 2 m above roof
 UA_{wal} [W/K] overall heat transfer coefficient for walls in Design Advisor
 UA_{win} [W/K] overall heat transfer coefficient for windows in Design Advisor

V [m/s] wind speed on roof

V_{air} [m/s] velocity of air between window glass and blinds

T_i' [K] temperature of i th node at next time step

Chapter 1

Roof Technologies

Many kinds of roofs are currently in the world's building stock. As shown in Fig. 1-1, this array of roofs varies widely in appearance. Less obvious may be the differences in energy performance of each roof, which will be discussed in this thesis for three types of roofs: cool roofs, modified-bitumen roofs, and green roofs.

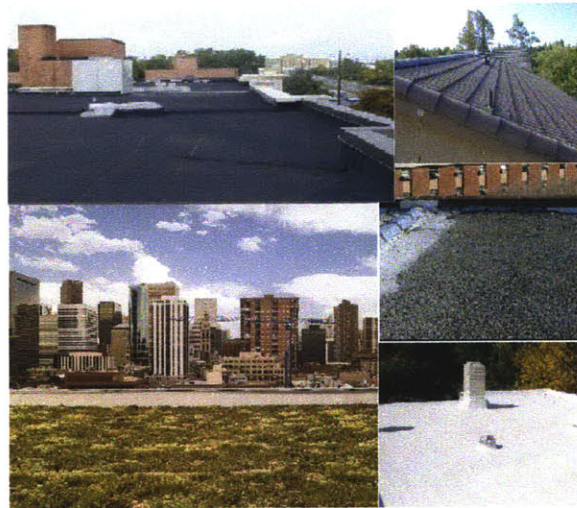


Figure 1-1: Numerous kinds of roofs used in today's building stock. Although the aesthetic differences between the roofs are apparent, the differences in energy impact are less obvious. Source [38][16][55][87][1]

1.1 Potential Impact of Roofs

In the United States and most developed countries the operation of buildings accounts for 39% of the nation's energy consumption [6]. The end-use of energy in buildings is dominated by the heating, ventilation, and air conditioning (HVAC) systems. Fig. 1-2 shows the end-use of energy across all U.S. buildings, demonstrating that the HVAC system accounts for roughly half of all U.S. building energy use (where the HVAC is defined to include the space heating, space cooling, and ventilation energies). Therefore, roughly 20% of the primary energy in the United States goes towards heating and cooling buildings.

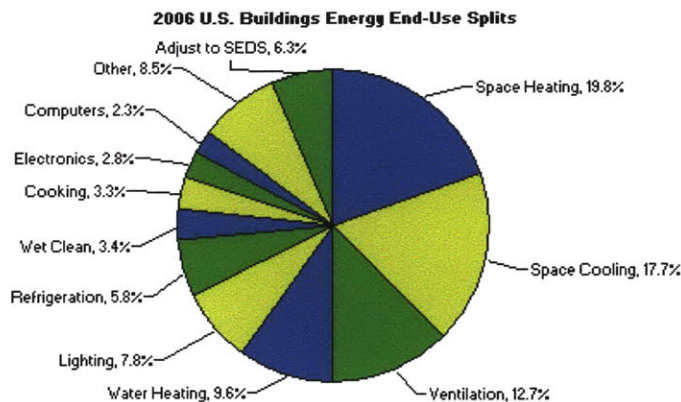


Figure 1-2: 2006 U.S. buildings energy end-use split. Source [2]

Numerous components affect the HVAC system energy use, including the building envelope, HVAC system components, the use of natural ventilation, the local climate, and many others. As part of the building envelope, roof technologies have received an increasing amount of attention in recent years. The state of California, for example, mandated cool roofs for both commercial and residential buildings in the 2008 revision of Title 24 [34]. Green Roofs for Healthy Cities (GRHC), a non-profit industry association aimed at promoting green roofs in North America, contracted independent Kendon Light, E.A. to poll all corporate members of GRHC. The study found that the square footage of green roofs in the U.S. grew 80% between the years of 2004-2005 to reach a total of 2.5 million ft^2 [39].

Consuming approximately 20% of the U.S. primary energy, the heating, cooling, and ventilation of buildings demands attention. The alternative roofing industry has responded through tremendous growth and publicization of their products' benefits, predominately energy savings. However, one roof technology will not solve all problems. Building owners must be informed of the benefits their particular building will realize by installing an alternative roof.

To help reduce building energy consumption by more fully informing building owners, this thesis seeks to investigate the energy saving potential of various roof technologies, which will be discussed in the following sections.

1.2 Cool Roofs

United States Secretary of Energy Steven Chu recently advocated cool roofs at the St. James Palace Nobel Laureate Symposium on May 26, 2009 where he stated that if all roads were made a paler color and all roofs converted to cool roofs, there could be “the equivalent effect of taking every car in the world off the road for 11 years” [43]. The potential for energy savings from cool roofs is discussed in this section.

1.2.1 General Overview of Cool Roofs

A cool roof, shown below in Fig. 1-3, is a roof that has a high ability to reflect the sun's radiation (wavelength of 0.3-2.5 μm) and emit absorbed thermal energy back to the sky (wavelength of 4-80 μm) [4] [23]. Thus, it often remains at a lower temperature than traditional roofing materials, up to 28-33 C cooler, which can lead to energy savings [90].

Two physical properties determine how “cool” a cool roof is: its reflectivity in the solar wavelength and its emissivity in the infrared wavelength. The relevance of these two properties for a roofing system is summarized in Fig. 1-4 below.

Although cool roofs are typically white Fig. 1-3, because of the color's inherit high solar reflectance and thermal emittance, commercial cool roof coatings are now available in an assortment of colors [60] [56]. Lawrence Berkeley National Laboratory

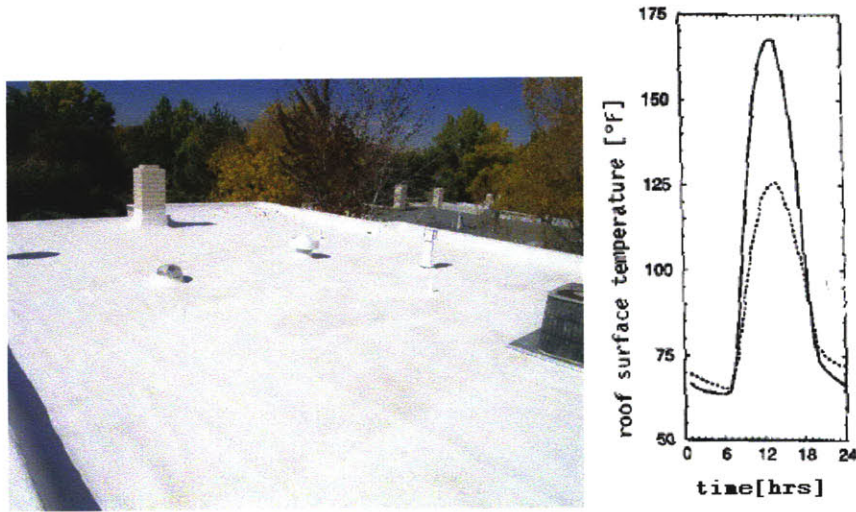


Figure 1-3: (left) This roof's white coating allows it to reflect much of the sun's radiation and emit absorbed energy well. (right) The measured roof surface temperature for a standard roof, solid line, and cool roof, dotted line, on a commercial building in Austin, TX. Source [16][51]

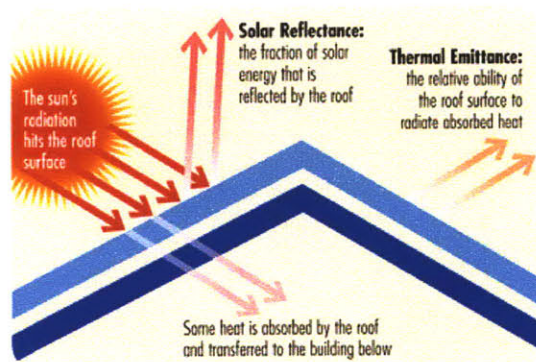


Figure 1-4: Both reflectivity and emissivity affect the incoming energy to the building through the roof. Source [4]

(LBNL) has developed an online database of a wide variety of “cool” color pigments [3]. Some of these “cool” colors are shown below in Fig. 1-5, as well as a home with a colored cool roof [55].



Figure 1-5: (left) A few of the “cool” color pigments analyzed by LBNL found in their online database. (right) A home with a colored cool tile roof installed. Source [55]

Some of these pigments were used in an experiment on homes in California, in which the researchers painted roof tiles six different colors in both “cool” and conventional colors [56]. Below, in Fig. 1-6 are figures from their paper comparing the surface temperatures and reflectivities of the tiles.

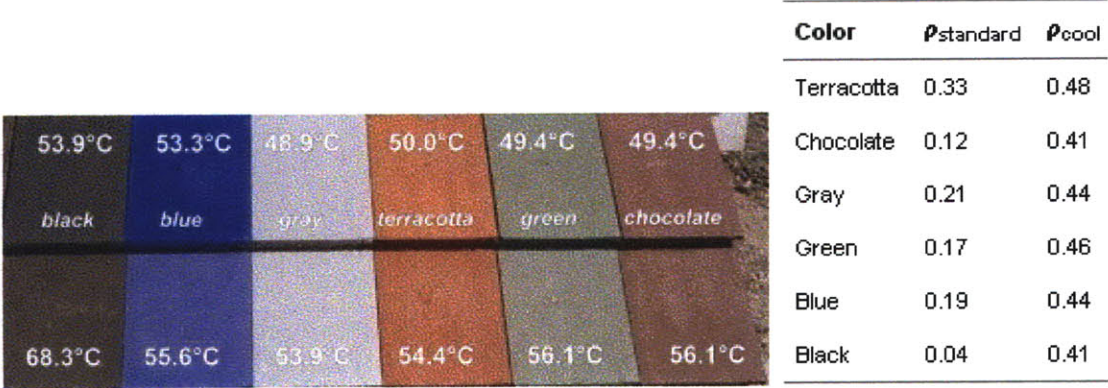


Figure 1-6: (left) Surface temperature of colored roof tiles. The “cool” roof tiles are on the top row and the conventional roof tiles are on the bottom. Surface temperatures were measured from 11:20 to 11:30 AM solar on 17 September 2003 (outside air temperature 27 C, horizontal global insolation $820 W/m^2$). (right) The measured reflectivities for the roof tiles shown on the left. Source [56]

1.2.2 Benefits of Cool Roofs

As previously mentioned, cool roofs can help significantly lower roof surface temperatures. This temperature reduction leads to numerous benefits, which are discussed below.

Cooling Energy Savings

Lower roof temperatures of cool roofs can lead to two primary benefits. First, cooling energy can be reduced as the net heat flux into the building decreases with lower roof temperature. The energy savings vary widely in the literature, as Hashem Akbari of the Heat Island Group at the Lawrence Berkley National Laboratory has shown savings to be as high as 80%, while Levinson et al has shown savings as low as 1% [21][56]. One study alone found a variance of 41% in homes with cool roofs [67].

Akbari compiled a table reviewing the measured summertime air-conditioning daily energy savings and demand from cool roofs [51]. The summertime air-conditioning savings alone, which are expected to be the highest of the year because of the high outdoor temperatures, vary from 1-63%. The lowest savings come from buildings with high insulation and small changes in roof reflectance, while the greatest changes come from buildings with little insulation and large changes in roof reflectance [51]. Akbari's summary is copied below in Fig. 1-7.

Another study shows the shift and reduction in peak power use with cool roofs during the summertime in Sacramento, CA , shown in Fig. 1-8 [21].

The investigators found that the high albedo (or high reflectivity) average daily summertime peak load lies about 0.5 kW below, and two hours after, the low albedo peak. Although the reduction in peak power is significant, for the majority of hours each day the average summertime cooling use is approximately the same for both conventional and cool roofs. During the evening hours, the cool roof actually has higher cooling energy use because of the shifted peak.

The same study investigated the reduction in summertime cooling load in an 89 m^2 one-story school also in Sacramento, CA with roof insulation 3.34 m^2C/W .

location	building type	roof area ft ²	roof system description			daily savings		reduced demand	
			R-val	duct	$\Delta\rho$	Wh/ft ²	%	W/ft ²	%
California									
Davis	medical office	31700	8	interior	0.36	6.3	18	0.31	12
Gilroy	"	23800	19	plenum	0.35	3.6	13	0.22	8
San Jose	retail store	32900	RB	plenum	0.44	0.4	2	0.15	9
Sacramento	school baglw	960	19	ceiling	0.60	4.4	46	0.63	20
Sacramento	residence	1830	11	crawl	0.59	1.3	63	0.33	25
Sacramento	office	24600	19	plenum	0.40	0.9	17	n/a	-
Sacramento	museum	4900	0	interior	0.40	1.9	26	n/a	-
Sacramento	hospice	6000	11	attic	0.40	1.0	39	n/a	-
Florida									
Cape Canaveral	residence	1400	11	attic	n/a	5.4	22	0.14	12
Cocoa Beach	"	1200	0	attic	0.63	12.7	43	0.72	28
Cocoa Beach	"	1300	0	attic	0.39	10.8	26	0.71	29
Cocoa Beach	"	1300	11	attic	0.52	7.9	25	0.51	28
Cocoa Beach	"	1500	19	attic	0.42	2.9	13	0.15	11
Merritt Island	"	1700	7	attic	0.44	6.8	20	0.58	23
Merritt Island	"	1800	25	attic	0.51	2.2	11	n/a	-
Miami	"	1400	11	attic	0.30	5.9	15	0.32	16
Palm Bay	"	1500	19	attic	0.44	2.1	10	0.24	16
Palm Bay	"	1800	19	attic	0.42	0.5	2	0.17	12
West Florida	"	900	0	none	0.53	6.2	25	0.55	30
Lakeland	"	2400	30	attic	0.65	n/a	17	n/a	-
Cocoa Beach	strip mall	12500	11	plenum	0.46	0.7	25	0.06	29
Cocoa Beach	school	10000	19	plenum	0.46	4.1	25	0.56	30
Georgia									
Atlanta	education	12000	11	plenum	n/a	7.0	28	n/a	-
Mississippi									
southern	office	n/a	11	n/a	n/a	n/a	22	n/a	-
Nevada									
Reno	regeneration	160	18	none	0.39	3.1	1	n/a	-

Figure 1-7: Hashem Akbari's summary of documented field studies of measured summertime air-conditioning daily energy savings and demand from cool roofs. $\Delta\rho$ is the change in roof reflectivity with the cool roof installation and RB is a radiant barrier. Note the positive correlation between $\Delta\rho$ and summertime air-conditioning savings along with the negative correlation between the insulation R-value and summertime air-conditioning savings. Source [51]

Because of the variable internal loads due to student occupation, the thermostat was set between 21-26 C throughout the experiment. The metal roof underwent multiple configurations: Metal (albedo = 0.34, emissivity = 0.30), Brown (albedo = 0.08, emissivity = 0.95), and White (albedo = 0.68, emissivity = 0.91) over the course of the experiment. Fig. 1-9 below plots the daily air conditioning use versus outside air temperature of the roof during the experimental session of June 17 through October 15 [21].

In Fig. 1-9, the regression lines of the different configurations immediately show the energy savings of using the White roof over the Brown or Metal for temperatures between 22-25 C . At temperatures lower than 22 C , there seems to be little difference between the A.C. use for different roof types. The significant difference between the

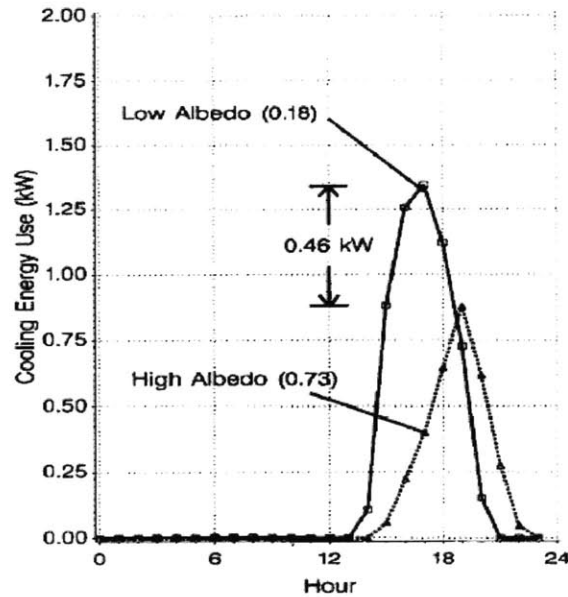


Figure 1-8: Average summertime cooling load shapes for a 170 m^2 one-story home in Sacramento, CA with roof insulation $1.94 \text{ m}^2\text{C}/\text{W}$. Average daily temperatures of data shown is between 23.1 and 25 C , and the thermostat is set to 26 C for cooling. Squares and solid line represent hourly load averages for low albedo days with cooling energy use. Triangles and dashed line represent hourly load averages for high albedo days with cooling energy use. The high albedo average daily peak load lies about 0.5 kW below, and two hours after, the low albedo peak. Source [21]

occupied and vacant White roofs indicates the importance of maintaining constant internal loads when considering the energy saving potential of roofs

All of the studies mentioned above were conducted in California, Florida, or other warm to hot climates where cooling loads dominate building energy use. Furthermore, the majority were conducted during the summer months, during which time the savings from cool roofs is expected to be highest. Studies have shown that cool roofs can save the most amount of energy in cooling-dominated climates because their high solar reflectance keeps heat from the roof, while their high thermal emittance allows energy to escape the roof [22]. However, in cold climates, those attributes lead to higher demand for energy [22] [96]. One comprehensive study by the National Institute of Standards and Technology (NIST) simulated building energy performance for cool roofs in six climates around the United States [96]. In every climate, the heating energy increased with the installation of a cool roof. Fig. 1-10 below shows

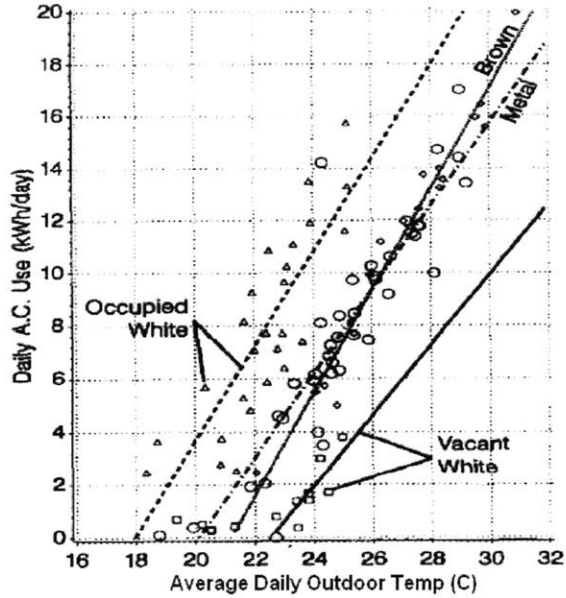


Figure 1-9: Daily summertime cooling energy use at an 89 m^2 one-story school in Sacramento, CA with roof insulation $3.34 \text{ m}^2\text{C}/\text{W}$. The thermostat is set between $21\text{-}26 \text{ C}$ throughout the experiment. Roof albedos: Metal (albedo = 0.34, emissivity = 0.30), Brown (albedo = 0.08, emissivity = 0.95), and White (albedo = 0.68, emissivity = 0.91). Squares and solid line represent data collected during the vacant white roof period. Triangles and dashed line describe data collected during the occupied white roof period. Circles and dot-dash line represent data collected in the metal roof period (vacant). Diamonds and dotted line represent data collected in the brown roof period (vacant). Source [21]

the increase in annual heating energy for a home in Bismark, North Dakota (which had the lowest percent increase in heating energy of the six climates).

Although the cool roof saves cooling energy for the home in Bismark, the increase in heating energy must be considered when looking at the net impact of the cool roof on the total annual energy consumption.

Reduced Urban Heat Island Effect

The second primary benefit of a lower roof surface temperature is a decrease in the Urban Heat Island (UHI) effect. This well researched phenomena occurs in urban centers where vegetation and open land are replaced with concrete and buildings and can lead to an increase in ambient temperatures of 2.5 K [20] [90] [80] [19]. Furthermore, it has been shown that each degree Kelvin rise in ambient temperature

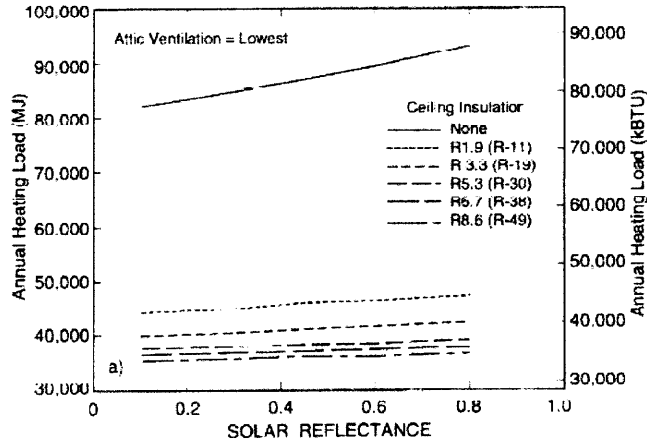


Figure 1-10: Simulated annual heating load in MJ for a one-story home in Bismark, ND with various roof reflectivities and insulation levels. Note the increase in heating energy as the roof reflectivity is increased. The percent increase in heating energy for Bismark is the smallest among the 5 climates considered in the study. Source [96]

increases energy demand by 2-4% [19]. Thus many cities around the world are paying for the UHI effect, like Los Angeles where it is estimated the city pays \$100 million a year for their 1-1.5 GW increase in energy demand from the UHI effect [19]. The UHI is a complex phenomena caused by numerous factors, including decreased urban albedo, increased thermal mass, increased surface roughness, increased heat released from buildings and vehicles, and decreased evaporative areas (or more impermeable areas) [80].

Cool roofs help decrease the UHI effect by raising the urban albedo, which reflects more of the sun's energy back to the sky [20] [90] [80].

Smog Reduction

As a result of lowering the peak summertime ambient temperature, cool roofs help decrease the amount of smog in cities. The Heat Island Group at the Lawrence Berkeley National Laboratory found that for every 1 C temperature rise above 22 C, incident smog in Los Angeles increased by 5% [20].

Minimal Cost Differential

Another benefit of cool roofs is their ease and cost of installation. Built-up roofs are typically coated with a protective layer, in lieu of which a cool roof coating can easily be used [30]. In many cases, choosing the cool roof over the traditional roof at the time of installation or repair can be done with no additional cost. In nearly all cases, the cool roof can be installed for less than 30% additional costs [30].

Prolonged Roof Life

Additionally, the lower surface temperatures of cool roofs on hot days decrease the amount of thermal stress on the roof. This decreased thermal stress is expected to lead to generally longer lifespans compared to traditional roofs [30].

Additional Consideration

However, nearly all cool roofs suffer a loss in performance over their lifespan, especially on flat roofs. Dirt and other particulates build up over time on the roof surface and lower the albedo, though the effect is less significant on a sloped roof [30]. Bretz found that multiple cool roofs that began with albedos of 0.5-0.7 were eventually dirtied to have albedos of 0.3-0.6 [30]. Most of the albedo decrease happens within the first months of installation. Although soap can easily restore the original albedo of many cool roof surfaces, Bretz's financial analysis concludes the additional maintenance costs of washing are not economical [30].

1.2.3 Areas for Research - Cool Roofs

It has been shown that the ability of cool roofs to reduce roof surface temperature can lead to cooling energy savings, reduce the UHI effect, potentially decrease the amount of smog, and help lower a city's energy use. Furthermore, it is known that cool roofs use more energy than conventional roofs in cold climates or during the winter in moderate to warm climates. However, in which climate does having a cool roof save energy over the length of a year? Lastly, the negative correlation between

the amount of insulation and energy savings has been shown, but the amount of insulation past which a cool roof has minimal savings over a conventional roof is yet to be determined.

1.3 Modified-Bitumen Roofs

The roofing surface of choice in the US and other OECD countries for flat roofs, modified-bitumen roofs are easily noticeable above most cities for their contrasting black color, as shown below in Fig. 1-11 [15].



Figure 1-11: Black modified-bitumen roofs fill Boston's residential Back Bay (left) and commercial downtown areas (right), as is the case in many OECD cities. Source [8]

1.3.1 General Overview of Modified-Bitumen Roofs

Modified-bitumen roofs consist of a blend of bitumen, or asphalt, and polymer that allows the asphalt to take on properties of the polymer [12]. Some of the beneficial properties include an increase in resistance to brittleness at cold temperatures, greater flow resistance at high temperatures, and a higher elasticity [11].

Modified-bitumen roofs were first developed in Europe in the 1960s, but were quickly introduced to the United States and Canada, where they have flourished [11]. They are designed for flat or low-sloped roofs and therefore are often used on commercial buildings. As shown in Fig. 1-12, they typically consist of a top coating, the bitumen-polymer layer, a waterproofing layer, and insulation above the

roof structural support. Although Fig. 1-12 shows a steel structural support, concrete is often used as well.

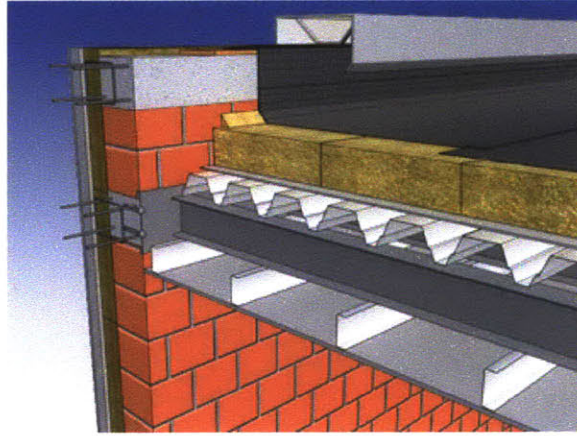


Figure 1-12: Cross section of a modified-bitumen roof, showing the top coat, bitumen-polymer, waterproofing, and insulation layers. Source [13]

Because of the low reflectivity of their topmost coating, conventional modified-bitumen roofs absorb up to 96% of the sun's radiation that reaches the Earth's surface [56]. This low reflectivity leads to high roof surface temperatures, reaching up to 76 C or higher [51]. Despite the wide-spread use of modified-bitumen roofs, they have helped increase city temperatures, leading to the UHI effect, as previously mentioned.

1.4 Green Roofs

The New York Times recently published an article on the green spots that are beginning to dot New York City's skyline, which are green roofs. See Fig. 1-13 for one such roof. In the article, Dr. Stuart Gaffin, Associate Research Scientist at Columbia's Center for Climate Systems Research, describes the vegetation that creates green roofs by saying, "They're nature's geniuses at staying cool" [33]. This section describes green roofs and investigates how "cool" they really are.



Figure 1-13: An extensive green roof in New York, New York. Source [14]

1.4.1 General Overview of Green Roofs

A green roof, sometimes called a living, sod, or vegetated roof, is one covered partially or entirely with vegetation growing in soil. Today, modern green roofs include numerous additional components to help protect the building, such as drainage, waterproofing, and insulation layers. The schematic of a characteristic green roof system is shown in Fig. 1-14 below.

Green roofs can be split into two broad categories. Intensive green roofs, shown below in Fig. 1-15, are characterized by heavier structural loads, high capital and maintenance costs, and accessibility to occupants. Additionally, intensive green roofs allow for a greater variety of plants including hardy perennials, native flowers, shrubs, and even trees. These plants require regular maintenance including watering and weeding. Soil depth is typically 15-61 *cm* (or more) and weight load is 390-732 *kg/m²* [64].

Extensive green roofs, also shown below, are characterized by lower capital and

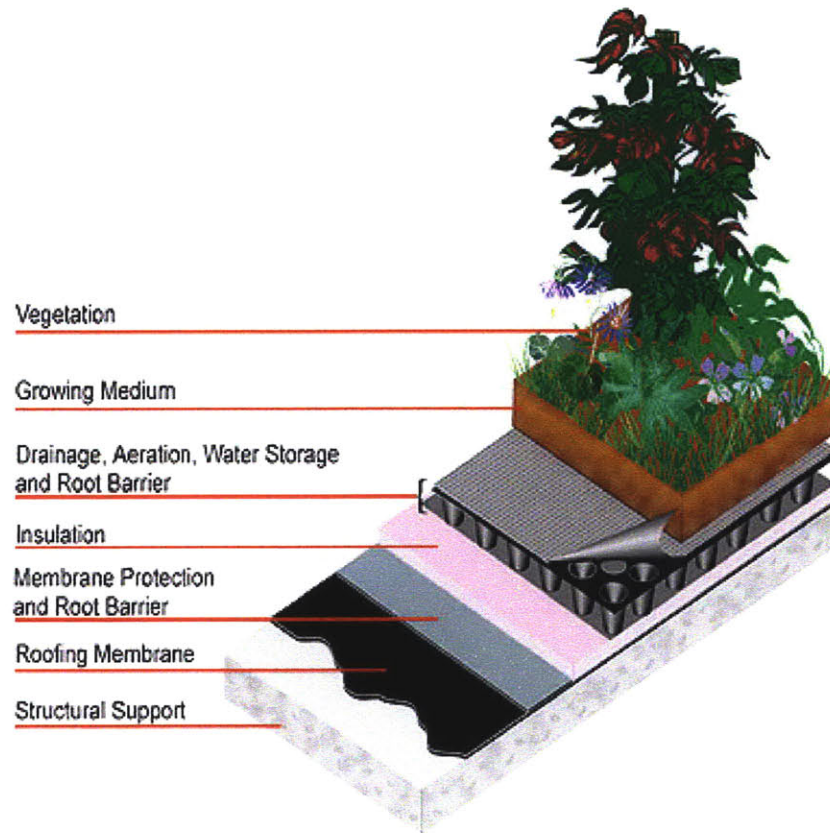


Figure 1-14: Typical construction schematic of a green roof. Source [10]

maintenance costs and lighter structural loads. Plants such as sedums and prairie flowers are utilized because they are low to the ground and require less maintenance (requiring occasional weeding and watering) and can tolerate many weather conditions. Soil depth is typically 2-15 *cm* and weight load is 73-244 kg/m^2 [64]

In their report Design Guildlines for Green Roofs, Canadian architects Steven Peck and Monica Kuhn weigh the advantages and disadvantages of intensive versus extensive green roofs in a table copied below in Fig. 1-16 [53]. It should be noted that this table is included to help compare the two types of green roofs and not make definitive statements about them. For example, an extensive green roof can be aesthetically pleasing or an intensive green roof may be less energy efficient than an extensive one.



Figure 1-15: (left) An intensive green roof, characterized by heavier structural loads, high capital and maintenance costs, and accessibility to occupants. (right) An extensive green roof, characterized by lower capital and maintenance costs and lighter structural loads. Source [64] [38]

Comparison of Extension and Intensive Green Roof Systems	
EXTENSIVE GREEN ROOF	INTENSIVE GREEN ROOF
<ul style="list-style-type: none"> • Thin growing medium; little or no irrigation; stressful conditions for plants; low plant diversity. 	<ul style="list-style-type: none"> • Deep soil; irrigation system; more favorable conditions for plants; high plant diversity; often accessible.
<p>Advantages:</p> <ul style="list-style-type: none"> • Lightweight; roof generally does not require reinforcement. • Suitable for large areas. • Suitable for roofs with 0 - 30° (slope). • Low maintenance and long life. • Often no need for irrigation and specialized drainage systems. • Less technical expertise needed. • Often suitable for retrofit projects. • Can leave vegetation to grow spontaneously. • Relatively inexpensive. • Looks more natural. • Easier for planning authority to demand as a condition of planning approvals. <p>Disadvantages:</p> <ul style="list-style-type: none"> • Less energy efficiency and storm water retention benefits. • More limited choice of plants. • Usually no access for recreation or other uses. • Unattractive to some, especially in winter. 	<p>Advantages:</p> <ul style="list-style-type: none"> • Greater diversity of plants and habitats. • Good insulation properties. • Can simulate a wildlife garden on the ground. • Can be made very attractive visually. • Often accessible, with more diverse utilization of the roof. i.e. for recreation, growing food, as open space. • More energy efficiency and storm water retention capability. • Longer membrane life. <p>Disadvantages:</p> <ul style="list-style-type: none"> • Greater weight loading on roof. • Need for irrigation and drainage systems requiring energy, water, materials. • Higher capital & maintenance costs. • More complex systems and expertise.

Figure 1-16: Comparative chart between extensive and intensive green roofs from Canadian architects' *Design Guidelines for Green Roofs*, which provides a succinct summary of the general differences between the two types of green roofs. It represents the opinions of the architects who created it, thus, for example, an extensive green roof can be aesthetically pleasing or an intensive green roof may be less energy efficient than an extensive one. Source [53]

1.4.2 Benefits of Green Roofs

Numerous benefits of green roofs have helped propel them to cover 10 million m^2 of roof area in Germany over a decade ago [53]. Similar widespread use spans other European countries and even the United States, where extensive green roofs have grown more than 50% for four subsequent years [59].

Reduced storm water runoff

One benefit of green roofs is their potential to reduce storm water runoff, a problem increasingly striking urban centers. Green roofs help reduce storm water runoff by absorbing rainfall in the growing media, which is later used for evapotranspiration by the vegetation and soil. This absorption and subsequent evapotranspiration, often referred to as retention, directly removes water from storm-water and sewage systems. The storm-water reduction benefits of green roofs are well documented through field studies and simulations, though consensus is not entirely reached on the extent of the benefits. One study compares an extensive green roof to a modified bitumen roof and found that for light rainfall, 2.1 mm , the retention of the green roof was 85.7%. However, in heavier rainfall, 12.1 mm , while the green roof delayed the runoff by 30 minutes, it failed to retain more than the conventional roof as both cases had the same runoff volume [84]. Another study found an average retention rate for an extensive green roof in Athens, GA to be 78% [32]. Nearly every storm that dropped less than 0.5 in (13 mm) of rainfall was retained by over 90%. The lowest retention occurred during a 2.12 in (53.8 mm) rainfall, and was found to be 39% [32]. A third experiment in Canada reports detailed data from a 34 mm rain event over an extensive green roof and reference modified bitumen roof, shown below in Fig. 1-18 [29].

All three experiments found that after the soil is saturated (or its field capacity reached), any additional rainfall will be runoff. For such rain events, green roofs provide retention in which rainfall is temporarily absorbed and later slowly released, thus reducing the surge of storm-water to the city's drainage system normally associated with conventional roofs [44]. The aforementioned Canadian experiment, which was

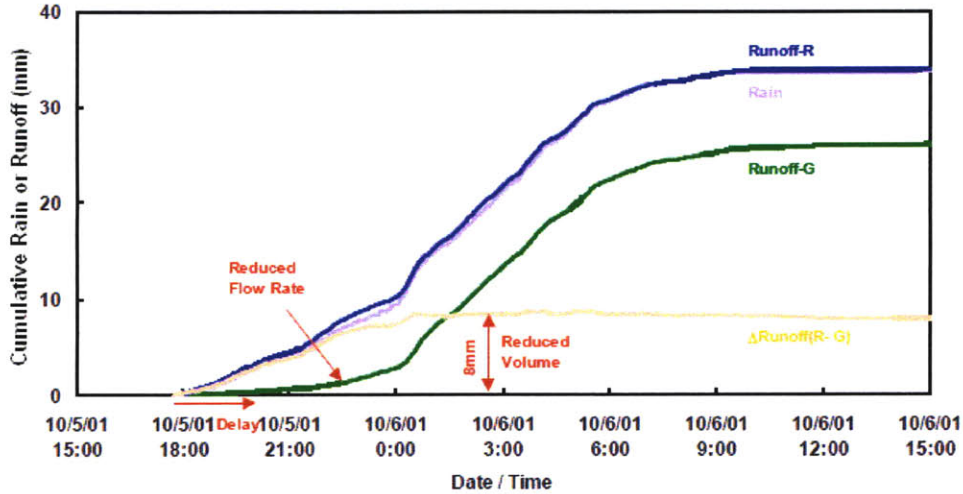


Figure 1-17: Rain event on Canadian extensive green roof on October 5-6, 2001. The purple line, Rain, is essentially matched by the blue line on top, Runoff-R, which is the measured cumulative runoff from a conventional roof, indicating that the traditional roof is completely impervious. The green line, Runoff-G, shows the initial delay then reduced runoff flow rate of the green roof. At approximately midnight, the green roof becomes saturated and follows the Runoff-R curve, though is always 8 mm lower indicating the 8 mm of rainfall retained by the green roof. Source [29]

conducted over 5 years, found the retention rate of an extensive green roof to vary significantly with month of the year [28]. Due to extremely cold winters, in which all precipitation was snow, only the spring and summer months should be noted for storm-water runoff data below in Fig. 1-18. Additional factors that affect the storm-water retention capability of a green roof are evaporation and transpiration potential, antecedent moisture conditions, and soil hydraulic properties [44]. Although the exact retention capability of green roofs vary, it is well accepted that they can significantly help reduce storm-water runoff.

Lower roof temperatures

It is well accepted that green roofs can significantly lower roof surface and membrane temperatures in warm climates [82] [76] [92] [29]. Roof surface temperature reductions over 30 C have been observed in multiple field experiments, one of which is shown in Fig. 1-19, in which summertime roof surface temperatures for a conventional and extensive green roof in Orlando, FL are plotted. As mentioned in Section 1.2.2, lower

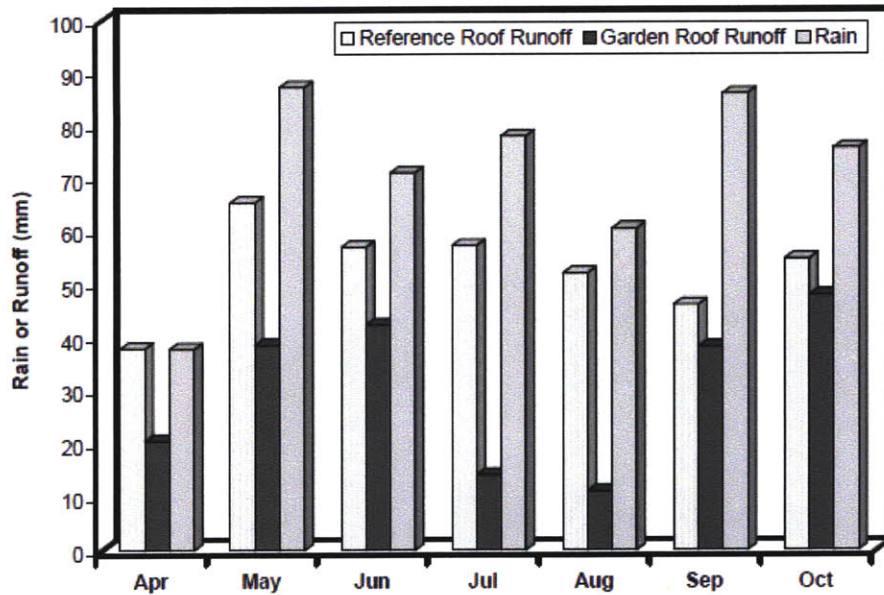


Figure 1-18: Cumulative monthly rainfall and runoff from the reference and extensive green roofs from Ottawa, Canada (averaged from 2002 - 2005). The minimal runoff during Jul and Aug is reported to be from increased evaporation potential (likely due to hotter ambient temperatures). Source [28]

surface temperatures can help mitigate the UHI effect.

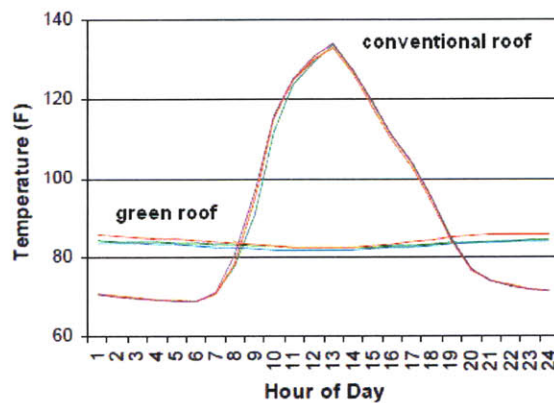


Figure 1-19: Average summertime surface temperature on a 307 m² building in Orlando, FL. Half of the roof is a conventional roof (upper curve) and half is an extensive green roof (lower curve). The amount of insulation varies from R-value 17-38. Different colors represent different temperature sensor locations. Source [35].

Prolonged Roof Life

Additionally, green roofs help moderate the temperature of roofs, as shown below in Fig. 1-20. Even in cold climates, such as northern Canada, green roofs can help moderate roof temperatures, though their impact is insignificant during the winter [29]. This temperature moderation often leads to longer roof membrane life. Two comparative studies between conventional roofs and green roofs have reported the life of a conventional roof membrane to be 10 and 15 years, while the membrane under a green roof is forecast to last 40 and 45 years [93][52]

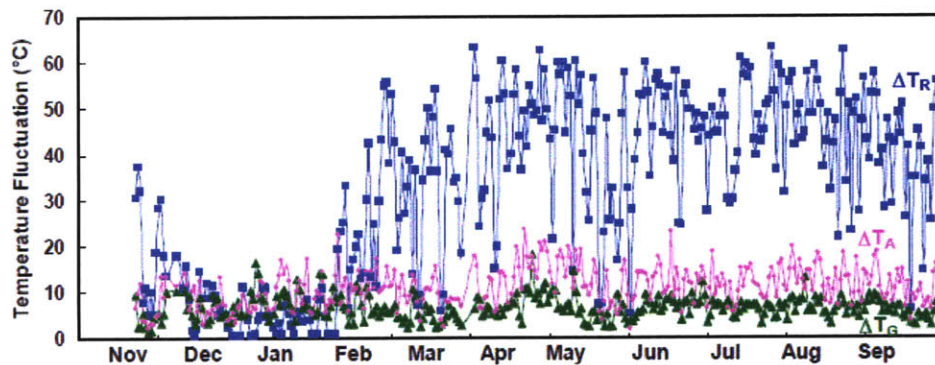


Figure 1-20: Daily temperature fluctuation for a traditional roof (blue squares), green roof (green triangles), and ambient air (pink circles) in Ottawa, Canada. Note the higher fluctuations of the traditional roof from Feb - Oct, which lead to higher thermal stress and shortens roof lifespan. During the winter months, there is an indistinguishable difference between to green and traditional roofs. Source [29]

Improved aesthetics

Green roofs often improve the aesthetics of the rooftop environment from an extremely hot black sheet of tar to a more tranquil vegetated area. This benefit of green roofs is difficult to quantify, but green roof advocates insist that green roofs increase property value, satisfy “the aesthetic needs of people” in surrounding buildings, and potentially increase employee productivity [9].

Energy saving potential

Onmura found a 50% reduction of heat flux through a concrete slab with vegetation compared to a bare concrete slab and extrapolated the results to green roofs in general [65]. Lazzarin conducted experiments on a hospital in Italy and found energy savings to be seasonal. In the summer, he found that the heat entering through the roof was nearly halved by a dry green roof and for a wet green roof, energy was actually leaving the building [54]. However, in the winter, he found that a green roof increased the amount of heating energy required [54]. Green roofs can, however, save energy during the winter. In a Canadian study, Bass and Baskaran measured the daily energy requirement for space conditioning in both a building with an extensive green and conventional roof in Ottawa, Canada. They found that the green roof saved total energy (space heating and cooling energy combined) in every month except January, where the green roof consumed roughly 10% more than the conventional [29]. Fig. 1-21 below summarizes the findings from nearly a year of measurements.

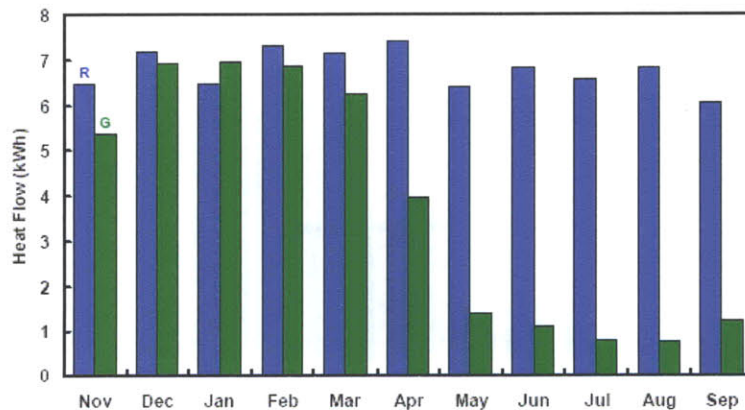


Figure 1-21: Average daily energy requirement due to the heat flow through the roof surfaces from Nov 22, 2000 - Sep 31, 2001 in Ottawa, Canada. The blue bars, denoted R, are for a reference conventional roof while the green bars, denoted G, are for an extensive roof. Source [29]

Some observed the impact of a green roof on a two-story building in Florida and found that during the summer, an average heat flux of 1.51 W/m^2 with a conventional roof was reduced to 1.23 W/m^2 with a green roof, an 18% reduction [76]. Although

these percentages may seem encouraging, they depend on numerous parameters (as will be later shown) and the impact on total building energy can be less substantial.

Reduced sound propagation

Numerical modeling suggests that green roofs can also reduce sound propagation through cities [69]. Under perfect conditions, a maximum 10 *dB* reduction in the adjacent urban canyon was simulated by switching from a conventional roof to an extensive green roof [69]. This maximum decrease was only noted in dense urban canyons [69]. Although this noise reduction may seem encouraging, 10 *dB* is the difference between a power saw at 3 *ft* and a motorcycle [5]. Additionally, by adding 3 *in* of expanded polystyrene insulation to concrete, a 36 *dB* reduction is reported from the environment to inside the building [7].

Pollution and air particulate removal

As with any vegetation, green roofs help remove particles and pollution from the air. It has been estimated that if all the roofs in Washington, DC were green roofs, 58 metric tons of air pollutants could be removed [36]. Such potential can be exciting, but when a more realistic total green roof area is used, the reductions are not as large. One study considered 71% (or 19.8 ha) of Chicago's green roof area, (the leading promoter of green roofs in the US) and found through simulation that green roofs removed 1675 kg of air pollutants in just under a year [94]. A field study on a 4000 m^2 green roof in Singapore found the particle and SO₂ concentration above the roof dropped 6% and 37% respectively by installing a green roof [95]. Similar results were found, however, using trees planted in the urban center. Based on a US Department of Agriculture report and Yang's simulations, a medium-sized tree will remove as many pollutants as a 19 m^2 extensive green roof, but will only cost \$400 rather than \$3059 [94][58].

Additional useable space

In the case of intensive green roofs, additional space is often provided for recreation, growing food, and numerous other activities, including a golf course and outpatient care space as shown in Fig. 1-22 [9].



Figure 1-22: (top) 6,500 ft^2 intensive green roof atop the Massachusetts General Hospital Yawkey Center for Outpatient Care and (bottom) 15,000 ft^2 intensive green roof in Berlin, Germany on the corporate offices of Giese + Giese. Source [9]

1.4.3 Areas for Research - Green Roofs

This investigation into the energy saving potential of various roof types does not seek to add another statistic to the long list of energy savings achieved by installing a green roof. Instead, it seeks to establish a common standard that can be used to compare the energy saving potential of numerous types of roofs. Therefore, it aims to fill a gap in the literature by providing a comparison between different roof technologies in different climates.

1.5 Roof Construction

Three different types of roofs have been described in detail thus far. Each of these roofs, however, can share multiple commonalities in how they are constructed.

1.5.1 Roof Insulation - Amount

Insulation is well known to help moderate temperatures in buildings and therefore help reduce building energy consumption. The magnitude of this moderation and reduction is discussed in this section.

Temperature Moderation

An experiment in Sri Lanka investigated the effect of insulation on the soffit temperature of small-scale buildings [42]. The soffit is the underside of the roof slab, and thus its temperature is the same as the ceiling underneath the roof, assuming no drop ceiling is used. In a tropical climate like Sri Lanka, it is ideal to have a lower soffit temperature. Fig. 1-23 shows the decrease in soffit temperature during a hot, cloudless day for a concrete roof with 0, 25, 38, and 50 mm of expanded cellular polyethylene insulation, corresponding to R values of 0.0, 0.71, 1.1, and 1.4 m^2C/W respectively.

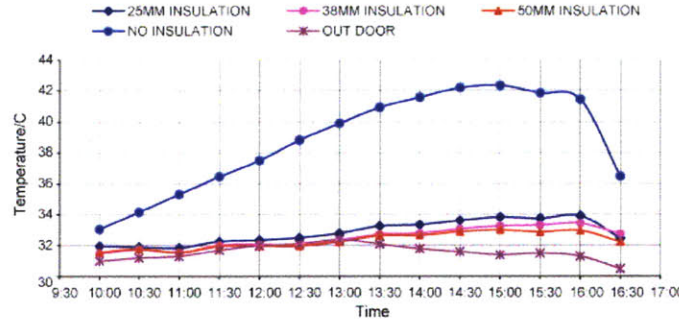


Figure 1-23: Soffit temperature on small-scale buildings in Sri Lanka on a hot, cloudless day for a concrete roof with R values of 0.0, 0.71, 1.1, and 1.4 m^2C/W , corresponding to 0, 25, 38, and 50 mm of expanded cellular polyethylene insulation. Note the near 8 C temperature difference between the roof with 0 and 25 mm of insulation. The variation of temperature between the cases with insulation is much less, only decreasing by 1 C when insulation is doubled. Source [42]

It is shown in Fig. 1-23 that a modest amount of insulation, 2.5 cm, can significantly reduce soffit temperatures in a building, by up to 8 C in the tropical climate of Sri Lanka [42]. In a building with no dropped ceiling, this cooler soffit is in direct contact with the indoor air, leading to cooler indoor conditions.

Building Energy Reduction

It has been shown that adding insulation can significantly lower soffit temperature, however, what is the impact of this lower temperature on energy use? The same Sri Lankan study calculated the heat flux into the building through the roof for the 0, 25, 38, and 50 mm insulation cases. Their findings are shown below in Fig. 1-24

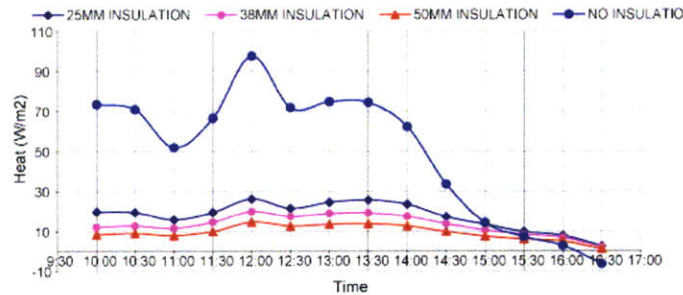


Figure 1-24: Heat flux into small-scale buildings in Sri Lanka on a hot, cloudless day for a concrete roof with R values of 0.0, 0.71, 1.1, and $1.4 \text{ m}^2\text{C}/\text{W}$, corresponding to 0, 25, 38, and 50 mm of expanded cellular polyethylene insulation. Note the peak reduction of nearly $90 \text{ W}/\text{m}^2$, or 90%, average daytime difference between the 0 and 50 mm insulation cases. By changing the amount of insulation, the 1 C decrease in soffit temperature shown in Fig. 1-23 results in an $10\text{-}15 \text{ W}/\text{m}^2$ decrease. Source [42]

This reduction in heat flux through the roof can be compared to the reduction caused by installing a green roof. A Japanese experiment measured surface and soffit temperature, net radiation, water content, and other parameters needed to estimate the different modes of heat transfer on a green and conventional roof [82]. The roof had no insulation, so the only difference between the two sets of data was the roof type. From the measured data, the heat flux into the building was determined. The calculated heat flux into the building during a hot summer day in Kobe, JP, is shown below in Fig. 1-25.

A comparison of Figs. 1-25 and 1-24 shows that both adding insulation and installing a green roof help reduce heat flux into buildings on a hot day. Because of the different experimental constructions between the Sri Lankan and Japanese studies, as well as different climates, it can not be determined whether adding insulation or installing a green roof more greatly reduces roof heat flux into buildings. Although the percent reduction in heat flux from adding insulation is higher, nearly 90% for

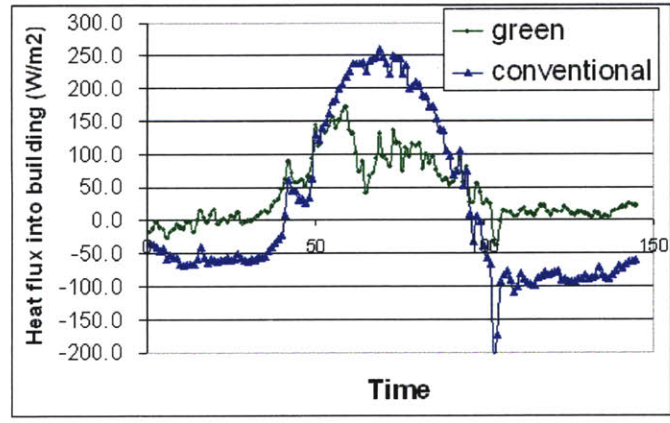


Figure 1-25: Heat flux into a full-scale building in Kobe, JP on a hot summer day with no insulation. Note the average daytime reduction of nearly 150 W/m^2 , or 60% from installing a green roof. The insulating effects of the green roof prevent any night cooling from happening, which occurs with the conventional roof, as evidenced by the negative heat flux. Source [82]

insulation compared to approximately 60% for a green roof, the absolute reduction from adding a green roof is nearly twice that of the reduction from adding insulation, approximately 150 W/m^2 for the green roof compared to approximately 45 W/m^2 for the insulation.

Few studies have tested the impact of varying the amount of insulation on green or cool roofs. A simulation of a green roof in Greece predicted that the annual total energy savings from a green roof were negligible, 2%, when “heavy insulation” was used, which resulted in an overall roof R value of $3.85 \text{ m}^2\text{C/W}$ (which included insulation and structural concrete slab). When “moderate insulation” was used with overall roof R value of $1.35 \text{ m}^2\text{C/W}$, an annual total energy savings of 4% were estimated [63]. The same comprehensive study by NIST mentioned in Section 1.2.2 considered, among a few other roof construction factors, the role of insulation on the annual heating and cooling energy for a building with various roof reflectivities [96]. The study found large savings in cooling energy when a cool roof was installed, but in nearly every case, the minimum cooling energy was realized when insulation was added in addition to a cool roof. Fig. 1-26 shows some of the key findings of these two studies with regard to the effect of insulation on the energy savings from green

and cool roofs.

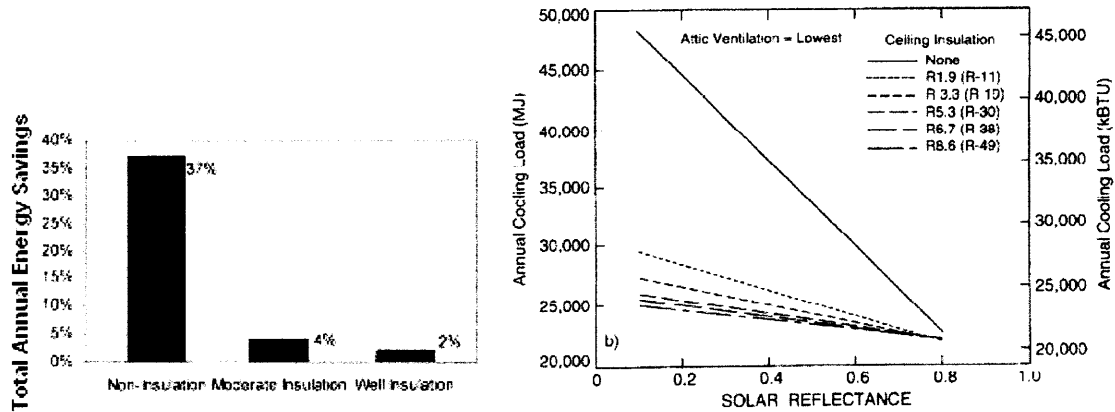


Figure 1-26: (left) Simulated annual total energy savings from installing an extensive green roof on a building in Greece. The overall roof R value for the non, moderate, and well insulation cases are 0.129, 1.35, and 3.85 m^2C/W respectively. (right) Simulated annual cooling load in MJ for a one-story home in Miami, FL with various roof reflectivities and insulation levels. Note the large potential savings of installing a cool roof, changing the reflectivity from 0.2 to 0.8, when no insulation is present. Source [63][96]

In Fig. 1-26, although the savings decrease when insulation is used, the total annual load is significantly reduced with a small amount of insulation, 1.9 m^2C/W , even without a cool roof. In both studies, the potential savings of installing the green or cool roof are greatly reduced when insulation is present, though the total cooling energy is reduced.

1.5.2 Roof Insulation - Location

Not only does the amount of insulation affect the building's performance, but where the insulation is added within the roof assembly also has an impact. A study in Turkey used a first-principle analytical model of a concrete roof to show the impact of insulation location within the roof assembly [66]. Twelve location configurations were modeled, many of which are physically difficult to reproduce, because insulation was added within the structural support slab. For each location, two amounts of insulation were considered, 6.0 and 9.0 *cm* of glass wool, corresponding to R values of 1.7 and 2.5 m^2K/W . The study found that the incoming heat flux was reduced

by 17% if all the insulation was placed on top of the roof slab instead of underneath [66]. Their calculated heat flux through the roof for various insulation locations is presented below in Fig. 1-27.

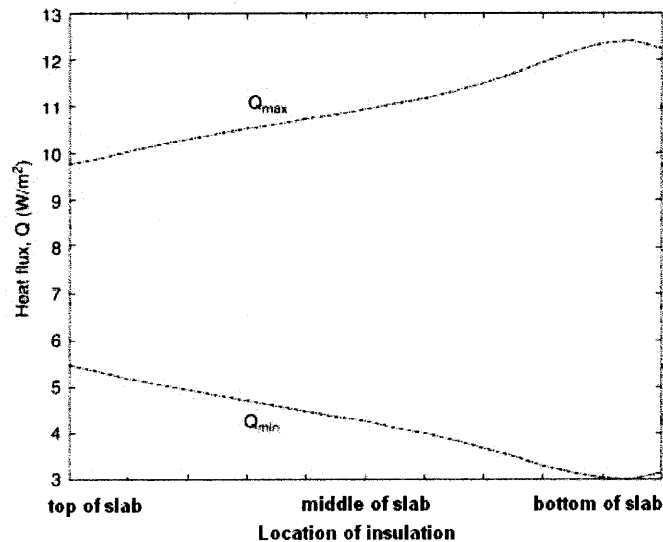


Figure 1-27: Analytical model of heat flux through a concrete roof as insulation location is varied, beginning at the top of the 20 cm concrete slab and moving downward. The two plots shown, labeled Q_{max} and Q_{min} , represent the max and min heat flux through the roof during the day. 6 cm of glass wool, R value of $1.7 \text{ m}^2\text{K}/\text{W}$ is used for this simulated roof in Elazig, Turkey during a typical summer day. Note the decreased maximum heat flux when the insulation is added on top of the slab. Source [66]

Although the above study is helpful in understanding the impact of insulation location on a building in Turkey with a concrete roof, the impact for different climates, roof types, and amounts of insulation is unknown. Another analytical study conducted in Saudi Arabia tested the impact of various kinds and locations of insulation as well, but concluded the optimal location for insulation is on the bottom of the slab [24]. Though this second study found the difference between the two locations to be minimal, such conflicting reports warrant further research.

1.5.3 Number of Floors in Building

One final aspect of the roof construction that will be considered may seem unrelated to roofs: the number of floors in a building. Because the roof only directly impacts

the floor beneath it, the roof of a one-story warehouse will affect the entire building's energy profile much greater than the roof on a twenty-story highrise. One analytical study in Italy predicted the impact of adding a green roof to a small two-story building with a basement, in Athens, Greece. The percent savings in cooling energy was roughly halved when the entire building was considered, which is expected for a two-story building [71].

1.5.4 Areas for Research - Roof Construction

It has been shown that roof insulation can significantly decrease building energy use, roof insulation location affects savings, and that the number of floors in a building should be considered when predicting the impact of the roof on the total building energy consumption. However, more research is needed in simultaneously considering the impact of these three factors on total building energy use.

1.6 Motivation for Thesis

As mentioned in the previous sections, there are multiple areas of research across the different roofs and roof constructions. Synthesizing these areas together leads to the addition this thesis will make to the literature. Although the cooling energy savings of cool roofs is well documented, the heating energy losses are less published. One addition this thesis will make will be to weigh the tradeoffs between cooling savings and heating losses associated with cool roofs. This net energy impact of a cool roof can then be compared to a modified-bitumen and green roof, providing a rare but informative perspective on the energy saving potential of all three roofs. Along with this comparison across technologies, aspects of roof construction will be considered, which have been shown to potentially have an equal or greater impact on total building energy use than the roof technologies.

This investigation will also compare the energy saving potential of these aspects of the roof to the potential of other building components (such as windows, building orientation, HVAC system, etc.), to verify the effectiveness of changing such aspects.

Finally, this thesis will empower building owners in cities around the world to quickly understand how various roof technologies will impact their building's energy consumption.

1.7 Outline of Thesis

To predict the tradeoffs between the three roof technologies, a first-principles analytical tool has been developed that estimates the energy entering a building through the roof. Weather parameters, which are easily attained from weather stations around the world, are the inputs to the tool, allowing any climate to be considered. Furthermore, the model is verified by comparisons to two data sets for both green and cool roofs in the literature. This tool is explained in detail, along with its verification, in Chapter 2.

The tool is incorporated into an existing online design aid, MIT's Design Advisor, that allows architects and designers to easily compare the energy requirements of various building configurations. This tool will thus become a new roof module for Design Advisor, which will allow users to quickly see the potential energy savings of different roof technologies and compare them to other potential savings in the building (for example, from improving windows, wall insulation, building orientation, etc). Design Advisor and the incorporation of the roof module will be discussed in Chapter 3.

Numerous trials and comparisons across the three roof technologies along with discussion of these results will be presented in Chapter 4.

Chapter 2

Energy Modeling

The aim of this thesis is to provide insight into the energy saving potential of various roof technologies, as mentioned in the previous chapter. In this chapter, the first principles used to analyze the energy impact of each roof are discussed, the numerical modeling techniques used to find solutions to the energy model are explained, and lastly, the model is validated.

The model developed is intended to be used with averaged weather data from numerous climates, predicting the expected energy savings of a certain roof technology throughout an “average” year. However, the model is verified by two sets of data, and accurately models both situations. Nevertheless, the design criterion of using average weather data for inputs justifies certain component approximations of the model that otherwise may not be justifiable.

2.1 Cool and Modified-Bitumen Roof Model

2.1.1 Cool and Modified-Bitumen Roof Energy Balance

The similar construction of both cool and modified-bitumen roofs allows for a single model to be used for both roofs, in which only a few parameters are altered.

A one dimensional model is used to consider the heat transfer through the roof, thus it is assumed at any given depth of the roof, temperature is uniform across the

horizontal plane at that depth. The model also assumes that the roof is large enough such that any potential edge effects are negligible. Although there can be many layers in either type of roof construction, as shown in Fig. 1-12, the thermal resistances of the surface coating and waterproofing layer are neglected.

Therefore, the roof model is composed of a 15 *cm* thick concrete slab with a variable amount of insulation on top or beneath the slab. In both cases, the upper surface of the roof is exposed to incident short-wave radiation from the sun, I_s , long-wave radiation exchange with the sky, $q_{ir,roof}$, and convective heat exchange with the outside environment, H_{roof} , all of which are in $[W/m^2]$. The case in which the insulation is beneath the slab is shown in Fig. 2-1. The roof is assumed to be a gray body, and thus only part of the incident short-wave radiation from the sun is absorbed, while the rest is reflected back to the environment. The roof's reflectivity, ρ , or albedo, determines this ratio as shown in Fig. 2-1.

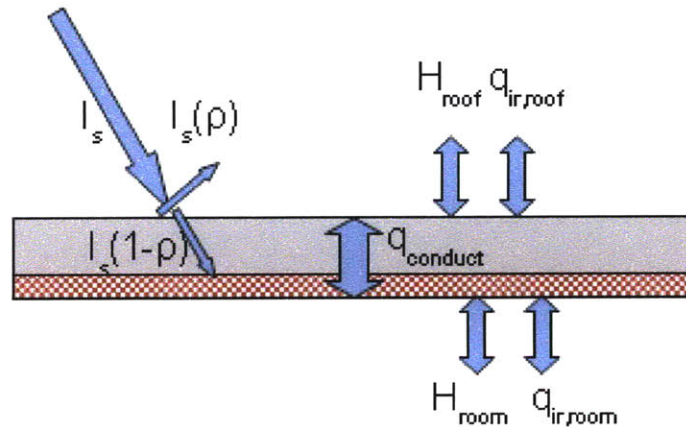


Figure 2-1: Cool roof energy balance with insulation beneath roof slab.

The sky is assumed to be a black body at a temperature T_{sky} of 10 *K* below the ambient temperature [57]. Furthermore, this assumption allows for the long wave radiation heat transfer to be linearized because of the small temperature difference

between the roof surface and the assumed sky temperature [47]. Thus, $q_{ir,roof}$, the heat flux per m^2 , becomes

$$q_{ir,roof} = h_{rad}(T_{sky} - T_{surface}) \quad (2.1)$$

where h_{rad} , in units of, $[W/m^2K]$ is defined as

$$h_{rad} \equiv 4\varepsilon\sigma T_m^3 \quad (2.2)$$

and ε is the emissivity of the roof (which is also equal to the absorbtivity of the roof for long-wave radiation from the gray body assumption), σ is the Stefan-Boltzman coefficient, $5.67e-8 J/sm^2K^4$, and T_m is the average temperature of the two bodies exchanging radiation, in this case, the roof surface and the sky. Although T_m changes slightly throughout the day and depending on location, any change is relatively small compared to the absolute temperature, thus its effect on h_{rad} is minimal and h_{rad} is assumed to be a constant $6 W/m^2K$.

The convective heat transfer between the environment and roof is found using a derived heat transfer coefficient for the average weather conditions on the roof, as shown in Eqs. 2.3 through 2.5.

$$H_{roof} = \bar{h}(T_{amb} - T_{surface}) \quad (2.3)$$

where T_{amb} is the ambient outdoor temperature in K and \bar{h} is determined from the average Nusselt number for turbulent flow over a flat plate [61]

$$\overline{Nu} = 0.664Re_{tr}^{\frac{1}{2}}Pr^{\frac{1}{3}} + 0.036Re_L^{0.8}Pr^{0.43} \left[1 - \left(\frac{Re_{tr}}{Re_L} \right)^{0.8} \right] \quad (2.4)$$

where Re_L is the Reynolds number based on total length and Re_{tr} is the transition Reynolds number, assumed to equal 50,000 here to account for the ease of transition from laminar to turbunlent on a roof (due to surface roughness and small vibrations in the building). The Prandtl number, Pr , for air is assumed to be 0.7. From Eq. 2.4, and average convective heat transfer coefficient can be derived from the definition of

Table 2.1: Variation of average heat transfer coefficient over a flat roof with wind speed

windspeed [m/s]	\bar{h} [W/m^2K]
1	2.88
2	5.05
3	7.00
4	8.83
5	10.6

the Nusselt number

$$\overline{Nu} = \frac{\bar{h}L}{k_{fluid}} \quad (2.5)$$

where L is the length of the roof over which the wind flows, and k_{fluid} is the conductivity of air, assumed to be $0.0257 W/mK$. Table 2.1 shows the variation of \bar{h} with a range of expected windspeeds on top of a square roof of length $25 m$.

Because average weather data will be used with this model, the range of windspeeds in Table 2.1 is expected to account for the majority of wind conditions on top of the roof. Fig. 2-2 shows the average wind speed at $10 m$ from 1976-1995 according to the National Center for Environmental Prediction (NCEP) and National Center for Atmospheric Research (NCAR) reanalysis data set.

Although a variation of nearly $8 W/m^2K$ is shown in Table 2.1, the temperature difference that drives convective heat transfer, Eq. 2.3, results in a comparatively small variation in the total heat transfer when the convective heat transfer is compared to other terms.

One might note that no natural convection is considered in this discussion of the convective heat transfer, which is correct. Natural convection is ignored on the roof because the wind, resulting in forced convection, dominates over bouyant forces, which result in natural convection. Analytically, the comparison between forced and natural convection can be made using the ratio of the square of Reynolds number, Re , to the Grashof number, Gr , a nondimensional number that approximates the ratio of bouyant to viscous forces

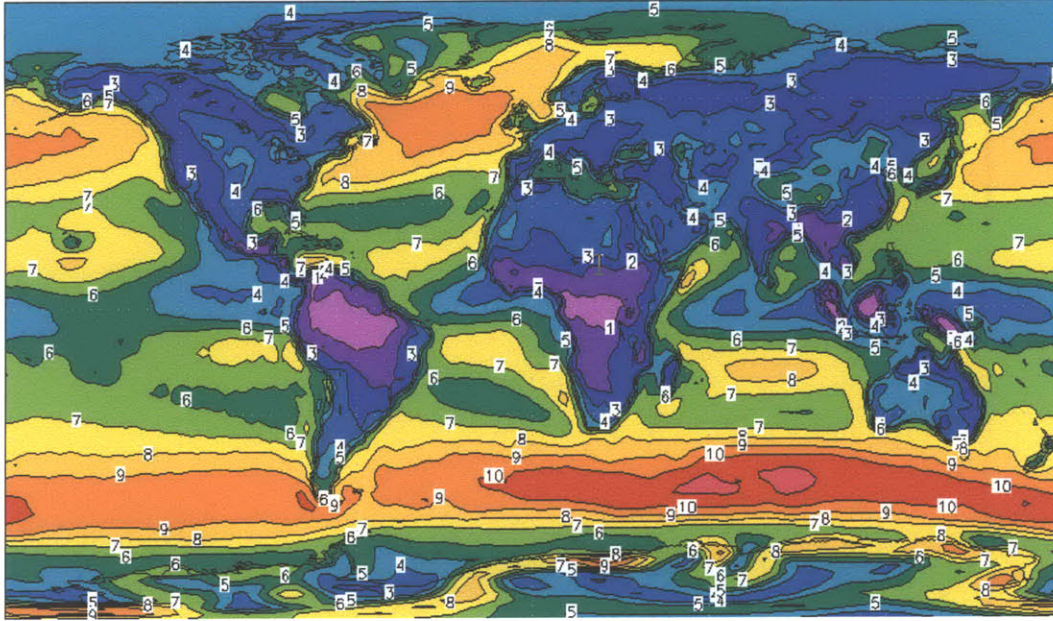


Figure 2-2: Average wind speed at 10 m from 1976-1995, according to the NCEP/NCAR reanalysis data set. Note the variation from purple, 1 m/s, to light blue, 5 m/s on all continents. [18].

$$\frac{Re^2}{Gr} = \frac{\left(\frac{VL}{\nu}\right)^2}{\left(\frac{gBL^3(T_{plate}-T_{amb})}{\nu^2}\right)} \quad (2.6)$$

where all properties are for the ambient air, V is the wind speed on the roof, L is the length of the roof as before, ν is the kinematic viscosity, g is the acceleration due to gravity, and B is the volumetric thermal expansion coefficient (approximated as $1/Temperature$ for ideal fluids, which is used for air).

If this ratio is much great than one, forced convection dominates, and if it is much less than one, natural convection dominates, but if it is approximately one, both types of convection are important to consider. The experimentally measured Re and Gr from a concrete roof at the University of Kobe shown in Fig. 2-3 reveals that forced convection dominates, thus natural convection is neglected in the model. It can be observed from Fig. 2-3 that the ratio drops during the day when a large temperature difference exists between the roof surface and ambient temperatures, thus increasing Gr .

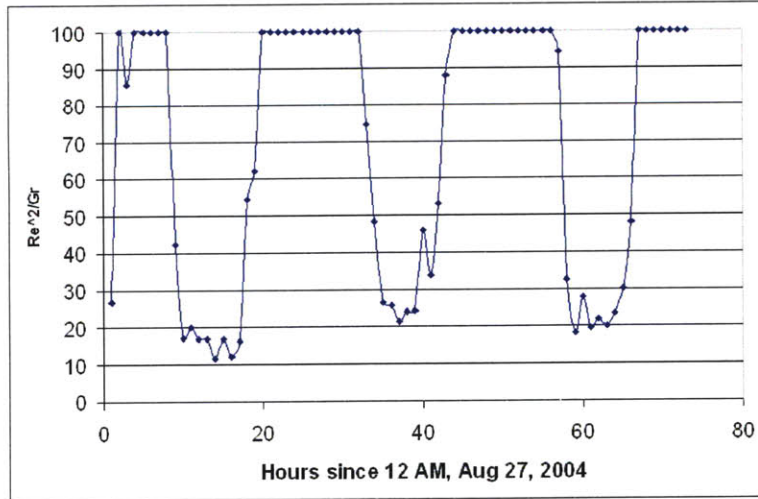


Figure 2-3: Ratio of measured $\frac{Re^2}{Gr}$ for a concrete roof at the University of Kobe that shows forced convection dominates on a roof because this ratio is much greater than one. To maintain a useful scale, all values are capped at 100, though the ratio reaches as high as 33949 at one point of the day. [81].

The thermal mass of the concrete slab, $mC|_{concrete}$, is accounted for, and it is assumed to have constant conductivity along with the insulation. However, the insulation is assumed to have no thermal mass on the basis that it would be negligible compared to the mass of the concrete and accounting for it would noticeably increase the complexity of the model [75]. A detailed description of the conduction through the slab and its thermal mass will follow.

Long-wave radiation and convective heat transfer are the two modes of thermal interaction between the top most room of the building and the roof. The radiation heat transfer occurs between the bottom of the roof, which is assumed to be the room ceiling, and other surfaces in the room. Because air is transparent, no heat is transferred to it by radiation. It is assumed that all surfaces that will radiate to the ceiling are at the room temperature, T_{room} . The temperature difference between the room and roof is small enough to allow for a linearization of the radiative heat transfer [47]. Convection from the ceiling to the air in the room will be either forced or natural convection, or a combination of the two, depending on the ventilation system. Following the reasoning laid forth by Bryan Urban in his master's thesis, the linearized radiation and convective heat transfer coefficients are lumped together to

Table 2.2: Thermal properties of roof used in model

	Cool Roof	Modified-Bitumen Roof
<i>Roof membrane</i>		
reflectivity [-]	0.7	0.1
emissivity [-]	0.95	0.95
<i>Structural support slab</i>		
Thickness [m]	0.015	0.015
Density [kg/m ³]	2300	2300
Conductivity [W/mK]	1.4	1.4
Heat Capacity [J/kgK]	880	880
<i>Insulation</i>		
Thickness [m]	not specified	not specified
R Value [W/m ² K]	variable, user specified	variable, user specified

form an effective heat transfer coefficient from the ceiling to the room, h_{room} , which is approximated as $10 \text{ W/m}^2\text{K}$ [88]. The thermal properties of the roof used in the model are summarized in Table 2.2.

Finally, to complete the energy balance for the cool and modified-bitumen roofs, consideration must be given to the energy storage capability of the concrete slab, which is discussed in the next section.

2.1.2 Cool and Modified-Bitumen Roof Numerical Modeling

Modeling Temperature Distribution through Roof

In order to account for the transient temperature gradient through the concrete slab, while minimizing calculation complexity, it is divided into numerous thin slices. An energy balance is then performed on each slice, assuming a lumped capacity model for each slice, to determine the effect of the thermal mass and to simplify the flux calculation through the slab.

In order to model each slice as a lumped system, heat must diffuse *through* the slice more quickly than it diffuses from the environment *into* the slice. The non-dimensional Biot Number, Bi , compares these two phenomena for the outermost slice and is defined as

$$Bi \equiv \frac{hl}{k}. \quad (2.7)$$

where h is the convective heat transfer coefficient, l is the characteristic thickness through which heat conducts (in this case the slice thickness), and k is the conductivity of the medium through heat transfers ($k_{concrete}$ in this case). Typically, in order to make the lumped capacity assumption, the Biot number must be less than 1/6 [61]. However, to be conservative in this case, the Biot number must be less than 0.1. In this model, because there is long-wave radiation in addition to convection on the roof, both modes of heat transfer must be included in determining what will be a quasi Biot number. The sum of the linearized radiation heat transfer coefficient and the convective coefficient creates an overall effective heat transfer coefficient, which is represented by h in Eq. 2.7. Thus, the maximum slices thickness, l_{max} , is

$$l_{max} = 0.1 \frac{k}{h} \quad (2.8)$$

Given the thermal properties listed in Table 2.2, the required slice thickness to validate the lumped capacity model is 0.83 *cm*. Dividing the 15 *cm* concrete slab by 0.83 *cm* and rounding up to the nearest whole number results in a total of $n = 18$ slices.

Nodal Energy Balance

The aforementioned energy balance on the entire roof must now be revisited to consider each of the 18 slices, or nodes, individually. Furthermore, the energy balance must be discretized for the sake of calculations. Though this task may seem daunting, the uniformity of many nodes greatly simplifies it. Because every node is made of concrete and are all of equal thickness, the mass and heat capacity of each node is uniform, and denoted m and C , respectively.

The thermal mass of each node allows energy to be internally stored in each. The change of this internal energy, in joules, is equal to the net energy flux in to or out of the node

$$\frac{dE_{internal}}{dt} = \dot{Q}_{in} - \dot{Q}_{out} \quad (2.9)$$

where $\frac{dE_{internal}}{dt}$ is the change in internal energy over time dt , \dot{Q}_{in} is the net energy entering the node, \dot{Q}_{out} is the net energy leaving the node. Because of the lumped capacity model, dt is small enough to assume that all temperatures (in the slab, ambient, and in the room) as well as all weather parameters (incident solar radiation) are constant over dt . The appropriate dt to justify this assumption is determined by ensuring that the Fourier Number, Fo is less than 0.5

$$Fo \equiv \frac{k\Delta t}{\rho cl^2} < \frac{1}{2} \quad (2.10)$$

where l is the characteristic length through which conduction takes place, in this case, the slice thickness. Solving for Δt using l_{max} will give the maximum time step for which a lumped system can be used

$$\Delta t_{max} = \frac{1}{2} \frac{\rho c (l_{max})^2}{k} \quad (2.11)$$

With the allowable time step now determined, the general nodal energy balance, Eq. 2.9, can be specifically defined for each node. For the case when insulation is beneath the roof slab, the roof is divided into slices as shown in Fig. 2-4.

The energy balance for the top node, $n = 1$, is the most complicated because of its direct interaction with the outside environment and is shown below

$$mC(T_1' - T_1) = \left[(1 - \rho)I_s - h_{rad,sky}(\bar{T}_1 - T_{sky}) - \bar{h}(\bar{T}_1 - T_{amb}) + \frac{k}{1.5l_{slab}}(\bar{T}_2 - \bar{T}_1) \right] \Delta t \quad (2.12)$$

where T_i is the current node temperature, T_i' is the node temperature at the next time step, Δt , l_{slab} is the thickness of a single node, and \bar{T}_i is the average temperature of the current and next time step, as defined below

$$\bar{T}_i \equiv \frac{T_i' + T_i}{2} \quad (2.13)$$

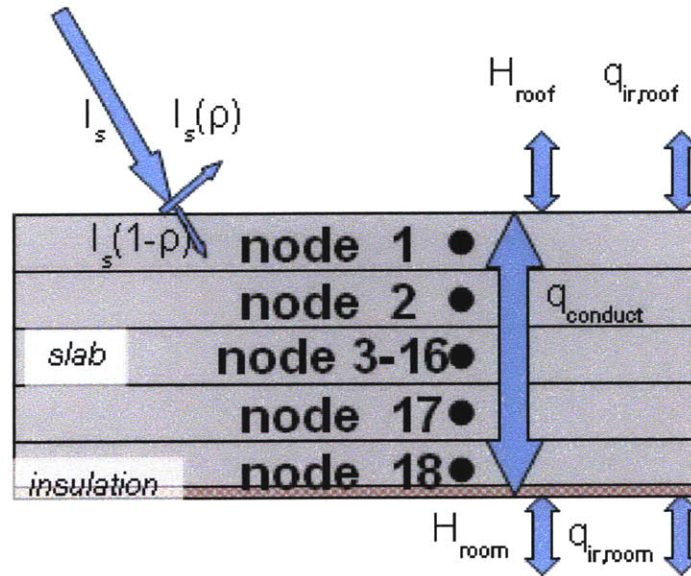


Figure 2-4: Nodal diagram of cool and modified-bitumen roof model, in which each node has a lumped capacitance. In this case, the insulation is beneath the roof slab and is included as part of the final node.

The incident solar radiation, I_s in W/m^2 is an input to the model, as is the ambient temperature in degrees Kelvin, T_{amb} , which also gives T_{sky} by

$$T_{sky} \equiv T_{amb} - 10 \quad (2.14)$$

The length in the conduction term, l_{slab} , is multiplied by 1.5 to account for the additional half length of slab through which the heat must conduct from node 2 to the surface, shown in more detail in Fig. 2-5

The last node of the concrete slab is also more complex because of its interaction with the room, additional half length in conduction term (for the same reasoning as the top node), and accounting for the insulation. The final node, node 18, has energy balance

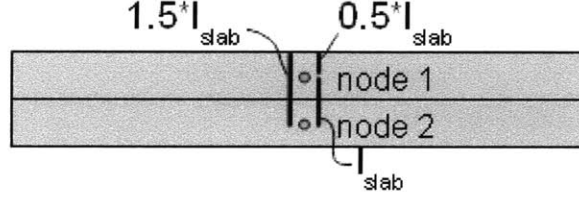


Figure 2-5: Diagram of nodes 1 and 2 that shows the additional half length through which heat must conduct from node 2 to the surface. Similarly, on the bottom of the roof slab, heat must also conduct an additional half length from the second-to-last node into the room beneath.

$$mC(T_{18}' - T_{18}) = \left[\frac{1}{R_{eff,room}} (T_{room} - \overline{T_{18}}) + \frac{k}{1.5 \cdot l_{slab}} (\overline{T_{18}} - \overline{T_{17}}) \right] \Delta t \quad (2.15)$$

where

$$R_{eff} \equiv \frac{1}{h_{room}} + R_{ins} \quad (2.16)$$

where R_{ins} is an input parameter in units of $m^2 K/W$.

Because of the additional half length in the conduction term of both nodes 1 and 18, nodes 2 and 17 will also be affected, and have the following energy balances, respectively

$$mC(T_2' - T_2) = \left[\frac{k}{l_{slab}} (\overline{T_3} - \overline{T_2}) + \frac{k}{1.5 \cdot l_{slab}} (\overline{T_1} - \overline{T_2}) \right] \Delta t \quad (2.17)$$

$$mC(T_{17}' - T_{17}) = \left[\frac{k}{1.5 \cdot l_{slab}} (\overline{T_{18}} - \overline{T_{17}}) + \frac{k}{l_{slab}} (\overline{T_{16}} - \overline{T_{17}}) \right] \Delta t \quad (2.18)$$

All other nodes, nodes 3-16, look the same in terms of the energy model and can be described by

$$mC(T_i' - T_i) = \left[\frac{k}{l_{slab}} (\overline{T_{i+1}} - \overline{T_i}) + \frac{k}{l_{slab}} (\overline{T_{i-1}} - \overline{T_i}) \right] \Delta t \quad (2.19)$$

Insulation Location

The above analysis is done for the cool or modified-bitumen roof with insulation underneath the concrete slab, thus leaving the concrete exposed to the outside environment. If the insulation is instead placed on top of the concrete slab, the slab will be exposed to the indoor conditions, helping to moderate indoor temperatures. Consequently, the Bi number will slightly change because the overall heat transfer coefficient in Eq. 2.7 changes. Using the new h determined from indoor conditions (which is assumed a constant $10 \text{ W/m}^2\text{K}$), the resulting l_{max} is 1.4 cm , which leads to $n = 11$ slab nodes and a time step of $\Delta t = 60 \text{ s}$. The basic energy balance for each node, Eq. 2.9 will remain the same, but some of the nodal equations will change for this case.

In the model, a $1/2 \text{ in}$ coverboard of conductivity $k_{board} = 0.133 \text{ W/mK}$, density $\rho_{board} = 746 \text{ kg/m}^3$, and heat capacity $Cp_{board} = 1090 \text{ J/kgK}$, is placed on top of the insulation, to protect it from the environment, as shown in the nodal diagram in Fig. 2-6. Because the Biot number for the coverboard fulfills the standard assumption for lumped capacitance, that is $Bi < 1/6$, the coverboard is added as a single node, and thus the total number of nodes is now 12.

Now, the top node, made of coverboard, will have an additional resistance in the conduction term (as well as the additional half length of coverboard), as shown in the energy balance

$$(mC)_{board}(T_1' - T_1) = \left[\begin{aligned} &(1 - \rho)I_s - h_{rad,sky}(\bar{T}_1 - T_{sky}) - \bar{h}(\bar{T}_1 - T_{amb}) \\ &+ \frac{1}{\frac{l_{board}}{k_{board}} + \frac{0.5l_{slab}}{k_{slab}} + R_{ins}}(\bar{T}_2 - \bar{T}_1) \end{aligned} \right] \Delta t \quad (2.20)$$

Due to the interaction between the first and second nodes and their different materials, both conductivities must be used, as the heat is transferring through both materials from node 2 to node 1. Because of this interaction, the second node is also affected, which has the following energy balance

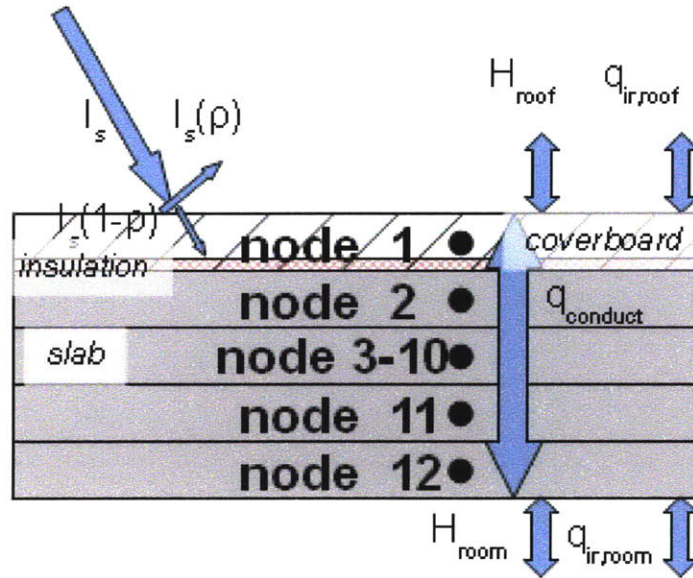


Figure 2-6: Nodal diagram of cool and modified-bitumen roof model, in which each node has a lumped capacitance. In this case, however, the insulation is on top of the roof slab and is included as part of the first node.

$$(mC)_{slab}(T_2' - T_2) = \left[\frac{1}{\frac{l_{board}}{k_{board}} + \frac{.5l_{slab}}{k_{slab}} + R_{ins}} (\bar{T}_1 - \bar{T}_2) + \frac{k}{l_{slab}} (\bar{T}_3 - \bar{T}_2) \right] \Delta t \quad (2.21)$$

The remaining interior nodes, nodes 3-10, are the same as before, and have the energy balance shown in Eq. 2.19. Similarly, the second to last node, now node 11 instead of node 17 for the previous case, has the same energy balance as it previously did, shown in Eq. 2.18.

However, now that the insulation is on top of the slab, the final node is changed as R_{eff} in Eq. 2.15 simply becomes the effective heat transfer coefficient between the ceiling and room, h_{room} , yielding the following energy balance for node 12, the final node

$$(mC)_{slab}(T_{12}' - T_{12}) = \left[h_{room}(T_{room} - \overline{T_{12}}) + \frac{k_{slab}}{1.5l_{slab}}(\overline{T_{12}} - \overline{T_{11}}) \right] \Delta t \quad (2.22)$$

Numerically modeling cool and modified-bitumen roofs

The discretization presented above, in which the current temperature and temperature at the next time step are averaged, is called the Trapezoidal Rule or Crank-Nicolson method. This method allows fewer limitations on the time step, making it more stable and the time step potentially larger, but is slightly more computationally demanding than other numerical methods. However, the stability and accuracy of this second-order approximation justify its use [88][78].

Combining Eqs. 2.12, 2.15, 2.17, 2.18, and 2.19 and also substituting in Eqs. 2.13 and 2.16 creates a large system of equations. By grouping all T' terms on the LHS and all T terms on the RHS along with all constants (as done below for a single equation, Eq. 2.19), the following system of equations is obtained.

Single example of grouping terms:

$$\begin{aligned} & \frac{-k}{2l_{slab}} \Delta t T'_{n-1} + \left(mC + \frac{k}{l_{slab}} \Delta t \right) T'_n - \frac{k}{2l_{slab}} \Delta t T'_{n+1} \\ & = \frac{k}{2l_{slab}} \Delta t T_{n-1} + \left(mC - \frac{k}{l_{slab}} \Delta t \right) T_n + \frac{k}{2l_{slab}} \Delta t T_{n+1} \end{aligned} \quad (2.23)$$

System of equations found by combining Eqs. 2.12, 2.15, 2.17, 2.18, and 2.19 and grouping terms as described above:

$$B \cdot \vec{T}' = (S \cdot \vec{T} + \vec{Q} \Delta t) \quad (2.24)$$

where B and S are the matrices containing all coefficients for the vectors \vec{T}' and \vec{T} , respectively, \vec{Q} is the vector containing all constants (such as ambient and room temperatures, as well as incident solar radiation), and Δt is the time step. It should be noted that the terms of \vec{Q} are constant only over a time step. Solving for \vec{T}' yields the final discrete energy balance

$$\vec{T}^i = B^{-1}(S \cdot \vec{T} + \vec{Q} \Delta t) \quad (2.25)$$

Now, using an iterative process, the temperature at the next time step can be predicted using the current temperature. An example system of $n = 4$ nodes with insulation on bottom of the slab is shown below in Eqs. 2.26 to 2.30.

$$B = \begin{bmatrix} mC + \frac{k\Delta t}{1.5l_{slab}} + \frac{(h_{rad}+h_{conv})\Delta t}{2} & \frac{-k\Delta t}{2 \cdot 1.5 \cdot l_{slab}} & 0 & 0 \\ \frac{-k\Delta t}{2 \cdot 1.5 \cdot l_{slab}} & mC + \frac{k\Delta t}{1.5 \cdot l_{slab}} & \frac{-k\Delta t}{2 \cdot 1.5 \cdot l_{slab}} & 0 \\ 0 & \frac{-k\Delta t}{2 \cdot 1.5 \cdot l_{slab}} & mC + \frac{k\Delta t}{1.5 \cdot l_{slab}} & \frac{-k\Delta t}{2 \cdot 1.5 \cdot l_{slab}} \\ 0 & 0 & \frac{-k\Delta t}{2 \cdot 1.5 \cdot l_{slab}} & mC + \frac{k\Delta t}{1.5 \cdot l_{slab}} + \frac{\Delta t}{2R_{eff}} \end{bmatrix} \quad (2.26)$$

$$S = \begin{bmatrix} mC - \frac{k\Delta t}{1.5l_{slab}} - \frac{(h_{rad}+h_{conv})\Delta t}{2} & \frac{k\Delta t}{2 \cdot 1.5 \cdot l_{slab}} & 0 & 0 \\ \frac{k\Delta t}{2 \cdot 1.5 \cdot l_{slab}} & mC - \frac{k\Delta t}{1.5l_{slab}} & \frac{k\Delta t}{2 \cdot 1.5 \cdot l_{slab}} & 0 \\ 0 & \frac{k\Delta t}{2 \cdot 1.5 \cdot l_{slab}} & mC - \frac{k\Delta t}{1.5l_{slab}} & \frac{k\Delta t}{2 \cdot 1.5 \cdot l_{slab}} \\ 0 & 0 & \frac{k\Delta t}{2 \cdot 1.5 \cdot l_{slab}} & mC - \frac{k\Delta t}{1.5l_{slab}} - \frac{\Delta t}{R_{eff}^2} \end{bmatrix} \quad (2.27)$$

$$\vec{Q} = \begin{bmatrix} (1 - \rho)I_s + h_{rad,sky}T_{sky} + \bar{h}T_{amb} \\ 0 \\ 0 \\ \frac{1}{R_{eff}}T_{room} \end{bmatrix} \quad (2.28)$$

$$\vec{T} = \begin{bmatrix} T_1 \\ T_2 \\ T_3 \\ T_4 \end{bmatrix} \quad (2.29)$$

$$\vec{T}' = \begin{bmatrix} T_1' \\ T_2' \\ T_3' \\ T_4' \end{bmatrix} \quad (2.30)$$

2.1.3 Differences between Cool and Modified-Bitumen Roofs

As mentioned at the beginning of this section, both cool and modified-bitumen roofs are numerically modeled by the same equations, Eqs. 2.26 to 2.30, though clearly have different performances. A large difference between a cool and modified-bitumen roof from an energy standpoint is their reflectivities, ρ . While a cool roof can reflect up to 80% of the incoming solar radiation, a modified-bitumen roof often reflects only 5%. This difference leads to significant energy implications. Although each roof company may manufacture a slightly different roof assembly, the general assembly of both roofs (top coat, the roof membrane, a waterproofing layer, and insulation above the roof structural support) often remains the same. Thus, it is assumed that the only difference affecting energy performance between a cool and modified-bitumen roof is the reflectivity, which is assumed to be 0.7 and 0.05 respectively.

2.2 Green Roof

Numerous similarities exist between the previous energy analysis and the green roof energy analysis, however, multiple key differences warrant a second energy analysis for the green roof, which follows.

2.2.1 Modeling Vegetation and Growing Media

Before applying an energy balance to a green roof, it is necessary to define what kind of green roof will be used. This definition as well as key assumptions are listed below.

Type of Green Roof

When deciding which kind of green roof would be modeled, the greatest consideration is given to the type of green roof that would potentially be used by the most number of people. The affordability, lighter weight, ease of retrofit, and low maintenance of an extensive green roof all motivated the selection of an extensive green roof for the model. A 12 *cm* clipped, cool-season grass is used as the vegetation, which is assumed to be actively growing over the entire roof.

The growing media is assumed to be a basic loam soil with constant conductivity 0.8 W/mK and a product of density and heat capacity equal to $1.4e6 \text{ J/m}^3\text{K}$ [48]. Although moisture levels within the growing media will certainly change, which in turn will affect the media conductivity, density, and heat capacity, it is assumed that over time the media moisture level is maintained high enough to support healthy grass growth. The above values are taken as the average between the saturated and wilting values for both conductivity and product of mass and heat capacity, where “saturated” is defined as the upper physical limit of water that loam can hold and “wilting” is the minimum amount of water in the loam that can support plant life [48].

For the purposes of the energy model, all other components of the green roof are not specified, that is, their thermal resistances are not included. This omission is made because of the variation not only between green roof compositions (for example, one roof could have a combined waterproofing and weed retardant layer, but another roof could have two separate layers), but also between the thermal resistances of those components (for example, one roof could use sand as a drainage layer, but another could use a porous rubber matting, both of which have significant differences in thermal resistance). Because of these variations, the thermal resistances are not included, though the user is able to account for thermal resistances if they are known. Some of the variation between green roof compositions and components is shown below in Fig. 2-7.

Roof type	Thickness (mm)	K-values	R-values (m ² K/W)	U-value (Btu/m ² K)
a. Rooftop garden with vegetation on the exposed roof				
Rooftop with 100% turfing				
Outside air film (R _o)	-	-	0.055	-
Turfing	-	-	0.360	-
Soil substrate (40% moisture content)	100	1.580	0.063	-
WOLFEN IB single layer polymerised	1.2	0.713	0.001	-
Cement and sand base screed to fall	50	0.533	0.094	-
RC slab	150	1.442	0.104	-
Inside air film (R _i)	-	-	0.162	-
			$\Sigma R = 0.840$	0.210
b. Rooftop garden with vegetation on the typical flat roof				
Rooftop with 100% turfing				
Outside air film (R _o)	-	-	0.055	-
Turfing	-	-	0.360	-
Soil substrate (40% moisture content)	100	1.580	0.063	-
Filter layer	1	0.035	0.029	-
INSULCELL	50	0.035	1.429	-
50--- drainage layer				
INSULFLEX	3	0.040	0.075	-
25--- protection layer				
'WOLFEN IB' membrane with root resistant ability (FLL tested)	1.5	0.713	0.002	-
Cement and sand base screed to fall	50	0.533	0.094	-
RC flat slab	150	1.442	0.104	-
Inside air film (R _i)	-	-	0.162	-
			$\Sigma R = 2.372$	0.074

Roof Layer	R Value [m ² K/W]
drainage layer	0.72
waterproofing layer	0.059
structural roof	0.79

Figure 2-7: (above) Detailed listing of the composition of two different types of green roofs that also includes the components' R-value. (below) Composition of a simple green roof used for an experiment in Singapore. R-values are listed, which shows the variation from roof to roof. Source [54][91].

Modeling Vegetation Layer

Accounting for Radiation within Vegetation Layer

The field of agriculture has long been interested in accurately approximating the amount of solar radiation absorbed by plants [85][70]. Essential processes in that field, such as photosynthesis and plant transpiration are dominated by the intercepted solar radiation. This well established field is useful in the current study by providing a model for the vegetation.

To approximate the amount of incident sunlight absorbed by a canopy of vegetation, the Beer-Lambert law is commonly used [85][70]. Beer-Lambert's law, also called Beer's law or Beer-Lambert-Bouguer's law, was originally developed in optics, specifically spectrophotometry, where it was used to determine the relationship between how much light is absorbed by a liquid through which it passes and the concentration of the liquid [85]. In 1953, Monsi and Saeki first applied the law in agriculture studies and showed that it is valid within plant canopies. In this application, the canopies can be thought of as a turbid or semi-opaque medium; the further sun light travels into them, the greater the decrease in irradiance [85]. The adapted form of Beer's law for agriculture describes the transmittance, τ , through vegetation as

$$\tau \equiv \exp(-\sqrt{\alpha} \cdot k_{ext} \cdot LAI) \quad (2.31)$$

where α is the fraction of light absorbed by an individual leaf, k_{ext} is the vegetation extinction coefficient, and LAI is the leaf area index of the vegetation. Both α and k_{ext} can vary with wavelength of light, thus two values for each are used, α_s and α_l , and $k_{ext,s}$ and $k_{ext,l}$ for short and longwave radiation respectively. Additionally, both values are most often empirically measured, as are the values used in this model. The leaf area index, LAI , is the total leaf area per unit ground area [85]. In the case of grasses, the LAI is directly proportional to the grass height, and can be found using the following relationship

$$LAI = 24height_{grass} \quad (2.32)$$

where $height_{grass}$ is the grass height in m [25]. Using this definition of transmittance, the amount of solar radiation absorbed by the vegetation layer can now be calculated. Not all of the incident solar radiation enters the vegetation layer, because it has a collective vegetation reflectivity, ρ_{veg} . Accounting for ρ_{veg} , the amount of solar radiation absorbed by the vegetation layer is

$$I_{s,veg} = (1 - \rho_{veg})I_s(1 - \tau_s) \quad (2.33)$$

where I_s is the total incident solar radiation, and τ_s is the short wave transmittance. Assuming that all incident solar radiation not reflected back to the sky is either absorbed by the vegetation or passes through to the soil, the solar radiation reaching the soil is

$$I'_{s,soil} = (1 - \rho_{veg})I_s\tau_s \quad (2.34)$$

of which only a fraction is absorbed, determined by the soil absorptivity, $\alpha_{soil} = 0.83$, while the rest is assumed to enter the environment [82].

$$I_{s,soil} = \alpha_{soil}(1 - \rho_{veg})I_s\tau_s \quad (2.35)$$

Vegetation Heat Capacity

The vegetation is assumed to have a heat capacity per leaf square meter of $640J/m^2K$, which Jones found for the “general plant leaf” [49]. This value is multiplied by the LAI to find the vegetation heat capacity per square meter of soil

$$C|_{veg} = 640LAI \quad (2.36)$$

where $C|_{veg}$ is the heat capacity for the vegetation in J/m^2K . All of the assumed values for the preceding parameters are listed below in Table 2.3

Table 2.3: Physical Vegetation Parameters

Parameter	Symbol	Value
<i>Vegetation</i>		
Reflectivity	ρ_{veg}	0.23 [-] [26]
Height	$height_{grass}$	0.12 [m] [26]
LAI (calculated)	LAI	2.83 [26]
Extinction coefficient, short wave	k_{short}	0.55 [-] [72][86]
Extinction coefficient, long wave	k_{long}	0.55 [-] [72] [86]
Transmittance, short wave (calculated)	τ_{short}	0.24 [-] [85]
Transmittance, long wave (calculated)	τ_{long}	0.49 [-] [85]
<i>Individual Leaf</i>		
Absorbptivity, short wave	α_s	0.8 [-] [85]
Absorbptivity, long wave	α_l	0.2 [-] [85]
Heat capacity per ground area	$C _{leaf}$	1.8e5 J/m ² K [49]
<i>Soil</i>		
Reflectivity	ρ_{soil}	0.83 [-] [82]
Conductivity	k_{soil}	0.8 W/mK [48]
Density and specific heat capacity product	$(MC_p)_{soil}$	1.4e6 J/m ³ K [48]

Evapotranspiration

The final aspect of the vegetation model to be explained is the accounting for evaporation from the soil and transpiration of the grass. Transpiration is defined as the vaporization of liquid water contained in plant tissues and the vapour removal to the atmosphere [26]. It occurs through small openings on plants called stomata, which cover the leaves, stems, flowers, and even roots of a plant [31]. These two phenomena are closely linked. Consider the case when there is little moisture in the soil. Consequently, minimal evaporation from the soil can occur, but also, minimal transpiration will occur because little water has been able to diffuse into the plant for it to transpire. The close link between these two phenomena has helped lead the agriculture field to develop a concept, evapotranspiration, that accounts for both phenomena.

In its simplest form, evapotranspiration is the transport of water from surfaces to the atmosphere [31]. Although evaporation from soil and plant transpiration dominate evapotranspiration, evaporation from wet plant canopies and evaporation from vegetation-covered bodies of water (as found in wetlands) can also contribute to evap-

otranspiration [31]. However, in the case of the extensive green roof at hand, the latter two contributors are not applicable.

The implication of evapotranspiration in the field of agriculture is enormous, as it largely determines irrigation rates. For this reason, it has been extensively researched and modeled and has been found to be affected by weather parameters (predominately radiation, but also air temperature, humidity and wind speed), crop factors (such as crop resistance to transpiration, height, roughness, reflection, ground cover and rooting characteristics), and management and environmental conditions (such as soil salinity, poor land fertility, limited application of fertilizers, the presence of hard or impenetrable soil horizons, the absence of control of diseases and pests, poor soil management, ground cover, plant density and the soil water content) [26]. These numerous parameters make predicting the amount of evapotranspiration from a given plant, in a given soil, for a given climate a challenging task. Although there are models that account for all such parameters, they often require a significant number of experimentally measured parameters, which severely restricts their scope of use [26] [25]. Because the motivation behind creating the green roof model in this thesis is to develop a general model that can be compared to a cool or modified-bitumen roof, such specificity rules out such complicated models.

Therefore, when choosing an evapotranspiration model, a high priority is given to a general model that can be used in a variety of climates, that models a representative grass (the green roof vegetation in this case), and applies for reasonable management and environmental conditions associated with green roofs. The model found that fits these criteria best is the hourly-based reference case of the FAO-56 Penman-Monteith equation [68][62][26] [25].

Penman first combined an energy balance with mass transfer in 1948 to develop an equation that computes evaporation from open water, bare soil, and grass, with only readily available climatic inputs [68] [45]. Howell well summarizes the evolution of the Penman equation, which took many transformations before the United Nations' Food and Agriculture Organization (FAO) saw the need for a widely adopted standard and published its "Crop evapotranspiration - Guidelines for computing crop

water requirements,” FAO Drainage and Irrigation paper 56 [45]. In the paper, the authors assume a reference crop against which all vegetation and management and environmental conditions could be compared [26]. An experimentally determined crop coefficient can be measured for any crop, that in turn can be compared to the reference case. This reference evapotranspiration, ET_0 , is fully described by climatic inputs. Thus, readily available weather data combined with a measured crop coefficient can accurately predict the evapotranspiration rates for any crop.

This method is widely accepted as one of the best models of crop evapotranspiration and is often used as the benchmark to which new evapotranspiration models are compared [37][50][79]. One major advantage of this equation to the green roof model at hand is that the reference case, ET_0 , assumes a hypothetical grass of uniform height 0.12 m, fixed bulk surface resistance of 70 s/m (implying a moderately dry soil surface resulting from about a weekly irrigation frequency), albedo of 0.23, that is actively growing and completely shading the ground [26]. The bulk surface resistance is defined by the FAO as “the resistance of vapour flow through the transpiring crop and evaporating soil surface” [26]. Elsewhere, this hypothetical grass is referred to as a clipped cool-season grass, which embodies these assumptions [25]. Furthermore, one dimensional heat and mass transfer is assumed, thus the grass must cover an area large enough to neglect edge effects [26]. Therefore, because this reference grass is exactly the grass suitable for the green roof model in this thesis, the calculated ET_0 based solely on weather data will accurately model the evapotranspiration from the green roof. No empirical crop coefficient is needed. This equation for ET_0 developed by the FAO varies slightly depending on time scale to account for changes in units, and thus the equation for hourly data is used (and is defined in the following section of this thesis, Section 2.2.2).

2.2.2 Green Roof Energy Balance

As with the cool and modified-bitumen roof, a one dimensional model is used for a large roof, so edge effects are neglected, that ignores the thermal resistance of all roof components except the structural support, insulation, and now soil. The concrete

structural slab is again assumed to be 15 cm thick, as is the layer of soil. The insulation is placed either underneath the slab or above it, directly under the soil.

A diagram of the energy balance for the green roof with insulation under the slab is shown below in Fig. 2-8.

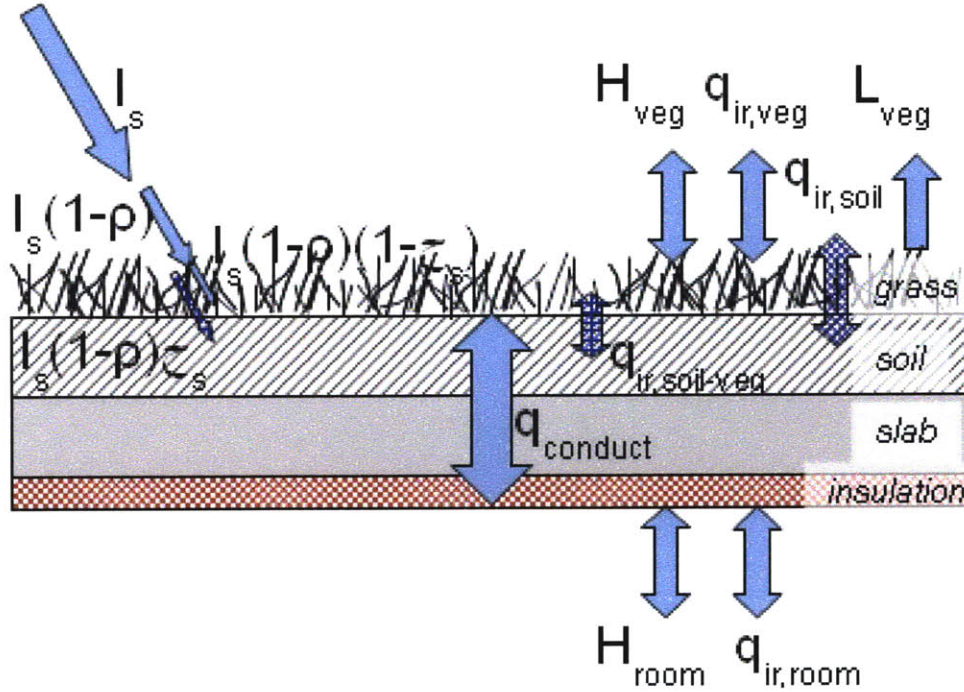


Figure 2-8: Green roof energy balance. All terms shown are energy fluxes with units $[W/m^2]$.

Now, instead of exposing the slab to the environmental conditions, the vegetation and soil buffer the roof from external conditions. The vegetation layer has short and long wave transmittances τ_s and τ_l , respectively. All of the following terms, and terms shown in Fig. 2-8 are energy fluxes in $[W/m^2]$. In addition to the convective, H_{veg} , short wave radiation, $I_s(1 - \rho)(1 - \tau_s)$, and long wave radiation, $q_{ir,veg}$, heat transfer between the vegetation and environment, (long wave radiation is between the vegetation and T_{sky} , again assumed to be 10 C lower than T_{amb}) a latent term, L_{veg} , is now present. The only interaction between the vegetation and soil occurs through long wave radiation, $q_{ir,soil-veg}$, although the soil interacts with the environment by receiving incident solar radiation, $I_s(1 - \rho)\tau_s$, as well as exchanging long wave ra-

diation, $q_{ir,soil}$ (again, T_{sky} is used). An exploded view of the interaction between the vegetation and soil layers, including all radiation terms, is shown in Fig. 2-9. Heat is conducted through the soil, slab, and insulation, denoted $q_{conduct}$. As before, convection, H_{room} , and radiation, $q_{ir,room}$, transfer heat to the room.

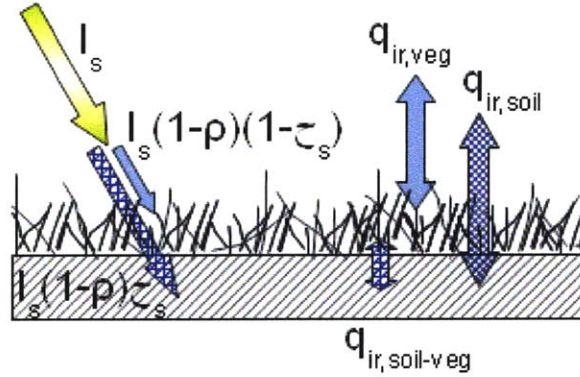


Figure 2-9: Exploded view of interaction between vegetation and soil layers that shows the only interaction between the two nodes is long-wave radiation, $q_{ir,soil-veg}$. All radiation terms for the green roof model are shown, including all terms involving the soil layer (blue hatched arrows), and all terms involving the vegetation and environment (light blue arrows). All terms shown are energy fluxes with units $[W/m^2]$.

All vegetation is assumed to be at the same temperature, T_{veg} , which is close enough to T_{sky} to warrant a linearized model for radiation heat transfer between the vegetation and sky. This same assumption is used in the preceding cool and modified-bitumen roof model, however, Eq. 2.1 now becomes

$$q_{ir,veg} = (1 - \tau_l) \cdot h_{rad}(T_{veg} - T_{sky}) \quad (2.37)$$

where h_{rad} is the same value as before, Eq. 2.2, but T_m is now the average between the vegetation and sky temperatures. Although the vegetation long-wave emissivity is slightly different than the roof emissivity, the difference has a negligible impact on the overall h_{rad} . However, because the vegetation layer is treated as a semi-opaque layer, not all longwave radiation is able to escape, as indicated by the $(1 - \tau_l)$ term. For the same reason, the longwave radiation heat transfer between the vegetation layer and soil takes a similar form and is expressed as

$$q_{ir,soil-veg} = (1 - \tau_l) \cdot h_{rad}(T_{veg} - T_{soil}) \quad (2.38)$$

in which the same h_{rad} is used from before, although small temperature differences would slightly increase the term, the increase is negligible compared to the driving term ($T_{veg} - T_{soil}$).

The long wave radiation between the sky and soil, $q_{ir,soil}$ takes a similar linearized form, but must pass through the vegetation layer, thus it is expressed as

$$q_{ir,soil} = \tau_l \cdot h_{rad}(T_{veg} - T_{sky}) \quad (2.39)$$

The convective heat transfer between the vegetation and environment, H_{veg} , will be slightly different from the convective heat transfer on the cool or modified-bitumen roof, Eq. 2.3. This difference arises from the surface resistances of the two roofs. In the case of the cool or modified-bitumen roof, the large flat roof will allow the boundary layer of air along the roof to grow fairly thick, decreasing the amount of heat that can be transferred. In the case of the green roof, the numerous small surface areas of the grass prohibit any substantial boundary layer from developing, thus increasing the amount of heat transfer. However, these small surfaces are also obstacles to the wind, which if flows parallel to the roof, can be greatly weakened by the end of the roof, slightly decreasing the heat transfer on the green roof. The flatness of the cool and modified-bitumen roofs provides little obstacle to the wind, which allows the wind to flow relatively freely over the roof, slightly increasing heat transfer. For the purposes of this model, these differences are considered negligible because of the small role the convective heat transfer has compared to the latent and radiation terms. Therefore, Eq. 2.3 is once again used in which T_{veg} is now used.

The latent heat transfer between the vegetation and the environment, L_{veg} , is found using the ET_0 method mentioned in the preceding section. The provided equation from the FAO for hourly ET_0 is [26]

$$ET_0 = \frac{0.408\Delta(R_n - G) + \gamma \frac{37}{T_{hr} + 273} u_2 (P_{sat(T_{hr})} - P_{act})}{\Delta + \gamma(1 + 0.34u_2)} \quad (2.40)$$

where ET_0 is the reference evapotranspiration [mm/hr],
 R_n is the net radiation at the grass surface [MJ/m^2hr],
 G is the soil heat flux density excluding evaporation [MJ/m^2hr],
 T_{hr} is the mean hourly air temperature [C],
 Δ is the saturation slope vapour pressure curve at T_{hr} [kPa/C],
 γ is the psychrometric constant [kPa/C],
 $P_{sat(T_{amb})}$ is the saturation vapour pressure at T_{hr} [kPa],
 P_{act} is the average hourly actual vapour pressure [kPa],
 u_2 is the average hourly wind speed 2 m above the vegetation [m/s].

ET_0 is normally defined as the amount of water depth loss per unit time (in this case, an hourly interval is used) [26]. The water depth loss can also be defined in loss of water volume as 1 mm/hr of depth loss equals 10 $m^3/(ha \cdot hr)$. Furthermore, assuming a water density of 1000 kg/m^3 and temperature 20 C , the depth loss can be converted into an energy flux per unit area as 1 mm/hr of depth loss equals 2.45 MJ/m^2hr . Thus, converting to SI units, ET_0 is related to the latent heat flux from the green roof, L_{veg} in [W/m^2], by the following relationship

$$L_{veg} = \left(\frac{2.45 \times 10^6}{3600} \right) ET_0 \quad (2.41)$$

R_n is found by subtracting the net longwave radiation leaving the green roof from the net incident radiation and converting to the proper units, using the fact that $1W/m^2 = 3.6 \times 10^{-3}MJ/m^2hr$

$$R_n = [I_s(1 - \rho)(1 - \tau_s) - Q_{ir,veg}] \cdot 3.6 \times 10^{-3} \quad (2.42)$$

G , the soil flux density, will be explicitly defined in the following subsection.

Δ is taken from the slope of the graph of water vapor saturation vapor pressure versus temperature, which is shown in Fig. 2-10

The curve shown in Fig. 2-10 arises from the fact that the amount of water vapor that can be stored in the air depends on the air temperature. As shown, the higher

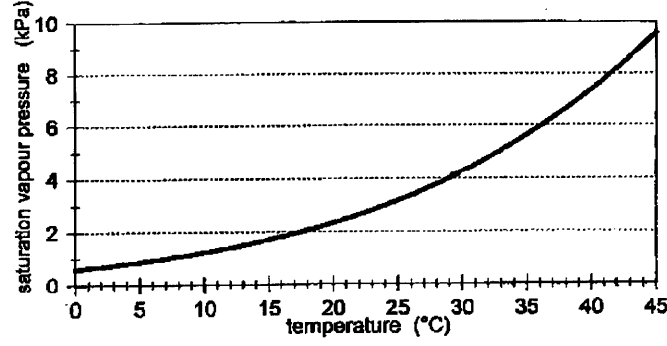


Figure 2-10: The saturation vapor pressure of water vapor in air as a function of temperature [26].

the temperature, the higher storage capacity the air has for water vapor. The greater the amount of water vapor in the air, the greater partial pressure exerted by the water vapor in the air. The curve shows the maximum, or saturated, vapor pressure of water vapor at the temperatures shown [26].

An equation for the slope of the curve in Fig. 2-10 is given for the FAO-56 Penman-Monteith equation, which is

$$\Delta = \frac{4098 \left[0.6108 \exp \left(\frac{17.27 T_{hr}}{T + 237.3} \right) \right]}{(T_{hr} + 237.3)^2} \quad (2.43)$$

γ , the psychrometric constant, which is defined as

$$\gamma \equiv \frac{C_{p_{air}} P_{act}}{\lambda_v \frac{MW_v}{MW_a}} = 0.665 \times 10^{-3} P_{act} \quad (2.44)$$

where $C_{p_{air}}$ is $1.013 \times 10^{-3} [MJ/kgC]$, λ_v is the latent heat of water vaporization $2.45 [MJ/kg]$, and MW_v and MW_a are the molecular weights of water vapor and air respectively.

$P_{sat(T_{hr})}$ is found using the well accepted Goff-Gratch equation, shown below [41]

$$\begin{aligned}
\log(10 \cdot P_{sat}(T)) &= -7.90298(T_{st}/T - 1) + 5.02808 \log(T_{st}/T) \\
&- 1.3816 \times 10^{-7}(10^{11.344(1-T/T_{st})} - 1) + 8.1328 \times 10^{-3}(10^{-3.49149(T_{st}/T-1)} - 1) \\
&+ \log P_{sat}(T_{st})
\end{aligned} \tag{2.45}$$

where P_{sat} is the saturated vapor pressure in $[kPa]$ at temperature T in $[K]$ and T_{st} is the so-called steam-point temperature, or boiling point at 1 atm, 373.15 K [41].

P_{act} is easily found with P_{sat} known by multiplying it by the outdoor relative humidity RH ,

$$P_{act} = RH \cdot P_{sat} \tag{2.46}$$

u_2 is defined as the average hourly windspeed in $[m/s]$ 2 m above the vegetation. In the green roof model, the windspeed measured from a weather station is used, which is measured 10 m from the ground. Although this height will not always be 2 m above the roof surface, it serves as a characteristic value and should not be drastically different from the actual value at 2 m.

To summarize the energy balance for the green roof, it is helpful to split the green roof into three separate sections for the vegetation, soil, and structural slab. The energy balance for each section will be described in the following subsection. A summary of the physical parameters for each section of the green roof is shown in Table. 2.4

2.2.3 Green Roof Numerical Modeling

Modelling Temperature Distribution through Roof

As with the cool and modified-bitumen roofs, a lumped capacity model is also used for the vegetation, soil, and structural slab sections of the green roof. Therefore, the same criterion of $Bi < 0.1$ must be achieved using Eq. 2.7, which will in turn give

Table 2.4: Thermal properties of green roof used in model

<i>Vegetation surface</i>	
reflectivity [-]	0.23 [26]
emissivity [-]	0.95
<i>Growing Media</i>	
Material [-]	loam [48]
Thickness [m]	0.15
Density · Heat Capacity [J/m^3K]	1.4e6 [48]
Conductivity [W/mK]	0.8 [48]
<i>Structural support slab</i>	
Material [-]	concrete
Thickness [m]	0.15
Density [kg/m^3]	2300 [46]
Conductivity [W/mK]	1.4 [46]
Heat Capacity [J/kgK]	880 [46]
<i>Insulation</i>	
Thickness [m]	not specified
R Value [W/m^2K]	variable, user specified

a maximum slice thickness for the soil and slab from Eq. 2.8. However, because the vegetation is not assumed to be a solid medium through which heat conducts, no Biot number is found for it, although all vegetation is assumed to be at the same temperature and is therefore modeled as a single slice.

Both soil and slab layers must be treated differently because of their different materials and location. Although the soil layer is not involved in any convective heat transfer, typically needed for a Biot number, a quasi Biot number, similar to the one used for the cool and modified-bitumen roof, is once again used. In this case, only h_{rad} is used as the effective heat transfer coefficient h in Eq. 2.7. Using the assumed constant soil conductivity with h_{rad} the maximum thickness of the soil slices is found with Eq. 2.8 to be 1.25 cm, resulting in a total of $n = 12$ soil slices.

To find the maximum slice thickness for the slab layer, not only is the slab conductivity used in Eq. 2.8, but a different heat transfer coefficient must also be used. Because the soil is now in direct interaction with the environment, rather than the slab, the indoor convective and radiation coefficients are used as the overall heat

transfer coefficient. Recall the sum of these values is assumed to equal $10 \text{ W/m}^2\text{K}$ [88]. Using this value with the conductivity of concrete, the max slice thickness of the slab layer is found to be 1.36 cm , resulting in a total of $n = 11$ concrete slices. Combining the 1 vegetation slice with 12 soil slices and 11 concrete slices results in a total of $n = 24$ slices for the green roof model.

Nodal Energy Balance

As in the cool and modified-bitumen roof model, each slice, or node, in the green roof model has an energy balance applied to it using Eq. 2.9. Before this can be done, the appropriate time step must be determined from Eq. 2.11. However, Eq. 2.11 will calculate a different time step depending on which material (soil or concrete) is used. Therefore, Δt_{max} is calculated for both, and the minimum value is used to be conservative.

With the time step determined, an energy balance is now applied to each node. In the case when the insulation is beneath the roof slab, as shown in Fig. 2-11, the vegetation node, or node $n = 1$, has the following energy balance.

$$C_{veg}(T_1' - T_1) = \{[(1 - \rho_{veg})(1 - \tau_s)I_s] - L_{veg} - [\bar{h}(\bar{T}_1 - T_{amb})] - [(1 - \tau_l) \cdot h_{rad}(T_{veg} - T_{sky})] - [(1 - \tau_l) \cdot h_{rad}(T_{veg} - T_{soil})]\}dt \quad (2.47)$$

where again T_i is the current node temperature, T_i' is the node temperature at the next time step, Δt , and \bar{T}_i is defined as before, Eq. 2.13. While L_{veg} is defined in Eq. 2.41, it is assumed to account for both transpiration from the vegetation and evaporation from the soil. However, in the green roof model, because the modeled grass covers the entire soil surface, it is assumed that most water loss occurs through plant transpiration rather than evaporation from the soil. The FAO shows that for a given harvestable crop, crop transpiration dominates the evapotranspiration when the crop is actively growing before harvest, which is similar to the case for the green roof model, because there is no harvest. Therefore, all latent heat flux is assumed to occur only in the vegetation layer.

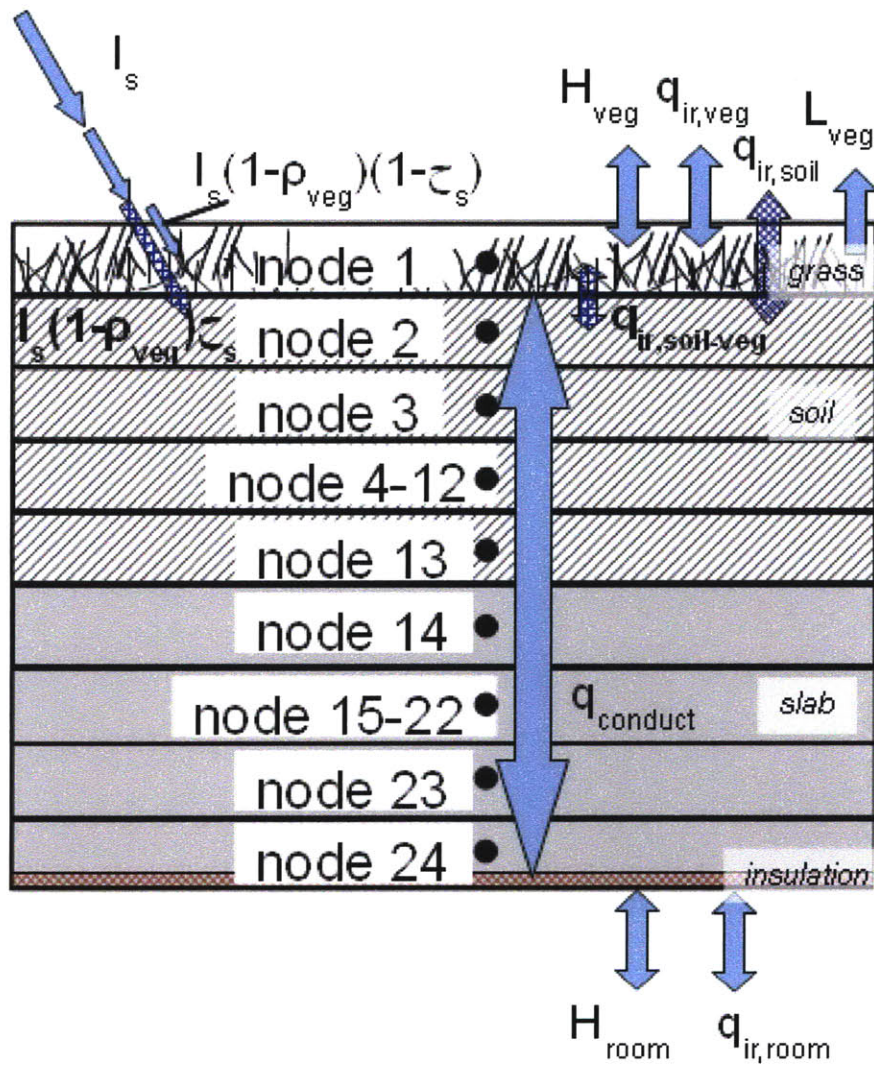


Figure 2-11: Nodal diagram of green roof model, in which each node has a lumped capacitance. In this case, the insulation is beneath the roof slab.

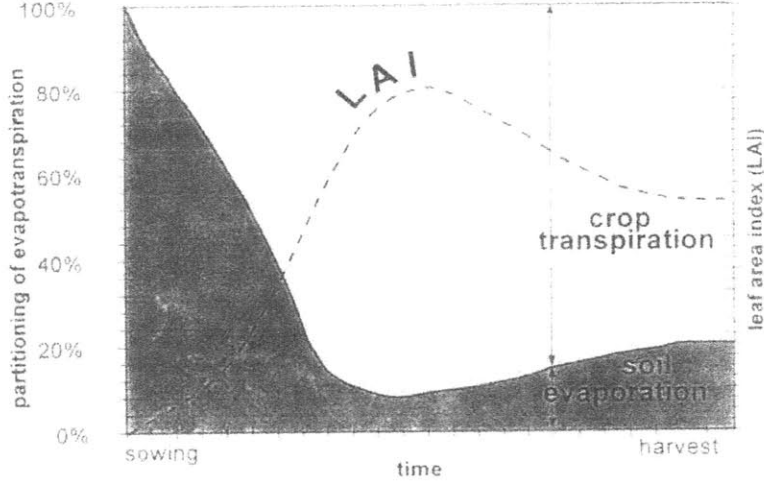


Figure 2-12: Relative crop transpiration and soil evaporation as percentages of the overall evapotranspiration over the growing period for an annual field crop. Source [26]

Thus, the first node of the soil, node 2, is defined

$$(mC)_{soil}(T_2' - T_2) = \{[(1 - \rho_{veg})(\tau_s)\alpha_{soil}I_s] - [(T_l) \cdot h_{rad}(\overline{T}_2 - T_{sky})] - [(1 - \tau_l) \cdot h_{rad}(\overline{T}_2 - \overline{T}_1)] + [\frac{k_{soil}}{1.5 \cdot l_{soil}}(\overline{T}_3 - \overline{T}_2)]\} \Delta t \quad (2.48)$$

where an additional half length is included in the conduction term for the same reason as described in Fig. 2-5. Consequently, node 3 is also affected, and has the energy balance

$$(mC)_{soil}(T_3' - T_3) = \left[\frac{k_{soil}}{l_{soil}}(\overline{T}_4 - \overline{T}_3) + \frac{k_{soil}}{1.5 \cdot l_{soil}}(\overline{T}_2 - \overline{T}_3) \right] \Delta t \quad (2.49)$$

Nodes 4 through 12, have similar energy balances, with the exclusion of the additional half length in the conduction term

$$(mC)_{soil}(T_i' - T_i) = \left[\frac{k_{soil}}{l_{soil}}(\overline{T}_{i+1} - \overline{T}_i) + \frac{k_{soil}}{l_{soil}}(\overline{T}_{i-1} - \overline{T}_i) \right] \Delta t \quad (2.50)$$

The energy balance for the final soil node, node 13, takes into account the interaction between the soil and slab layers by considering the conductivities and thicknesses

of both, as shown below.

$$(mC)_{soil}(T_{13}' - T_{13}) = \left[\frac{k_{soil}}{l_{soil}}(\overline{T_{12}} - \overline{T_{13}}) + \frac{1}{\frac{.5l_{soil}}{k_{soil}} + \frac{.5l_{slab}}{k_{slab}}}(\overline{T_{14}} - \overline{T_{13}}) \right] \Delta t \quad (2.51)$$

The first slab node, node 14, is also similarly affected, and has the following energy balance

$$(mC)_{slab}(T_{14}' - T_{14}) = \left[\frac{1}{\frac{.5l_{soil}}{k_{soil}} + \frac{.5l_{slab}}{k_{slab}}}(\overline{T_{13}} - \overline{T_{14}}) + \frac{k_{slab}}{l_{slab}}(\overline{T_{15}} - \overline{T_{14}}) \right] \Delta t \quad (2.52)$$

The interior slab nodes, nodes 15-22, have the energy balance

$$(mC)_{slab}(T_i' - T_i) = \left[\frac{k_{slab}}{l_{slab}}(\overline{T_{i-1}} - \overline{T_i}) + \frac{k_{slab}}{l_{slab}}(\overline{T_{i+1}} - \overline{T_i}) \right] \Delta t \quad (2.53)$$

The second to last node, node 23, must include the additional half length in its conduction term, and thus has the energy balance

$$(mC)_{slab}(T_{23}' - T_{23}) = \left[\frac{k_{slab}}{l_{slab}}(\overline{T_{22}} - \overline{T_{23}}) + \frac{k_{slab}}{1.5 \cdot l_{slab}}(\overline{T_{24}} - \overline{T_{23}}) \right] \Delta t \quad (2.54)$$

Lastly, the final node of the slab, node 24, which includes the insulation, additional half length, and interaction with the interior room, has the energy balance

$$(mC)_{slab}(T_{24}' - T_{24}) = \left[\frac{1}{R_{eff}}(T_{room} - \overline{T_{24}}) + \frac{k_{slab}}{1.5 \cdot l_{slab}}(\overline{T_{24}} - \overline{T_{23}}) \right] \Delta t \quad (2.55)$$

where R_{eff} is defined as it is in the cool and modified-bitumen case, by Eq. 2.16.

Insulation Location

The preceding nodal analysis is done for the green roof with insulation beneath the roof slab. When the insulation is moved above the roof slab, directly under the soil layer, some of the analysis changes. Fig. 2-13 below shows the nodes for this new case.

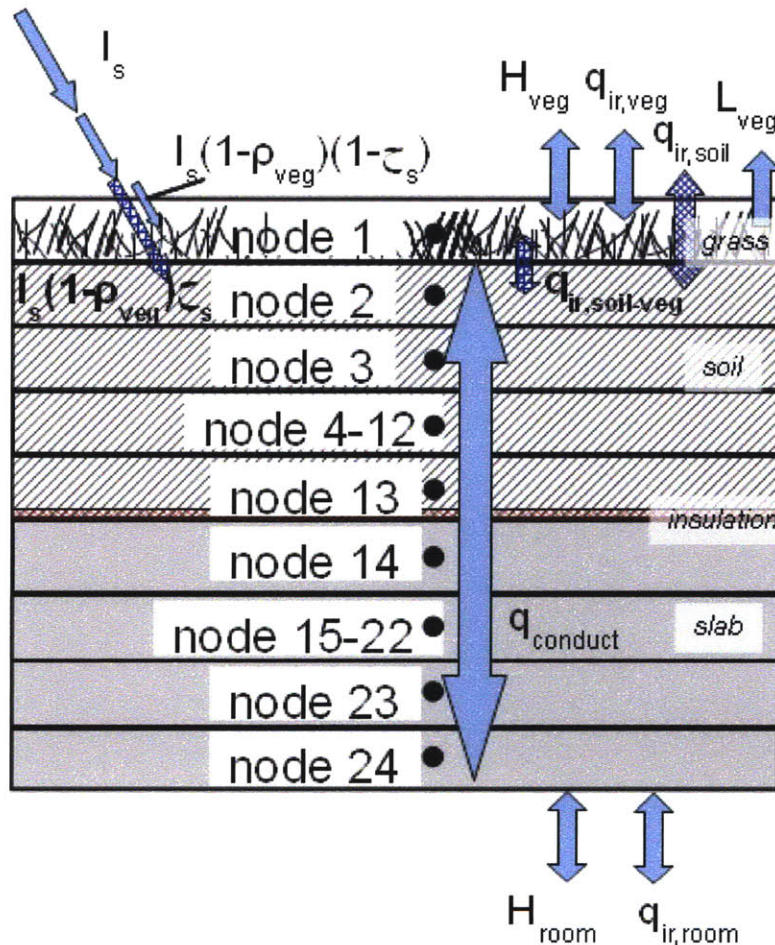


Figure 2-13: Nodal diagram of green roof model, in which each node has a lumped capacitance. In this case, the insulation is above the roof slab.

A comparison of Figs. 2-13 and 2-11 reveals numerous similarities. One such similarity is that nodes 1-12, the vegetation and soil nodes, are unaffected by moving the insulation. Thus, they are modeled using the same equations above, Eqs. 2.47 through 2.50. The first difference between the two cases arises in node 13, where insulation is now present. The new energy balance for node 13, the last soil node,

now becomes

$$(mC)_{soil}(T_{13}' - T_{13}) = \left[\frac{k_{soil}}{l_{soil}}(\overline{T}_{12} - \overline{T}_{13}) + \frac{1}{\frac{.5l_{soil}}{k_{soil}} + \frac{.5l_{slab}}{k_{slab}} + R_{ins}}(\overline{T}_{14} - \overline{T}_{13}) \right] \Delta t \quad (2.56)$$

Additionally, node 14, the first slab node, is also affected, and now becomes

$$(mC)_{slab}(T_{14}' - T_{14}) = \left[\frac{1}{\frac{.5l_{soil}}{k_{soil}} + \frac{.5l_{slab}}{k_{slab}} + R_{ins}}(\overline{T}_{13} - \overline{T}_{14}) + \frac{k_{slab}}{l_{slab}}(\overline{T}_{15} - \overline{T}_{14}) \right] \Delta t \quad (2.57)$$

The remaining interior slab nodes are not affected by the change of insulation location, and thus are described by Eqs. 2.53 and 2.54. However, the final slab node must be adjusted because no insulation is now present. Thus, the energy balance for the final slab node is

$$(mC)_{slab}(T_{24}' - T_{24}) = \left[h_{room}(T_{room} - \overline{T}_{24}) + \frac{k_{slab}}{1.5 \cdot l_{slab}}(\overline{T}_{24} - \overline{T}_{23}) \right] \Delta t \quad (2.58)$$

Numerically Modeling a Green Roof

As is done in the cool and modified-bitumen roof model, the Trapezoidal rule is used again to numerically model the above system of equations using Eq. 2.25. Analogous matrices for B , S , \vec{Q} , \vec{T}' , and \vec{T} are formed from the preceding energy balances, which allows the temperature at the next time step to be predicted from the current temperature.

2.3 Validation of Models

Recall the chief motivation of this thesis, to provide a common basis on which to compare the energy performance of different roof technologies in different climates. In order to fulfill this motivation, a certain level of generality in the models must be

achieved. However, the models still must have a sufficient level of specificity to maintain an acceptable level of validity in modeling the natural world. To prove both the generality and specificity of the models, they are validated by two sets of experimental data that have been obtained from different regions of the world, graciously shared by Jeff Sonne of the Florida Solar Energy Center (FSEC) and Professor Hideki Takebayashi of Kobe University. The models' generality is shown by successfully modeling the roof conditions in two different regions of the world without tweaking any parameters except those that physically change and were measured (such as roof albedo or structural slab thickness). Simultaneously, the models' specificity is shown by accurately predicting roof conditions.

2.3.1 Experimental Setups

FSEC Green Roof Study

The FSEC Green Roof Study initially began as a green roof project led by the University of Central Florida's Stormwater Management Academy, located in Orlando, FL, under a grant from the Florida Department of Environmental Protection (FDEP). While the primary purpose of the project was to evaluate rainwater runoff benefits of the green roof, FDEP, through a U.S. Department of Energy State Energy Program Grant also funded Jeff Sonne of the FSEC to evaluate the energy performance of the green roof [35][76][40].

One half of this project's 3,300 square foot roof was a conventional, light-colored membrane roof (with measured reflectivity of 0.50 as determined by the ASTM Standard E1918-97 methodology) [35]. The other half of the roof had the same membrane roof with a planted green roof completely covering the surface. The study considered an extensive green roof with 6 to 8 *in* of plant media and a variety of primarily native Florida vegetation up to approximately 2 feet in height, shown in Fig. 2-14. Although the green roof model assumes a 12 *cm*, or 4.7 *in*, clipped grass, this difference in vegetation will test the generality of model.

Symmetry was used in the roof geometry and drainage systems to allow both



Figure 2-14: The extensive green roof with native Florida vegetation up to 2 *ft* in height, planted in 6 to 8 *in* of plant media. The conventional light-colored membrane roof is visible on the far right of the picture [35]

the conventional and green roofs to have similar “mirror image” insulation levels and corresponding thermocouple locations. More specifically, the roof assembly was comprised of the roof membrane, a Georgia Pacific 1/2” Dens Deck ©cover board, polyisocyanurate insulation, and a metal deck. Because concrete was not used as the structural support of the roof, the cover board is used in lieu of the concrete slab for the purposes of the model. The amount of insulation was approximated using a laser level at each sensor location, which measures the insulation thickness, from which a corresponding R-Value is determined [77]. In the middle of both green and conventional roofs, where there was the least amount of insulation, the R-Value is $2.99 \text{ m}^2\text{C}/\text{W}$, but closer towards the edges of the roof, it was $6.69 \text{ m}^2\text{C}/\text{W}$. A section view of the roof is shown in Fig. 2-15.

Special limits type-T thermocouples, were used to measure temperatures that include the roof surface, bottom of roof deck, ambient air, interior air, and green roof plant media surface. The combined accuracy of the thermocouples and multiplexer was $\pm 1.4\text{C}$ [89] [73]. These temperature measurements were taken at each of the three locations for the green and conventional roof indicated in Fig. 2-16, which

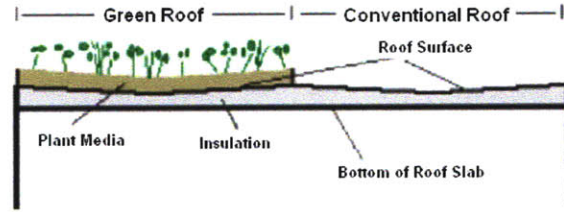


Figure 2-15: Section of the green and conventional roofs in the FSEC green roof study, which shows the symmetric design of the roof. Note the varying amount of insulation, which is determined to be $2.99 \text{ m}^2\text{C}/\text{W}$ in the middle of both green and conventional roofs, and $6.69 \text{ m}^2\text{C}/\text{W}$ on the edges of both types of roof. Source [35]

were the exact locations where insulation thickness measurements were taken, in the center [35]. Thermocouples on the roof surface “were attached to the membrane with a structural sealant and the three conventional roof sensors were painted to match the roof color as closely as possible.” [35].

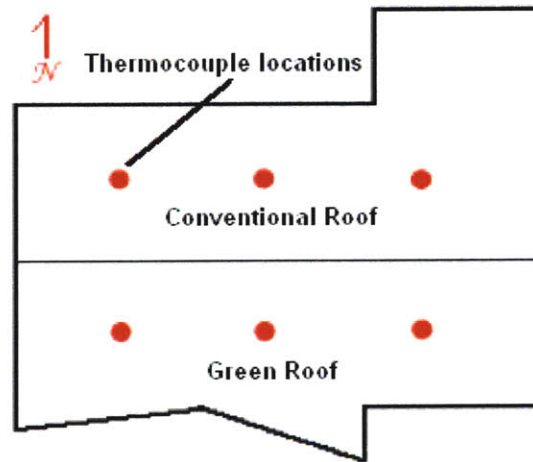


Figure 2-16: Roof diagram showing symmetric thermocouple placement on both green and conventional roofs. Source [35]

Meteorological measurements taken on site include ambient air temperature, rainfall, total horizontal solar radiation, wind speed and direction. All sensors were sampled every 15 seconds, though hourly averages are used in comparisons to the roof models. The green roof was irrigated twice a week for approximately 15 minutes each time so the soil was not lacking water as assumed in the green roof model. Although

Table 2.5: Summary of FSEC Experimental Roof Construction - * indicates value is specified in model and not obtained from experiment

	Cool Roof	Green Roof
<i>Top surface</i>	roof membrane	vegetation
reflectivity [-]	0.50	0.23*
emissivity [-]	0.95*	0.95*
<i>Growing Media</i>		
Material [-]	n/a	loam*
Thickness [m]	n/a	0.178
Density·C [J/m^3K]	n/a	1.4e6*
Conductivity [W/mK]	n/a	0.8*
<i>Structural support slab</i>		
Material [-]	Dens Deck ©cover board	Dens Deck ©cover board
Thickness [m]	0.0127	0.0127
Density [kg/m^3]	746	746
Conductivity [W/mK]	0.133	0.133
Heat Capacity [J/kgK]	1090	1090
<i>Insulation</i>		
Thickness	not specified	not specified
R Value [W/m^2K]	2.97	2.97

the FSEC study did not measure humidity, hourly outdoor relative humidity data collected from the Orlando weather station is obtained from Weather Underground and the National Severe Storms Laboratory [17][97]. Data collected during both summer—July 17-23, 2006—and winter—February 3-9, 2006—are used to test the models’ validity in both seasonal extremes.

All physical parameters used in the model are summarized in Table 2.5

Kobe University Roof Study

Hideki Takebayashi and Masakazu Moriyama of Kobe University investigated numerous kinds of roof technologies on the roof of a university building on their campus from July 2003 through February 2006 [82]. The total roof area of $42.9 m^2$ was divided into numerous sections, each of which had a different kind of roof technology, as shown in Fig. 2-17. The sections considered in this thesis included an extensive, turf grass green roof, a bare concrete roof, and a white cool roof, which are circled in

Fig. 2-17 [82].

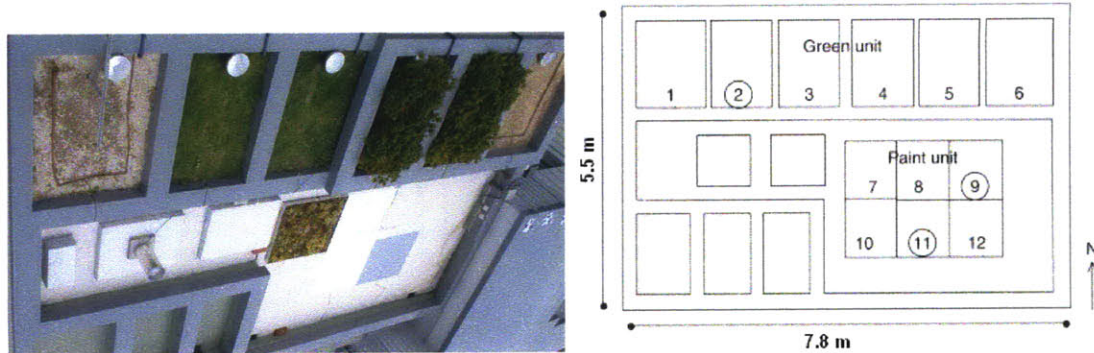


Figure 2-17: (left) Photograph of the 42.9 m^2 roof of Kobe University building, in Kobe, JP. (right) Diagram of experimental layout of roof. The circled numbers are considered in this thesis and include an extensive, turf green roof (2), a concrete roof (9), and a white cool roof (11). Both photograph and diagram are in the same orientation. Source [83]

Whereas the FSEC vegetation had a greater height and plant diversity than the green roof model, the clipped grass used in this study is much closer to the vegetation assumed in the model. The roof construction consisted only of a concrete structural slab (20 *cm* thick) for both the concrete and cool roof, though their measured reflectivities were 0.37 and 0.74 respectively. The green roof had a water barrier, which is neglected for the purposes of the model, between the growing media (21 *cm* thick) and the same concrete slab [82].

Measurements taken included growing media surface, roof surface, and soffit temperatures. They also included weather parameters gathered at a nearby weather facility: ambient air temperature, relative humidity, solar radiation, infrared radiation, precipitation, wind direction and velocity [82]. Data used from the Kobe University experiment were taken over three days, from August 27-29, 2004.

A summary of the roof constructions used in all three cases from the University of Kobe study is presented in Table 2.6 (with the concrete and cool roofs differing only by their reflectivities).

Table 2.6: Summary of University of Kobe Experimental Roof Construction - * indicates value is specified in model and not obtained from experiment

	Concrete & Cool Roof	Green Roof
<i>Top surface</i>	roof membrane	vegetation
reflectivity	0.37 (concrete), 0.74 (cool)	0.23*
emissivity	0.95*	0.95*
<i>Growing Media</i>		
Material [-]	n/a	loam*
Thickness [m]	n/a	0.21
Density · Heat Capacity [J/m^3K]	n/a	1.4e6*
Conductivity [W/mK]	n/a	0.8*
<i>Structural support slab</i>		
Material	concrete	concrete
Thickness	0.2 m	0.2 m
Density	2300 kg/m^3 *	2300 kg/m^3 *
Conductivity	1.4 W/mK *	1.4 W/mK *
Heat Capacity	880 J/kgK *	880 J/kgK *
<i>Insulation</i>		
Thickness	n/a	n/a
R Value	0 W/m^2K	0 W/m^2K

2.3.2 Model Validation

The first section of this chapter describes the cool, modified-bitumen, and green roof models developed in this thesis. In order to be validated, the models must be altered to account for the two different experimental roof constructions. Therefore, for this section only, input parameters are changed to reflect construction of the test roofs.

Data obtained from both the FSEC and University of Kobe studies is used to validate the roof models, which are validated by simulating the roof surface temperature measured in both studies. Although the models ultimately predict the energy flux into the building associated with either type of roof, the roof surface temperature is used to validate the models because the energy flux into the building is easily calculated with the roof surface temperature provided an indoor air temperature and known overall resistance of the roof. The indoor air temperature will be specified by the user depending on comfort conditions and the overall roof resistance will be known from the roof construction and amount of insulation. Therefore, since both

Table 2.7: Variation of concrete properties - *Indicates a heat capacity that is not reported, thus it is held constant. Source: ^a [46] ^b [47]

type of concrete	k [W/mK]	ρ [kg/m ³]	C_p [J/kgK]
stone mix ^a (used in model)	1.4	2300	880
limestone gravel ^b	0.6	1850	880*
sand and gravel ^b	1.4-2.9	2400	880*

indoor air temperature and overall roof resistances will be known, the models will accurately predict the energy flux into the building if they can accurately predict the roof surface temperature. Thus, the predicted roof surface temperature from the models is compared to the measured surface temperature from both studies to validate the model.

Cool and Modified-Bitumen Roof Model Validation

The cool and modified-bitumen roof model is validated using the concrete and cool roofs from the University of Kobe study. Fig. 2-18 shows the modeled and experimental roof surface temperature for the concrete and cool roof on the University of Kobe building during August 27-29, 2004. Although a modified-bitumen roof was not used in the study, the model was still validated by the experimental data because two roof surfaces of different albedo were used, concrete and a cool roof. The model is shown to successfully model these roofs with different albedos, as shown in Fig. 2-18. Thus, because the only assumed difference in allowed energy flux between cool and modified-bitumen roofs is the albedo, the model is validated by the experimental data.

For both concrete and cool roofs in Japan, concrete is the only component of the roof construction, apart from different surface coatings. Although the concrete properties chosen for the model are well accepted, other values are also reported in the literature for different types of concrete, which are summarized in Table. 2.7 [46] [47]. The modeled roof surface temperature corresponding to these different physical concrete parameters is shown in Fig. 2-19.

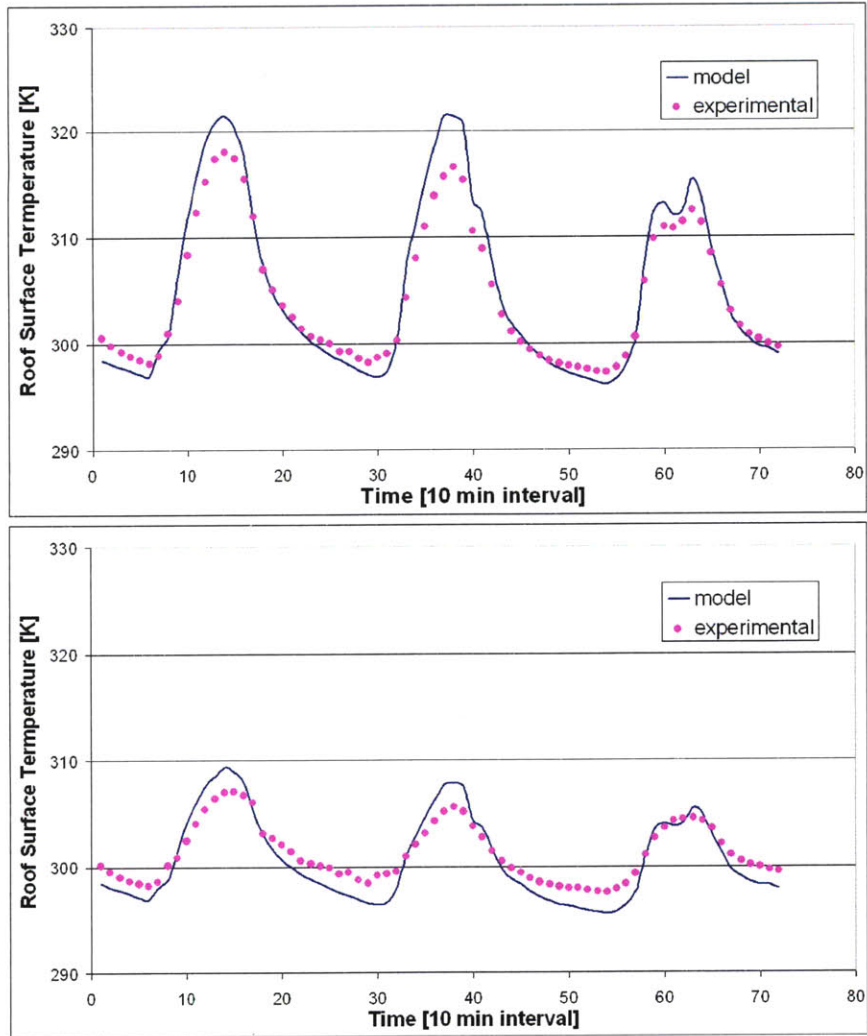


Figure 2-18: Simulated and experimental roof surface temperatures for a (top) 20 cm concrete roof with albedo = 0.37 and (bottom) cool roof with albedo = 0.74 and 20 cm concrete slab in Japan with no insulation. Experimental data, provided by Hideki Takebayashi and the University of Kobe, is from August 27-29, 2004, which includes measured weather parameters that are used with the roof model to simulate the roof surface temperature. Source [83].

The comparison of roof surface temperatures in Fig. 2-19 suggests any discrepancy between the simulated and experimental temperatures arises from slightly different physical concrete properties. This dependence on the physical properties of the concrete is likely from the lack of insulation, which when present dominates the resistance to heat transfer, thus decreasing the influence of concrete physical properties.

The cool roof model is also validated by experimental data from the FSEC study.

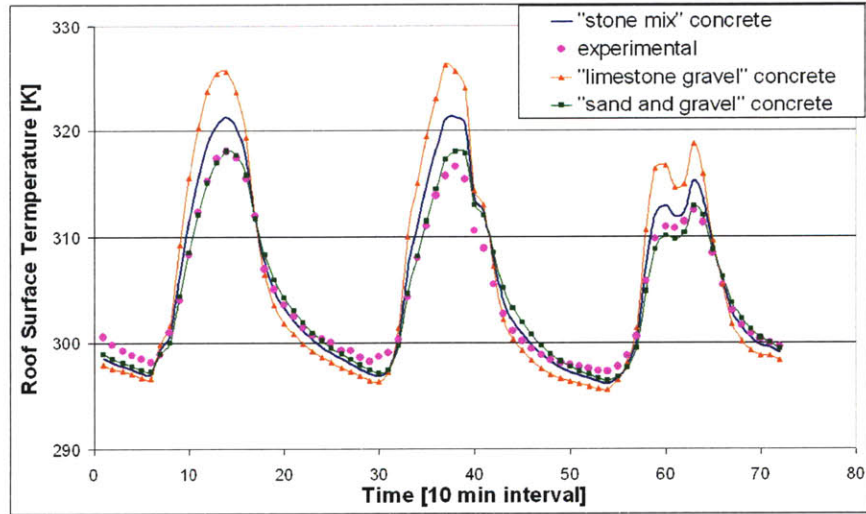


Figure 2-19: Simulated and experimental roof surface temperatures for a concrete roof with albedo = 0.37 in Japan with no insulation. Each type of concrete is listed in Table. 2.7. Source [83].

Although a “conventional roof” is used in the FSEC study, it is a light-colored roof with a measured albedo of 0.50, which by some standards is considered a “cool roof” [30]. Fig. 2-20 shows the simulated compared to the experimental roof surface temperature during the winter, February 20006, while Fig. 2-21 shows the same comparison for two weeks during the summer months of July and August 2006 [40]. The uncertainty of the measurements and model predictions are included in both figures.

The strong correlation between the cool roof model and experimental data is shown in Figs. 2-18 through 2-21. When predicting the roof surface temperature of the University of Kobe and FSEC studies, the predicted roof surface temperature of the model agrees with the measured value within 10 and 7.2%, respectively, of the peak roof surface temperature fluctuation. As previously described in Sec. 2.3.2, the model’s ability to predict roof surface temperature, which is an upper boundary of the heat conduction through the roof into the building, implies sufficient ability to predict heat flux into the building through the roof.

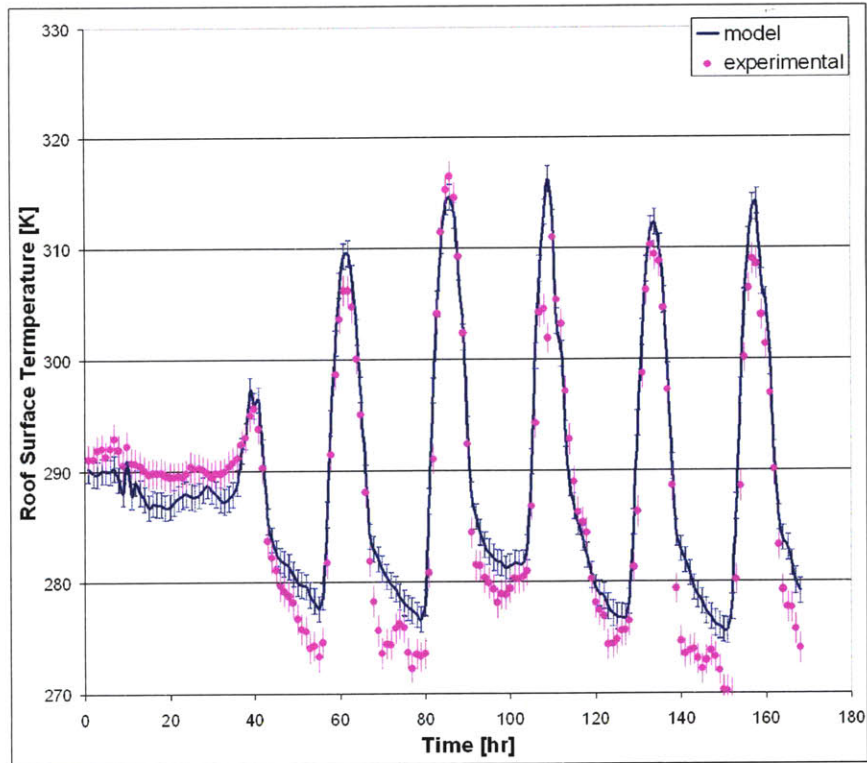


Figure 2-20: Simulated and experimental roof surface temperatures for a conventional roof with albedo = 0.5 in Orlando, FL constructed of a roof membrane on top of 1/2" cover-board, $2.97 \text{ W/m}^2\text{K}$ insulation, above a metal roof deck. Experimental data, provided by Jeff Sonne and the FSEC, is from February 3-9, 2006, which includes measured weather parameters that are used with the roof model to simulate the roof surface temperature. During the first 40 hours of the experiment, substantial rain fell, thus significantly moderating roof surface temperatures. Experimental temperatures are accurate to $\pm 1.4 \text{ C}$, while simulated temperatures are accurate to $\pm 1.16 \text{ C}$, or 7% of peak roof surface temperature fluctuations. Source [40].

Green Roof Model Validation

Similar to the cool and modified-bitumen roof model, the green roof model is also validated by both the University of Kobe and FSEC studies. Although the vegetation in the studies differs (recall a short turf is used in Japan, shown in Fig. 2-17, and tall native Floridian plants up to 2 ft in height are used in Florida, shown in Fig. 2-14), the vegetation and its evapotranspiration in the green roof model are not changed in any way to simulate both cases. Rather, they are held constant to show that the green roof model can simulate various kinds of green roof vegetation with relative

accuracy.

Similarly to the cool roof model, the green roof model is also shown to predict roof surface temperatures (the vegetation temperature in Japan and soil temperature in Florida), as shown in Figs. 2-22 through 2-24. The green roof model predicts surface temperatures that agree with measured values within 26 and 14% of peak roof surface temperature fluctuations in Japan and Florida respectively. There is likely less agreement with the Japanese data because of the high impact of physical concrete and soil properties, as previously discussed for the cool roof. The lack of insulation in the Japanese case leads to a higher dependence on accurate physical property values, which were not experimentally determined. However, in most applications roof insulation is present so typical physical property values will suffice.

This correlation not only validates the model's ability to predict green roof surface temperatures, but also its generality by modeling two green roofs of different vegetation sufficiently well. As with the cool roof model, the ability to predict roof surface temperatures implies an ability to predict the heat flux into the building.

The next chapter will discuss how this calculated heat flux from the model is incorporated into MIT's existing early-stage design software, the MIT Design Advisor.

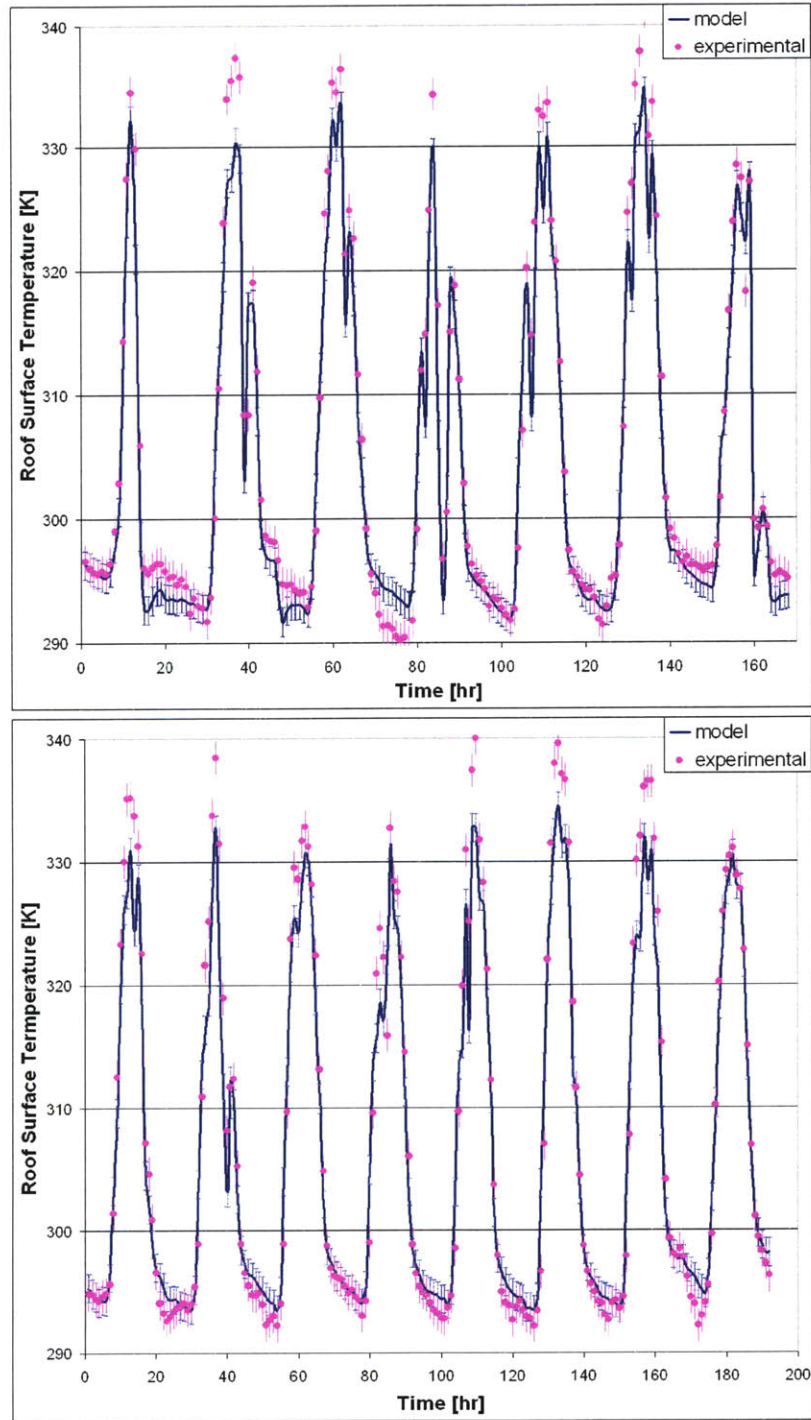


Figure 2-21: Simulated and experimental roof surface temperatures for a conventional roof with albedo = 0.5 in Orlando, FL constructed of a roof membrane on top of 1/2" coverboard, $2.97 \text{ W/m}^2\text{K}$ insulation, above a metal roof deck. Experimental data, provided by Jeff Sonne and the FSEC, is from (top) July 17-23, 2006 and (bottom) August 4-11, 2006, which includes measured weather parameters that are used with the roof model to simulate the roof surface temperature. Experimental temperatures are accurate to $\pm 1.4 \text{ C}$, while simulated temperatures are accurate to $\pm 1.16 \text{ C}$, or 7% of peak roof surface temperature fluctuations. Source [40].

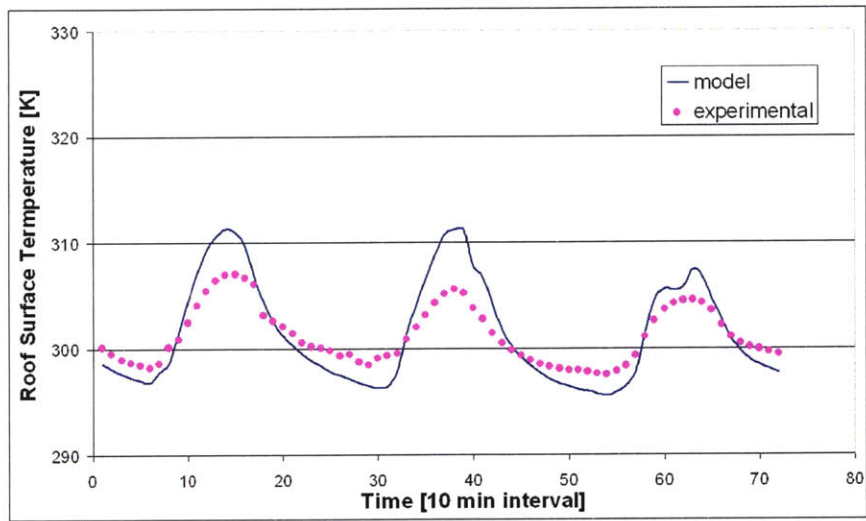


Figure 2-22: Simulated and experimental vegetation surface temperatures for an extensive turf green roof in Japan with no insulation. The turf is planted in 21 *cm* of growing media on top of a water proofing barrier above a 20 *cm* concrete roof slab. Experimental data provided by Hideki Takebayashi and the University of Kobe is from August 27-29, 2004, which includes measured weather parameters that are used with the roof model. Source [83]

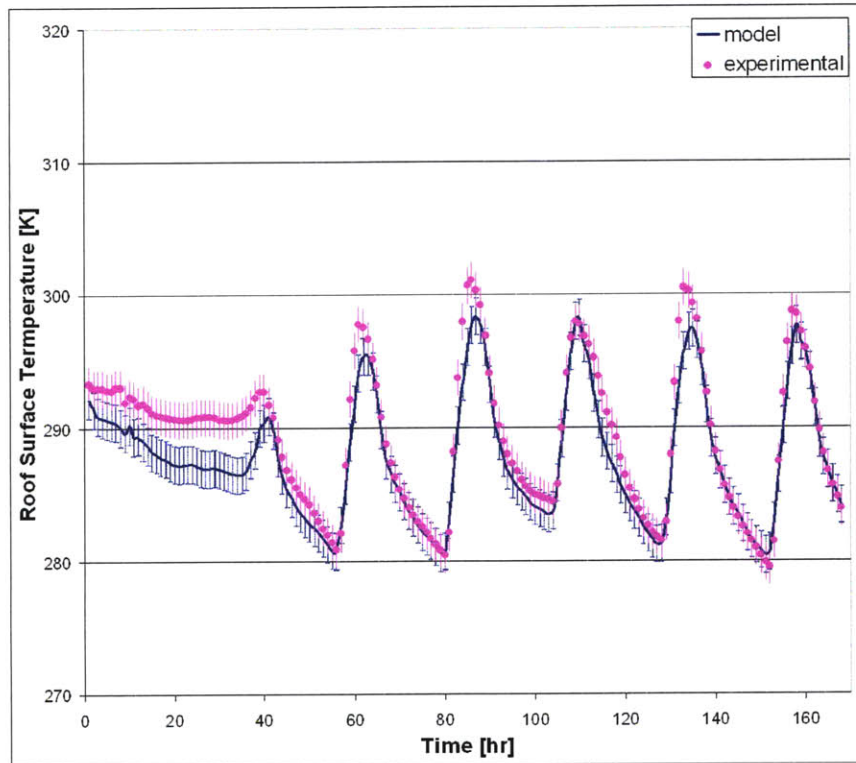


Figure 2-23: Simulated and experimental soil surface temperatures for an extensive green roof in Orlando, FL. The vegetation used in the experiment is native Floridian plants up to 2 ft in height. Although reported growing media is 6-8", an average of 7 " is used in the model, which sits on top of a 1/2" cover board, above $2.97 \text{ W/m}^2\text{K}$ insulation, that protects a metal roof deck. Experimental data, provided by Jeff Sonne and the FSEC, is from February 3-9, 2006, which includes measured weather parameters that are used with the roof model. Although the vegetation used in the green roof model is assumed to be 12 cm cool season grass, the model still accurately simulates the 2 ft native Florida plants. No vegetation parameters are changed in the model. During the first 40 hours of the experiment, substantial rain fell, significantly moderating roof surface temperatures. Experimental temperatures are accurate to $\pm 1.4 \text{ C}$, while simulated temperatures are accurate to $\pm 1.38 \text{ C}$, or 14% of peak roof surface temperature fluctuations. Source [40]

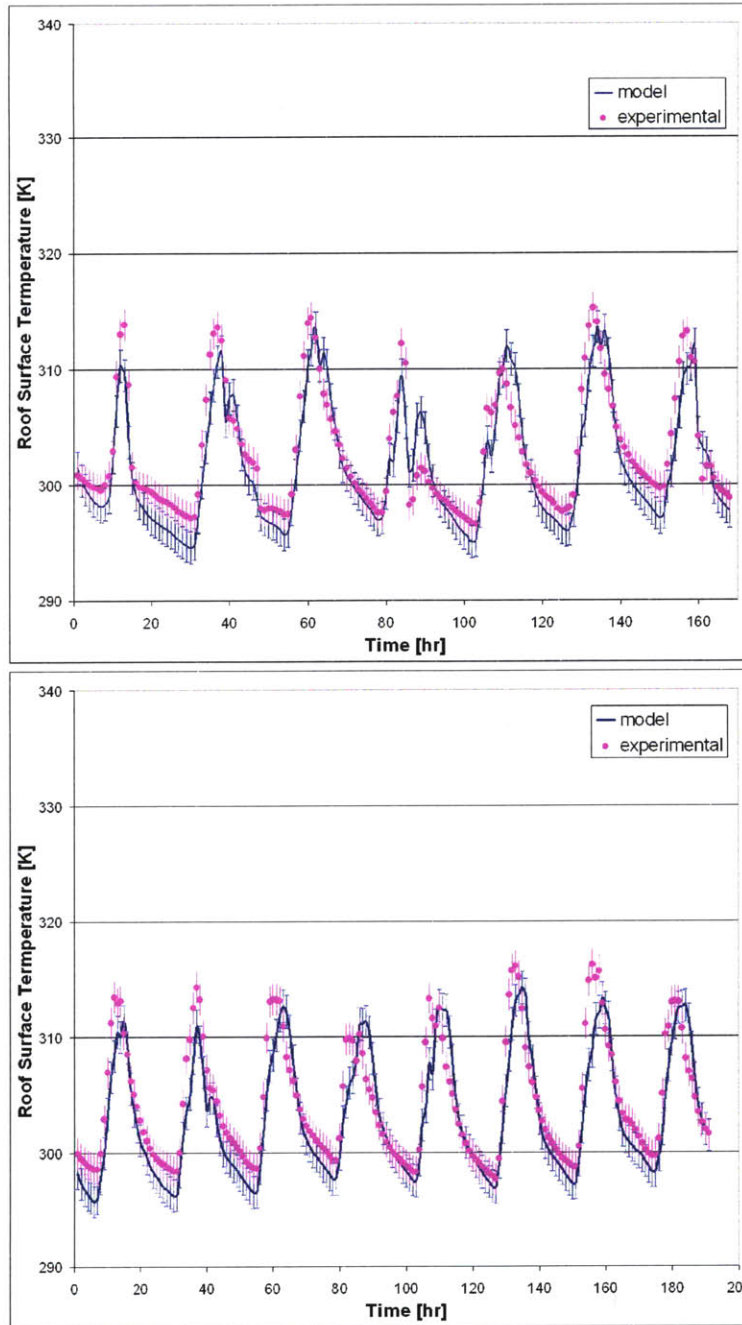


Figure 2-24: Simulated and experimental soil surface temperatures for an extensive green roof in Orlando, FL. The vegetation used in the experiment was native Floridian plants up to 2 ft in height. Although reported growing media was 6-8", an average of 7" is used in the model. The growing media sat on top of a 1/2" cover board, above 2.97 W/m²K insulation that protected a metal roof deck. Experimental data provided by Jeff Sonne and the FSEC was from (top) July 17-23, 2006 and (bottom) August 4-11, 2006, which included measured weather parameters that are used with the roof model. Although the vegetation used in the green roof model was assumed to be 12 cm cool season grass, the model still accurately simulates the 2 ft native Florida plants. No vegetation parameters are changed in the model. Experimental temperatures are accurate to +/- 1.4 C, while simulated temperatures are accurate to +/- 1.38 C, or 14% of peak roof surface temperature fluctuations. Source [40]

Chapter 3

Model Integration to Building

Simulator: MIT's Design Advisor

The first-principles model described in the previous chapter has been shown to accurately predict the energy flux into a building. In this chapter, that model is integrated into a building simulation tool, MIT's Design Advisor, to allow users to see how the energy flux through the roof will affect the entire building's energy performance. An overview of the current version of Design Advisor will be followed by a list of new parameters introduced to the tool for the added roof module, and finally the integration of the model into Design Advisor will close the chapter.

3.1 Overview of Design Advisor

The MIT Design Advisor (DA) is called by its originator “a simple and rapid building energy simulation tool, developed specifically for architects and building designers” [88].

3.1.1 High Level Overview

A high level overview of how the tool works is taken from the originator's thesis [88]:

A logic diagram, [copied in Fig. 3-1], shows how the software works. First,

the user selects building options on a simplified user interface, [copied in Fig. 3-2]. When completed, the data are sent to a simulation engine. Weather data are retrieved for the building’s location. A simulation engine models the available daylight, which can be displayed graphically for several times of day. This daylight information is used to predict how much artificial lighting is needed to light the indoor space. Electric lighting loads are then computed hourly for the entire year. An HVAC loads module then uses the weather and building information to predict the monthly and annual heating, cooling, and lighting energy needs. Information about occupant comfort is also produced. These results are then displayed to the user graphically. The entire simulation process and data interpretation takes less than a minute’s time. Once a simulation is completed, the user may revise the design options and repeat the process, comparing results side-by-side. Instant design feedback allows the user to quickly learn which components have large influences on building energy consumption.

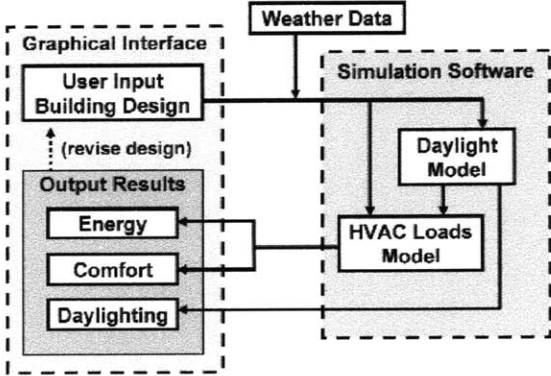


Figure 3-1: Logic diagram of the DA simulation tool. Source [88].

The daylight model as well as the key components of the HVAC load model (including internal loads, thermal mass, envelope loads, and their combination to form the HVAC loads model) are explained in more detail below.

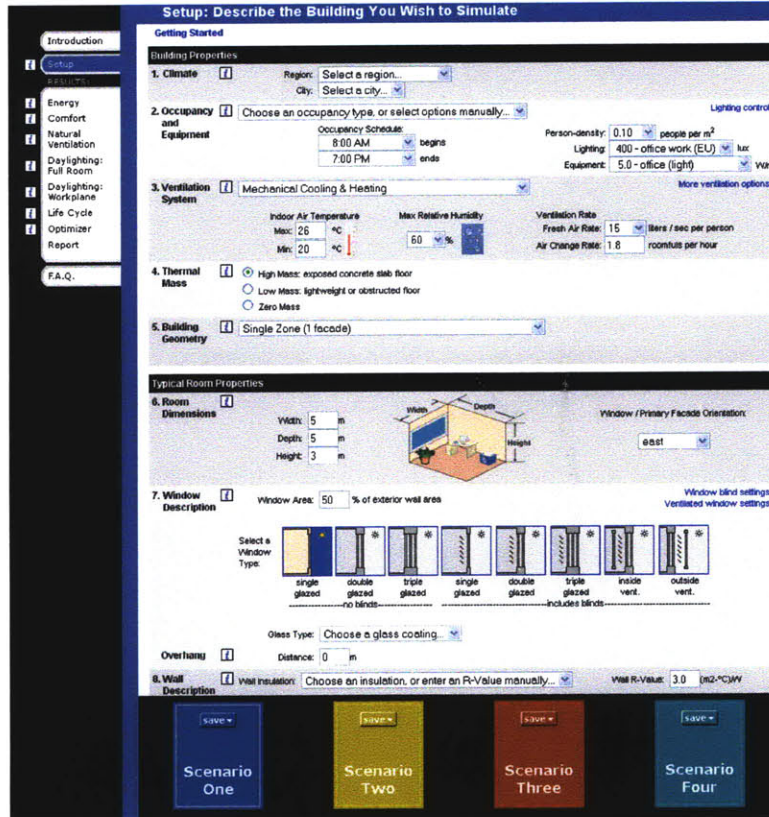


Figure 3-2: A portion of the single-page MIT Design Advisor interface.

3.1.2 Daylight Model

The daylight model includes both direct and diffuse daylight as obtained from the TMY2 weather data files. For one day of each month, the distribution of diffuse and direct solar daylight as it is reflected onto each subarea of the room is calculated by radiosity methods. For direct daylight, the elevation and azimuth of the sun, along with window area, coating, and blind information is used each hour to determine the area of the walls and floor that is directly illuminated. For each subsequent day of the month, the contribution of direct and diffuse daylight to each subarea is set proportional to the direct and diffuse intensity given in the weather file for that particular hour and day.

Multiple reflections are accounted for assuming diffuse reflections for all daylight. As specified in ASHRAE 90.1, we assume surface reflectances of 80% for ceilings,

50% for walls, and 20% for floors. Reflections from the surfaces on blinds are also included assuming the blinds reflect diffusely *only* for lighting calculations, and both diffusely *and* directly for radiosity calculations, which affect solar gains. To find the daylighting on a workplane 0.8 m above the floor, any shadows or blockage due to furniture or equipment are neglected.

Lighting energy is found using one of two strategies. The first strategy is to assume that the lighting for each room subarea is separately controlled so that only enough electrical lighting is provided so that the total of daylight and electrical light equals the required lighting level on the workplane. The second strategy uses the assumption that all of the room lights are controlled together. In this case, the electrical light in the room is uniform and adjusted so that the darkest part of the room receives the required lighting level. In both cases, the lights are assumed to maintain a constant efficiency when dimmed so that the light output per unit of electrical energy remains at 53 *lumens/watt* (typical for fluorescent lights). A graphic representation of the room subareas and workplane is shown in Fig. 3-3

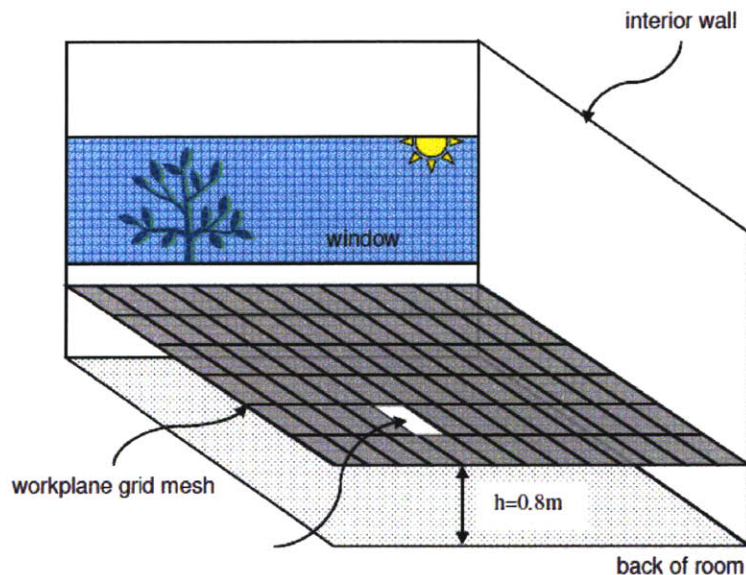


Figure 3-3: Two-dimensional workplane grid used to determine the lighting level in each subarea. Source [88]

3.1.3 HVAC - Ventilation

DA's modeling of building ventilation begins with a user specification of the minimum ventilation rate in air changes per hour. One air change is defined as replacing the entire volume of air currently in the building with the same amount of fresh air. In the tool, air changes can be specified directly, or the air change rate can be linked to a representative number of people in a room. Because ventilation rates often change with building occupancy, different rates can be specified for occupied and unoccupied times.

Although fresh air usually enters a building in one of three ways, mechanical systems, natural ventilation, or infiltration, only the first two are considered in the tool. However, if infiltration levels are known, they can be accounted for by including them in the minimum air change rate. Three ventilation options are possible: mechanical, natural, and hybrid ventilation (where hybrid combines the previous two). All three options share the assumptions that: (1) fresh air is brought into the building at the outdoor air temperature, (2) indoor air is exhausted from the building at the indoor air temperature, (3) no energy is recovered from the exhaust air, and (4) fan energy is not considered.

The specific assumptions for each of the three ventilation options taken from the DA website are listed below:

1. Mechanical Ventilation Cooling and Heating

- * The amount of fresh air intake and indoor air exhaust are exactly determined by the specified ventilation rate.
- * No heat is recovered from the indoor air exhaust.
- * If the indoor air temperature falls below the minimum temperature set-point, heating energy is supplied to maintain a comfortable temperature.
- * If the indoor air temperature rises above the maximum temperature set-point,

cooling energy is supplied to maintain a comfortable temperature.

- * If the indoor air humidity rises above the maximum humidity set-point, cooling energy is supplied to remove moisture from the air.

2. Natural Ventilation Cooling, Mechanical Heating

- * Windows can be opened or closed to help mediate the indoor environment.
 - o If the indoor air temperature is approaching the maximum temperature set-point, and the outdoor air temperature is cooler, the windows are opened.
 - o If the indoor air temperature is approaching the minimum temperature set-point, and the outdoor air temperature is warmer, the windows are opened.
 - o If the indoor relative humidity reaches the maximum humidity set-point, the windows will close if the outdoor humidity ratio is greater to prevent excess indoor humidity.
- * When a window is opened, the fresh-air flow rate through the window is calculated based on a cross-flow model that involves wind speed, window dimensions, and room dimensions.
 - o If the amount of natural ventilation is less than the minimum required air change rate, the mechanical system will bring in enough additional fresh air to meet the minimum requirement.
 - o If the amount of natural ventilation is greater than the minimum air change requirement, then no mechanical assistance will be used.
- * If the indoor air temperature falls below the minimum temperature set-point, heating energy is supplied to maintain a comfortable temperature.
- * If the indoor air temperature rises above the maximum temperature set-point, *no* cooling energy is supplied. Instead, the upper-temperature is allowed to float freely.

- * If the indoor air humidity rises above the maximum humidity set-point, *no* cooling energy is supplied. Instead, the indoor humidity level is allowed to float freely.

3. Hybrid Ventilation: Natural and Mechanical Cooling, Mechanical heating

This case is identical to Natural Ventilation Cooling except that:

- * If the indoor air temperature rises above the maximum temperature set-point, the windows are closed and cooling energy is supplied.
- * If the indoor air humidity rises above the maximum humidity set-point, the windows are closed and cooling energy is supplied.

Two types of ventilated window systems may be selected. These windows are multi-layered windows in which air can flow between two panes of glass. The user can select where the intake and exhaust air streams are connected (either indoors or outdoors). If a ventilated window system brings air from the outdoor environment into the indoor environment, this counts towards meeting the minimum air change requirement. In this case, the mechanical ventilation rate is then reduced by the amount of air brought in through the active window. It is possible to configure an advanced window that exhausts air from the indoor environment. In this case, if the flow rate exhausted by the window exceeds the mechanical ventilation rate it is assumed that additional conditioned air is automatically supplied to the room.

Both Cooling and Heating energy are explained in more detail below, as is done on the DA website.

Cooling and Heating Energy

When the indoor air temperature climbs above the high temperature setpoint, a (sensible) cooling load is required. Similarly, when the indoor air relative humidity climbs above the maximum-humidity setpoint, a (latent) cooling load is required. As expected, when the indoor air temperature falls below the low temperature setpoint, a (sensible) heating load is required.

If Natural Ventilation Cooling is chosen, then no chiller system is available and the cooling load is reported as zero. The air temperature will float freely above the minimum temperature. In this case the user can view a histogram of the hours spent at a given air temperature to determine how often the building would be uncomfortably hot without using a mechanical chiller. If Hybrid Ventilation is chosen, a chiller is used when opening the windows does not maintain a comfortable indoor environment. Factors that contribute to the cooling and heating load include:

Combined Cooling and Heat Assumptions:

- * Solar gains: direct and diffuse radiation passing through window/ blind system, as explained with the preceding Daylight model explanation.
- * Heat passing through the building envelope (walls and windows).
- * Heat from electric lights at 53 lumens/watt.
- * Heat from equipment, specified by user.
- * Heat from occupants: 75Watts/person (sensible)
+ 55Watts/person (latent).
- * Specified Ventilation (which can include infiltration) air flows:
 $MassFlowXCp_{air}X(T_{inside}T_{outside})$.
- * No energy is recovered from exhaust air.
- * Fan energy is neglected.

Cooling Assumptions:

- * Cooling energy represents the combined sensible and latent loads
- * Chiller Coefficient of Performance (COP) =
delivered-cooling-energy/electricity-consumption.
COP is assumed to be 3.0 and is constant for latent and sensible loads.
To provide 1 kWh of cooling energy requires (1 kWh /3.0) =
1/3 kWh of electricity.
- * Overall efficiency of power generation and distribution system = 30%.
Efficiency = Electrical energy delivered to building / Primary energy

consumed at power plant. So to provide 1 *kWh* of cooling energy requires 1/3 *kWh* of electricity, which requires $(1/3 \text{ kWh} - e)/30\% = 1.11 \text{ kWh}$ of primary energy.

Heating Assumptions:

* Furnace efficiency = 100%, with fossil fuel consumed on site.

To provide 1 *kWh* of heating energy requires 1 *kWh* of primary energy.

3.1.4 HVAC - Envelope Loads

The building envelope in the current version of DA consists of all exterior walls and windows through which heat and light may be exchanged with the outdoor environment. To simplify DA's simulation, the contributions of the ground to the energy balance have been neglected.

The following assumptions for the windows are taken from the DA website:

- * Conductivity and optical properties for standard single, double, and triple glazed windows are taken from ASHRAE Fundamentals.
- * Variation of glass optical properties with angle of incidence and radiant spectrum considered using Fresnel relations and Snell's Law.
- * Heat transfer through single-, double-, and triple- glazed windows is modeled with a resistive network including conduction, convection, and linearized radiation. Radiation heat transfer coefficients are calculated dynamically as glass temperature changes.
- * Heat transfer and solar transmission through windows that have blinds is computed using a radiosity method.
- * The windows are assumed to be continuous horizontal strip windows. The windows are centered vertically on the inside wall and the window height is adjusted based on the percent of envelope surface occupied by glazing.
- * Blinds can be set to actively respond to the environment in 2 ways, with

closed blind angle specified by the user:

1. Temperature sensitive: blinds close/open when they cross the upper alert temperature threshold (too hot).
2. Solar Intensity sensitive: blinds close when the direct normal illuminance is more than 50,000 *lux* (glare).

- * The exterior horizontal overhang is located at the ceiling level. Shadows cast by the overhang are considered in the direct solar on the window and the daylighting.
- * The frames for both single and double skin faades are assumed to occupy 16% of the glazing area with a U-value of 4.2 W/mK between the inside and outside.

Inside blinds are taken as a separate layer whose temperature is calculated by an energy balance between the inside glass and the room. This includes IR radiation and convection from both surfaces of the blinds. The blinds also absorb and reflect solar energy passing through the windows. The radiation properties of the blinds vary with blind material and color. The blinds reflect diffuse light diffusely and reflect the direct solar by a combination of specular and diffuse reflection. The latter includes the view factors between the blind surface and the room sub-areas as well as shadowing by neighboring blinds. The blind width is taken equal to the blind spacing.

For double skin facades, the temperature of each glazing layer is calculated by a thermal balance of conduction, convection, IR radiation, and solar absorption. For the blinds, a four body radiosity calculation is used for the IR between the upper and lower blind surfaces and the two adjacent glass layers. The air flow in the cavity is assumed to form two flow channels that do not mix with each other. The air temperature is calculated at five vertical layers along the flow channel by an energy balance. The convection heat transfer between the flowing air and the flat glass surface and the blinds is computed based on the air velocity: $h_{blinds} = 5.8 + 4 * V_{air} [W/m^2K]$. The program will calculate the performance of inside ventilated (inside air enters channel and is exhausted back to the room), outside ventilated (outside air enters and exists

the flow channel) as well as advanced designs where the air can enter from the outside and exhaust to the inside or vice-versa.

Heat transfer through the exterior walls is calculated using a series resistance network between the outdoor and indoor air temperatures. The outdoor and indoor long-wave radiation and convection resistances are used in addition to the conductive resistance of the wall and any insulation.

A graphical illustration of the heat transfer through both the windows and walls is shown in Fig. 3-4.

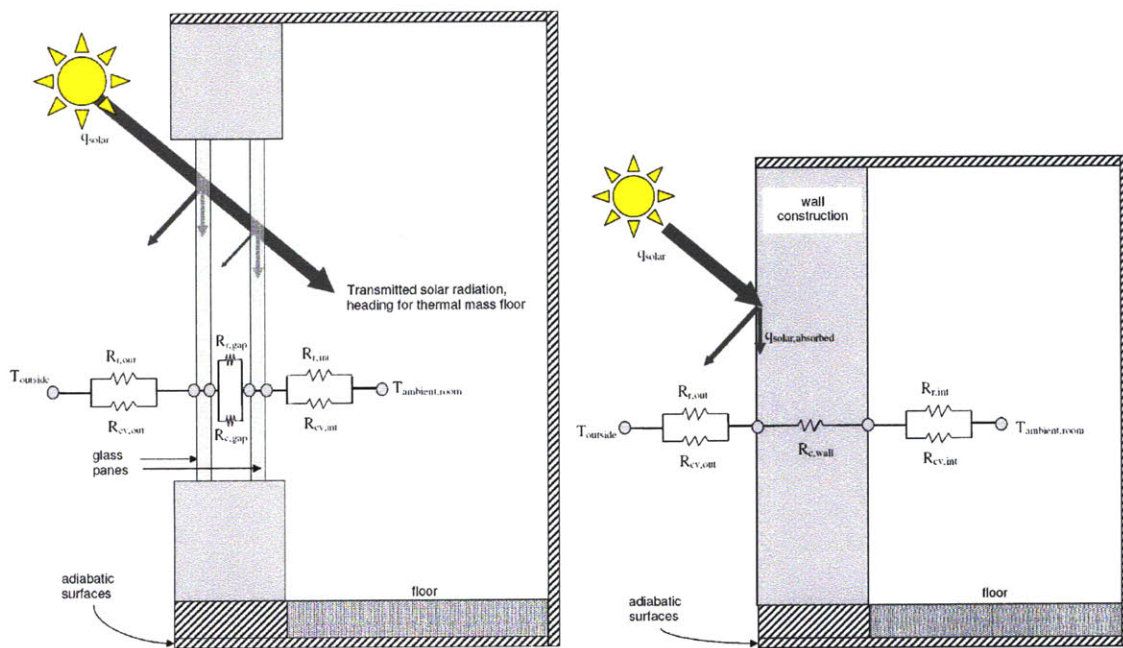


Figure 3-4: Illustration of the heat transfer through the windows (in this case, double pane) and walls that comprise the building envelope of the previous version of DA. Source [88]

3.1.5 HVAC - Thermal Mass

The user can add thermal mass to the floor of each room in DA. Fig. 3-5 shows a diagram of how the thermal mass is represented, and the following list of assumptions is taken from the Design Advisor website.

* The balance includes heat transfer between the air and thermal mass.

- * The thermal mass temperature is calculated by dividing it up into 10 equal-thickness layers and doing a heat balance for each layer.
- * For heavy thermal mass the floor area is assumed to be 10 cm thick concrete with a bare surface.
- * For light building construction, the concrete floor is assumed to be 2 cm thick.
- * Concrete for thermal mass has a specific heat capacity of 880 J/kgK and a density equal to 2400 kg/m^3 .
- * The heat transfer coefficient between the floor surface and air is taken to be $8 \text{ W/m}^2\text{K}$.
- * Heat transfer to the walls and ceiling is not included.
- * All of the incoming solar energy is assumed to be uniformly absorbed over the floor surface.

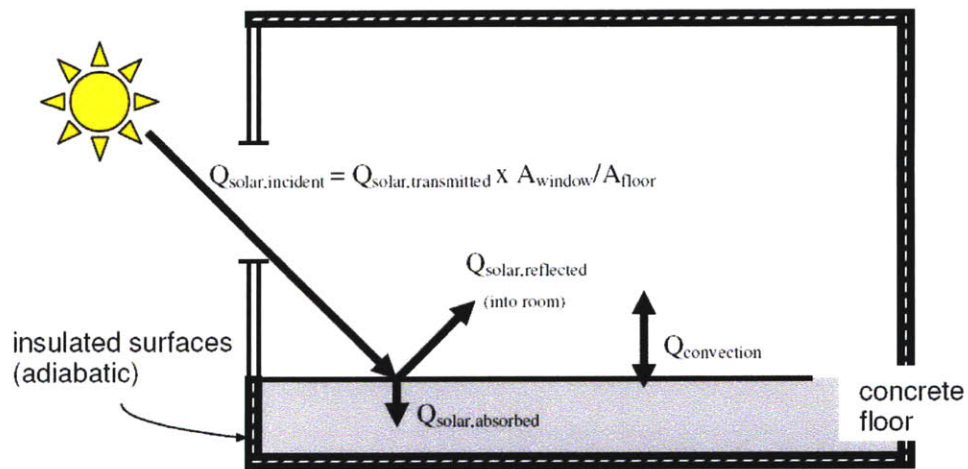


Figure 3-5: Schematic of heat transfer involving the thermal mass stored in the floor of a building in DA. Source [88].

3.1.6 HVAC - Combination of Components

In order to find the energy associated with the HVAC system, temperature bounds are defined for the building and as previously mentioned, when the room temperature,

Table 3.1: Variables used in the DA room Energy Balance

component	units	computational frequency
<i>Weather Data</i>		
Outdoor Air Temperature	K	hourly
Thermal Solar Flux	W/m^2	hourly
Visible Solar Illuminance	lux	hourly
<i>Internal Loads</i>		
Equipment	W/m^2	hourly
People	W/m^2	hourly
Lighting	W/m^2	hourly
<i>Temperature-dependent loads</i>		
Envelope gains	W/m^2	5 min.
Ventilation	W/m^2	1 min.
Thermal mass (including reflected solar thermal)	W/m^2	about 30 sec.
<i>Resultant Values</i>		
Room Air Temperature	K	1 min.
Heating / Cooling Load	W/m^2	1 min.

T_{room} , leaves these bounds, heating or cooling energy is required to return T_{room} within the desired temperature range. DA uses an energy balance applied to the room to find the room temperature every minute. The numerous parameters used in the energy balance, their units, and calculation frequency are shown in Table 3.1

To help understand how these parameters affect the heat transfer in the room, Fig. 3-6 is copied from Urban's thesis that illustrates the different modes of heat exchange with the air in a room in the original DA program (before the roof module is added).

Before the roof module is added, the energy balance of the room is

$$m_{a,rm}Cp_a \frac{\partial T_{room}}{\partial t} = (T_{hr} - T_{room}) [(UA)_{win} + (UA)_{wal} + \dot{m}C_p] + Q_{int} + Q_{tm} \quad (3.1)$$

where $m_{a,rm}$ is the mass of the air in the room, Cp_a is the specific heat capacity of air (assumed to be constant), T_{hr} is the ambient outdoor temperature, UA_{win} and UA_{wal} are the overall heat transfer coefficients for the windows and walls respectively,

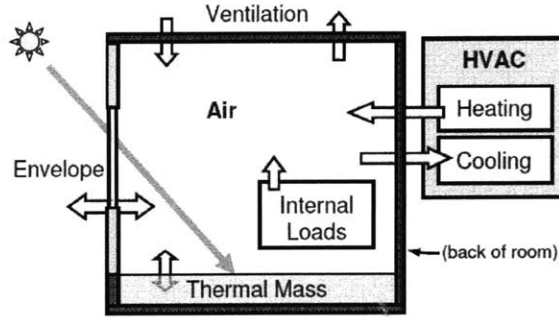


Figure 3-6: Heat exchange with air in a room, with arrows indicating possible directions of heat flow. Source [88].

\dot{m} is the mass flow rate of air into the room from the ventilation system, Q_{int} is the sum of internal plug and lighting loads, and Q_{tm} is the heat flux from the thermal mass in the floor. This energy balance can be solved to find T_{room} at the next time step (which in this case is a minute) as follows

$$T'_{room} = \frac{m_{a,rm} C p_a T_{room} + \Delta t \{ (T_{hr}) [(U A)_{win} + (U A)_{wal} + \dot{m} C p_a] + Q_{int} + Q_{tm} \}}{m_{a,rm} C p_a + \Delta t [(U A)_{win} + (U A)_{wal} + \dot{m} C p_a]} \quad (3.2)$$

As a final summary of the previous version of DA, a logic diagram is shown in Fig. 3-7.

3.2 New Roof Parameters in Design Advisor

In order to incorporate the energy impact of different kinds of roofs into DA, various new parameters have to be introduced, which are listed in this subsection. Each parameter must be specified by the user before an energy simulation is run. Fig. 3-8 shows the user interface for the roof model, which contains each of the following four new parameters.

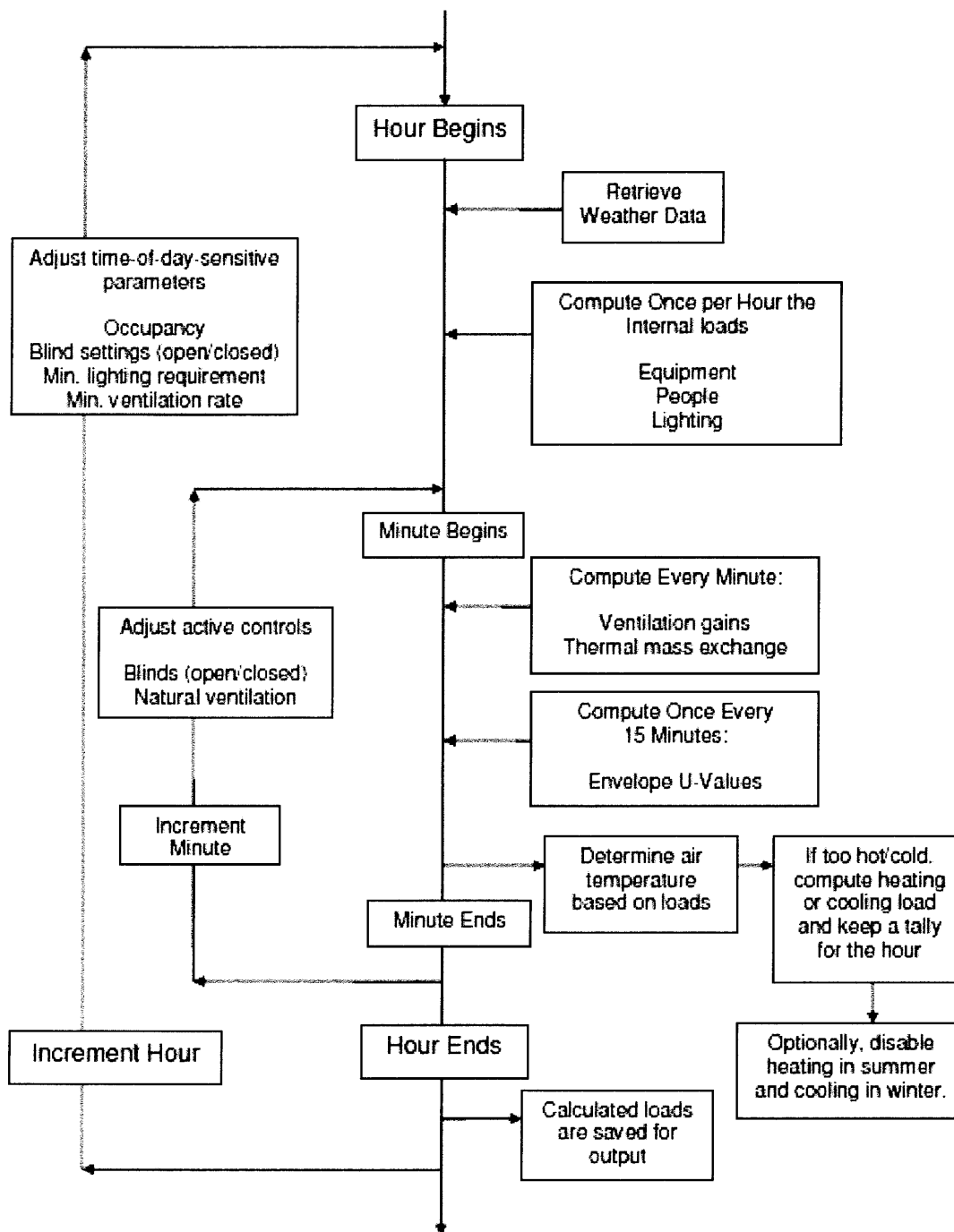


Figure 3-7: Hourly logic used for the DA software. Source [88].

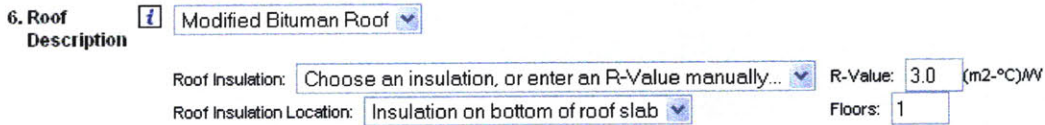


Figure 3-8: User interface for roof module, which allows user to specify the roof type, amount and location of roof insulation, and the number of floors in the building.

3.2.1 Type of Roof

The user must first specify what kind of roof will be simulated among four options: adiabatic, modified-bitumen, cool, or green roof. The adiabatic roof assumes no heat transfer through the roof (as previously assumed in DA), and thus only considers envelope loads through the walls and windows. The other three types of roofs are described in sections 2.1 and 2.2.

3.2.2 Roof Insulation R-Value

The user must also chose the R-value for the roof insulation, which can be done in one of two ways. In the first option, the user may select the amount of insulation from a list a typical insulation values compiled by Bryan Urban, a screen shot of which is shown in Fig. 3-9 [88]. The second option allows the user to specify the exact value of the insulation.

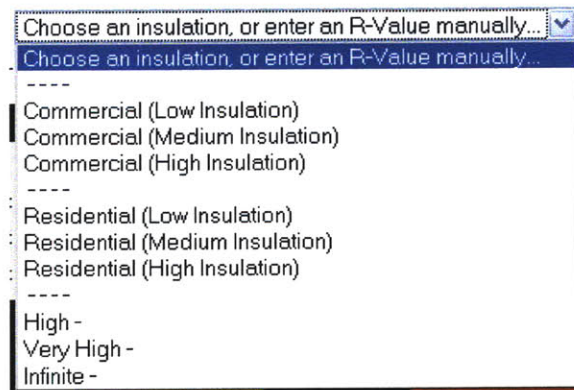


Figure 3-9: Screen shot of the types of insulation that can be chosen in DA. The user can also specify the exact value if it is known. Source [88].

3.2.3 Roof Insulation Location

In addition to the amount of insulation, the user must specify whether it is above or beneath the roof structural slab. Recall from Sec. 2.1.2 that for the cool and modified-bitumen roof model, if the insulation is placed on top of the slab, a 1/2" coverboard is placed on top of the insulation to protect it from environmental stressors. However, roof insulation placed beneath the slab is simply added to the bottom of the slab. Similarly, the green roof model assumes insulation is simply added to the bottom of the slab as well, if it placed beneath the structural slab. If it is placed above the slab, it is added between the soil and slab layers with no additional material. Refer to Sec. 2.2.3 for further discussion and diagrams of the roof insulation used in the green roof model.

3.2.4 Number of Floors in the Building

Another important parameter added to DA is the number of floors in the building that is modeled. A more detailed discussion of how this parameter is used in DA follows, but a simple example reveals the importance of knowing the number of floors when considering the energy impact of a roof. For example, a large roof on a single-story warehouse has a much greater impact on the total building energy use than a small roof atop a 30 story highrise.

3.3 Integration of Roof Model into Design Advisor

The integration of the aforementioned roof model, discussed in Chapter 2 and new DA parameters into the existing DA program is discussed in this section. Specific references to the Java source files and html code that comprise the program are not included in this section, but can be found in Appendix A.

After all changes to the DA program, essentially only two aspects are changed. First, there is now a heat flux through the roof. Second, multi-story buildings can now be modeled, in which a total building average energy use per square meter is

found. These changes are discussed below in more detail.

3.3.1 Accounting for Heat Flux through Roof

The primary change to DA from this thesis is the addition of a heat flux term from the roof. The heat flux from the roof is modeled similarly as the flux from the thermal mass in the floor. Every minute, a flux is calculated from the roof that in turn affects the energy balance in the room. Thus, the new energy balance for the room becomes

$$m_{a,rm}Cp_a \frac{\partial T_{room}}{\partial t} = (T_{hr} - T_{room}) [(UA)_{win} + (UA)_{wal} + \dot{m}C_p] + Q_{int} + Q_{tm} + Q_{roof} \quad (3.3)$$

where the only change from Eq. 3.1 is Q_{roof} , which is the heat load from the roof, defined as

$$Q_{roof} = A_{roof} \cdot h_{room}(T_{slab,n} - T_{room}) \quad (3.4)$$

where A_{roof} is assumed to equal the floor area (which is defined by the user), h_{room} is the effective heat transfer coefficient between the bottom of the roof slab and the room (which accounts for any added insulation beneath the slab, as explained in Chapter 2), and $T_{slab,n}$ is the temperature of the final node of the roof slab. The current room temperature is used to predict Q_{roof} , thus the new expression for T'_{room} becomes

$$T'_{room} = \frac{m_a Cp_a T_{room} + \Delta t \{T_{hr} [UA_{win} + UA_{wal} + \dot{m}C_p] + Q_{int} + Q_{tm} + Q_{roof}\}}{m_a Cp_a + \Delta t [UA_{win} + UA_{wal} + \dot{m}C_p]} \quad (3.5)$$

As before, all weather data is updated on an hourly basis, and likewise, all other components of the software logic shown Fig. 3-7 remain the same.

3.3.2 Accounting for Multiple Building Floors

The second aspect of the DA software that has been changed is the ability to account for multiple floors in a building. Before a roof is considered, and because no heat flux from the ground is considered, no consideration was needed for multiple story buildings. However, now that the top floor of the building, directly under the roof, has an additional heat load, Q_{roof} , the top floor must be treated differently than all other floors. There are two scenarios that are now considered for the number of floors in the building.

When there is only one floor, no additional modifications are made to the existing software, apart from the additional Q_{roof} term described above. However, if there are multiple floors, only the top floor considers Q_{roof} , while all remaining floors are assumed to have adiabatic roofs due to similar indoor air temperatures on each floor. The energy requirement per square meter for the top floor is averaged with that of all remaining floors to obtain an average energy requirement for the entire building.

Chapter 4

Results

One might argue the most important result of this thesis is the production of a tool that can quickly and easily assess the potential energy savings of various roof technologies in cities around the world. This tool is freely available online at <http://designadvisor.mit.edu>

However, insight into these various roof types and constructions has been obtained through running numerous simulations, which will be presented in this chapter.

4.1 Roof Type

As the primary focus of this thesis, the energy impact of various types of roofs is first presented. It has been shown many times that cool roofs can save cooling energy in warm climates such as California [21]. It is also known that in cold climates, cool roofs may actually require more heating energy because they reflect useful heat from the sun [22] [96]. However, the climate in which the cooling energy savings equals the heating energy losses is more uncertain. Therefore, the same building will be simulated in a hot, cold, and a few moderate climates to evaluate in which ones a cool roof leads to net energy savings. The model parameters used are listed in Appendix B under Table B.1.

As expected, it is shown in Fig. 4-1 that the cool roof performs roughly the same as the modified-bitumen roof in Minneapolis, a very cold climate. This equality in

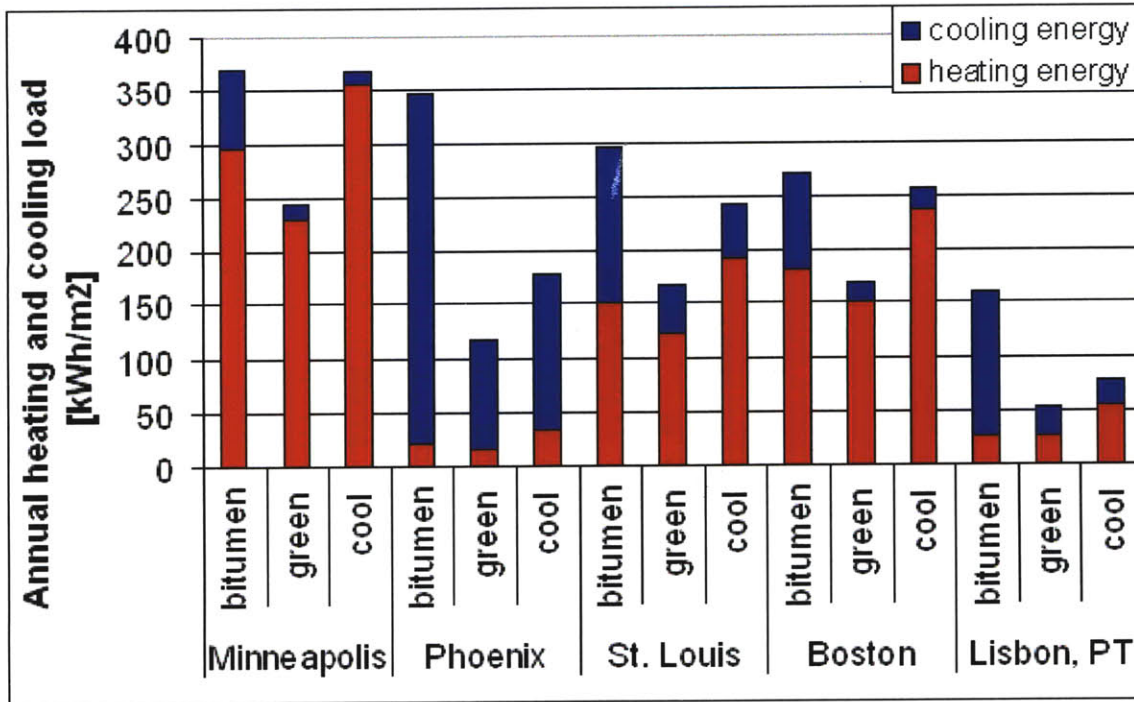


Figure 4-1: Annual heating and cooling load for a single-story residential building with no roof insulation. See Table B.1 in Appendix B for all input parameters.

energy demand results from an increased heating load for the building with a cool roof, because less of the sun's heat enters the building. Not just isolated to Minneapolis, this increase in heating energy occurs in every city when a cool roof is used. In a hot climate like Phoenix, the cool roof nearly halves the energy consumption of the building with a traditional roof. In the three moderate cities simulated, switching to a cool roof leads to at least minimal savings, even in Boston. In each of the five cities considered, the green roof leads to the lowest energy consumption, as the soil helps insulate the roof, which otherwise has no insulation. Furthermore, because the vegetation is assumed to always be healthily living, the green roof provides passive cooling to the roof when the incident radiation and ambient temperature are high enough to allow evapotranspiration. The water required for this evapotranspiration varies significantly with location, climate, and time of year. However, in the most extreme conditions, during the Phoenix summer, a weekly irrigation rate of 3.3 *in/wk* is needed to allow the modeled evapotranspiration. This weekly rate averages to 13

in/month of required water in the summer, of which 0.99 *in* could be met by the average July precipitation at the Phoenix Sky Harbor International Airport [74]. The large effect of roof type on energy consumption, up to a 60% reduction, suggests enormous potential by changing roofs, however particularly in hot arid climates, substantial water is needed for the roof.

However, such dramatic drops in energy consumption are not always realized. If the exact same building modeled in Fig. 4-1 is built as a four-story building rather than a single-story building, the energy impact of each type of roof changes significantly, as shown in Fig. 4-2.

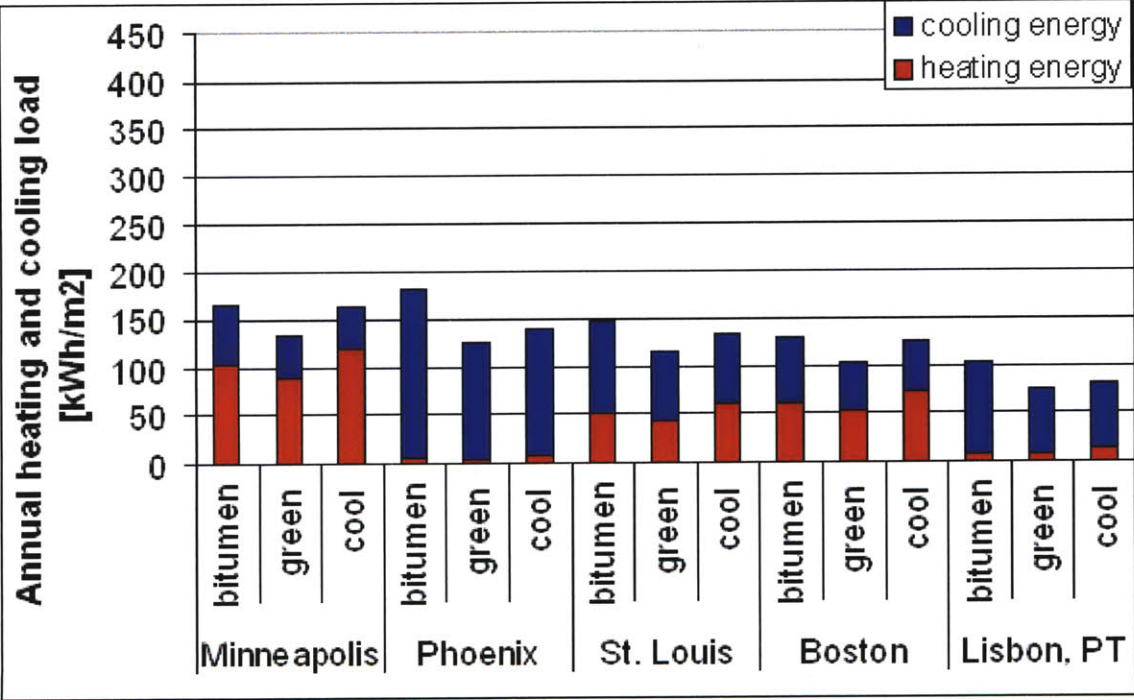


Figure 4-2: Average total annual heating and cooling load for the four-story equivalent of the building modeled in Fig. 4-1 (residential building with no roof insulation). See Table B.1 in Appendix B for input parameters, except the number of floors in the building, which is 4.

As observed in Fig. 4-2, both the relative and absolute change in energy consumption from changing roof types is significantly reduced when a four-story building is modeled. The reason for this reduction is the interior floors, which are not exposed to the heat flux through the roof, help moderate the average total building energy

consumption. The effect of the number of floors in the building will be discussed in more depth later in this chapter.

An even greater change in the energy consumption of the building shown in Fig. 4-1 occurs if insulation is added to the roof. The exact one-story building modeled before is re-simulated with $3 \text{ m}^2\text{K}/\text{W}$ of insulation, or 8.6 cm of polystyrene foam, placed on top of the roof slab, the results of which are shown in Fig. 4-3 [27].

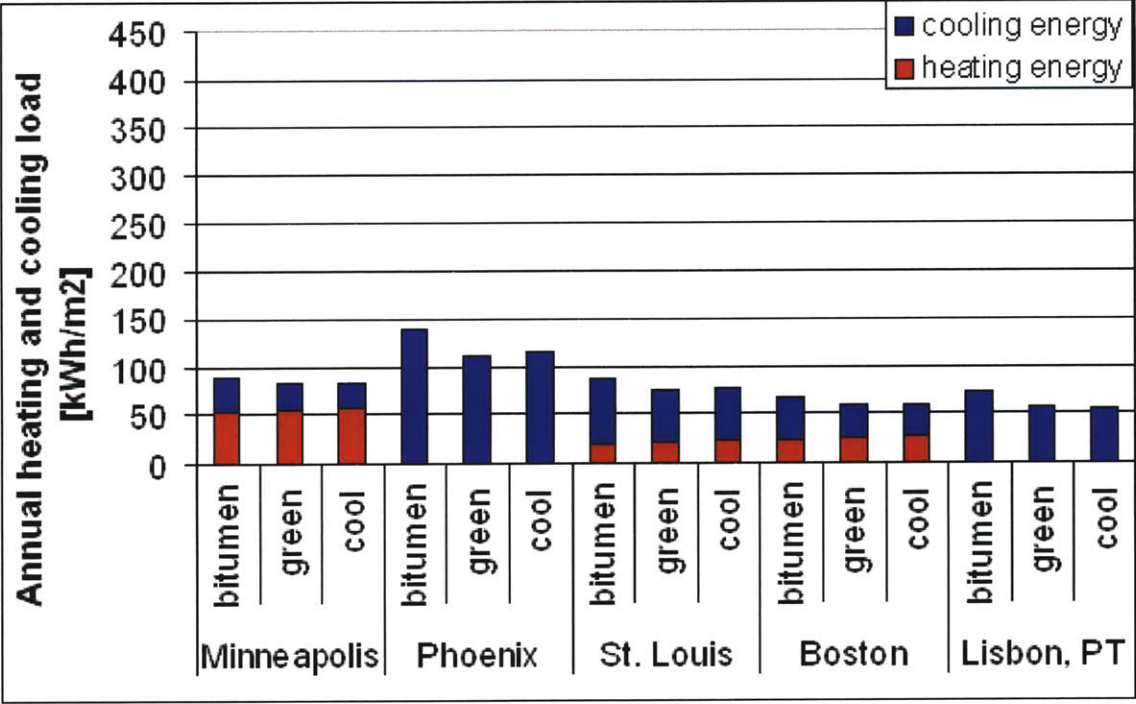


Figure 4-3: Average total annual heating and cooling load for the equivalent building of that modeled in Fig. 4-1, save $3 \text{ m}^2\text{K}/\text{W}$ insulation added above the roof slab. See Table B.1 in Appendix B for input parameters, except the roof insulation amount, which is now $3 \text{ m}^2\text{K}/\text{W}$.

With insulation, the absolute difference between the 3 types of roofs is drastically reduced. In climates dominated by heating energy, such as Minneapolis and Boston, the difference in energy consumption associated with each type of roof is much smaller than the difference in cooling dominated or moderate climates, roughly 6% in Minneapolis. However, in climates dominated by cooling loads, such as Phoenix and Lisbon, both green and cool roofs can save up to 25% in total energy consumption. It should also be noted that in every climate, the green and cool roofs now perform

nearly identically, whereas the green roof out performs the cool roof in every city when no insulation is used, as shown in Fig. 4-1. Both types of roofs now perform similarly because the added insulation severely limits heat transfer in both cases. With no added roof insulation, as in Fig. 4-1, the green roof performs best because the insulative effect of the soil somewhat limits heat transfer through the roof. When $3 \text{ m}^2\text{K}/\text{W}$ of insulation is added, however, the insulative effect of the added insulation dominates that of the soil, thus heat transfer is mostly limited by the added insulation. So, because heat transfer through the cool roof is also limited by the added insulation, though not the insulative effect of the soil, both roofs perform similarly.

4.2 Roof Insulation

Two aspects of the roof insulation are investigated in more detail in this section, both the amount and location of insulation used on the roof.

4.2.1 Roof Insulation - Amount

As shown in Fig. 4-3, $3 \text{ m}^2\text{K}/\text{W}$ of roof insulation seems to even the energy consumption of the building across all roof types in certain climates. Knowing at what amount of insulation this happens can help lead to smarter building designs. Figs. 4-4 through 4-7 plot the total energy consumption for a one-story building with moderate plug loads in four different climates. A full summary of input parameters is available in Appendix B under Table B.2.

In Figs. 4-4 through 4-7, notice how the energy consumption associated with all three roof technologies approaches the same value as insulation is increased. It should be noted, however, that in every case the modified bitumen roof has the worst energy performance. The degree to which a green or cool roof out performs the modified bitumen roof depends highly on climate. With an R-value of $7 \text{ m}^2\text{K}/\text{W}$, in the sunny and hot climate of Sacramento, the cool roof performs best and saves $10 \text{ kWh}/\text{m}^2$, or 9 %, annually over the modified bitumen roof. When solar gains are high, as they are in Sacramento, cool roofs perform very well as they prevent much of the solar

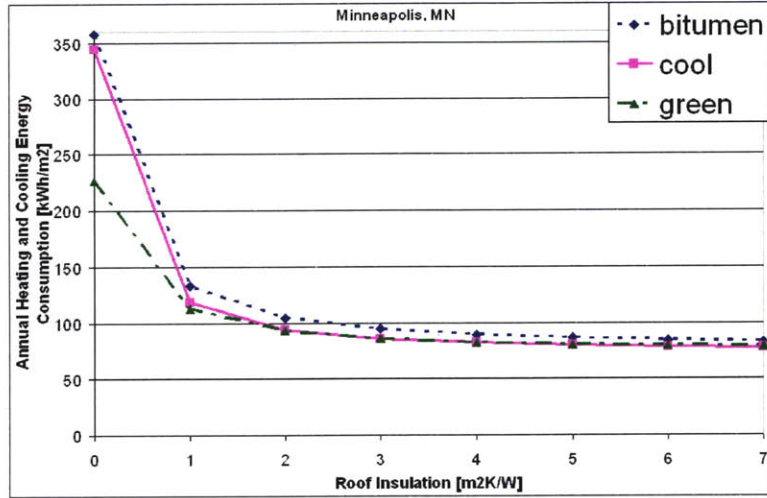


Figure 4-4: Average total annual heating and cooling load for a one-story building with moderate plug loads as a function of roof insulation in Minneapolis, MN. See Table B.2 in Appendix B for input parameters, except for the city and insulation amount, which are specified in the figure.

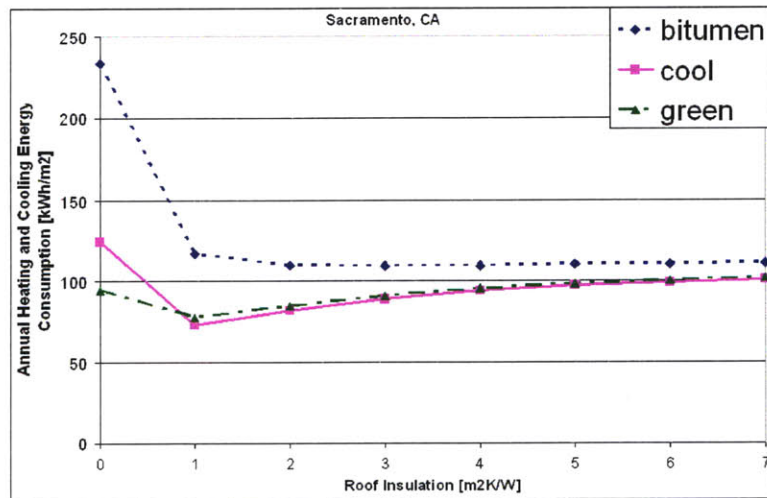


Figure 4-5: Average total annual heating and cooling load for a one-story building with moderate plug loads as a function of roof insulation in Sacramento, CA. See Table B.2 in Appendix B for input parameters, except for the city and insulation amount, which are specified in the figure.

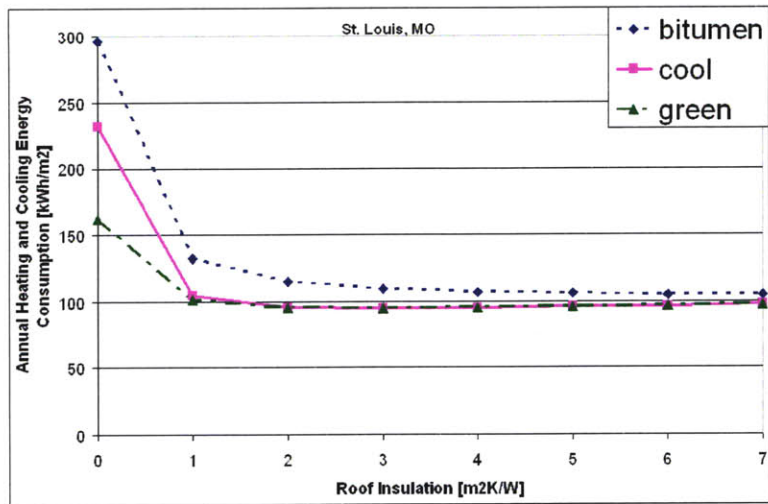


Figure 4-6: Average total annual heating and cooling load for a one-story building with moderate plug loads as a function of roof insulation in St. Louis, MO. See Table B.2 in Appendix B for input parameters, except for the city and insulation amount, which are specified in the figure.

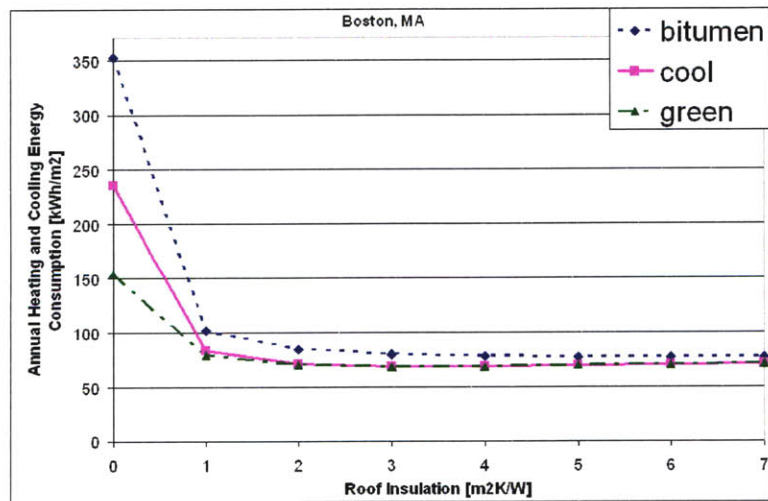


Figure 4-7: Average total annual heating and cooling load for a one-story building with moderate plug loads as a function of roof insulation in Boston, MA. See Table B.2 in Appendix B for input parameters, except for the city and insulation amount, which are specified in the figure.

energy from entering through the roof. However, in the cold climate of Minneapolis (again with roof insulation of $7 \text{ m}^2\text{K}/\text{W}$), the green roof performs best, saving $4.5 \text{ kWh}/\text{m}^2$, or 5 %, annually over the modified bitumen roof. The additional insulation and thermal mass of the green roof helps lower energy consumption during the winter, while the evapotranspiration and shading from the grass helps lower consumption in the summer. Thus, in colder climates, a green roof is expected to perform best.

In Fig. 4-5, there appears to be an optimum amount of insulation for the cool and green roofs at $1 \text{ m}^2\text{K}/\text{W}$. This optimum value arises because of two dominating factors: when no insulation is present, the solar heat flux through the roof dominates. When the roof is heavily insulated, the heat generated from the plug loads can not escape through the roof, especially at night when the cool night sky could help offset the heat from the plug loads. The optimum value of $1 \text{ m}^2\text{K}/\text{W}$ occurs where there is enough insulation to significantly reduce the solar heat flux through the roof, but not too much to keep the heat from internal loads trapped inside.

4.2.2 Roof Insulation - Location

Not only does the amount of roof insulation affect the energy consumption of the building, but also the insulation location. Assuming a concrete roof slab is used, when the insulation is above the slab, the concrete's thermal mass adds to that of the room, whereas when insulation is beneath the slab, the concrete's thermal mass is not in direct contact with the room because of the resistance of the insulation. Adding more thermal mass helps moderate the room temperature, thus lowering energy bills, whether during a hot summer or cold winter.

When the insulation is above the slab, the thermal mass is exposed to the indoor air temperature, helping to moderate it and lead to lower energy demands. Furthermore, during the day, the absorbed energy on the roof surface can not easily pass through the insulation and consequently the roof surface temperature is higher than when insulation is beneath the slab. This higher surface temperature allows more energy to be transferred back to the environment and not to the building, which is protected from the insulation. To better understand these tradeoffs, Fig. 4-8 shows

the energy consumption of a large office building in Lisbon, Portugal plotted as a function of roof insulation R-value for all three types of roof and two insulation locations. All input parameters are shown in Appendix B under Table B.3.

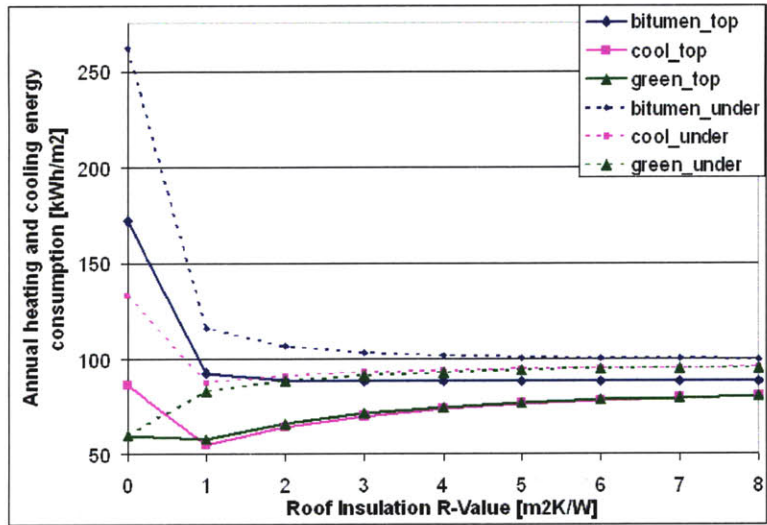


Figure 4-8: Average total annual heating and cooling load for a one-story office building as a function of roof insulation in Lisbon, Portugal. See Table B.3 in Appendix B for input parameters, except for the insulation amount and location (on top or under the concrete roof slab), which are specified in the figure.

Observation of the annual heating and cooling load when no insulation is present shows the impact of simply adding a coverboard on top of the roof. Recall when the insulation is placed on top of the roof, a half-inch coverboard is used to protect the insulation from the environment. This additional layer helps limit the amount of heat flux through the roof, thus significantly reducing the energy load of the building. In the case of the green roof with no insulation, the energy demands are equal, because no coverboard is needed to protect the insulation. As more insulation is added, the difference between the two configurations narrows, although the case with insulation on top of the roof slab always requires less energy.

To summarize the insulation section, a building with no roof insulation can generally realize much higher energy savings by adding as little as $1 \text{ m}^2\text{K}/\text{W}$ roof insulation instead of installing a new roof. Furthermore, that insulation should be added on top of the roof structural slab, especially if it is thermally massive. However, if a building

already has roof insulation, a green or cool roof can lead to additional energy savings, on the order of 5-10% in the single-story buildings and locations presented here.

4.3 Number of Floors

One component of building construction that is often unmentioned when the energy savings of a cool or green roof is mentioned is the number of floors in the building. It has been shown that such roof technologies have the potential of saving energy, however the eleven-story Chicago City Hall likely does not save much energy with its roof garden, because ten out of the eleven floors remain unchanged with the new roof. This section shows how the average energy consumption of the building changes with the number of floors in the building.

To illustrate this change, the average total heating and cooling energy per square meter is plotted as a function of the number of floors in the building. Recall the average total energy is found by assuming the interior floors of the building have adiabatic ceilings while the top floor must consider the heat flux through the roof. The average total energy is the floor-weighted average of these values. Two locations are considered, Lisbon, Portugal (a cooling dominated climate) and Boston, MA (a heating dominated climate). In each location, a building with 0 and 3 m^2K/W roof insulation is modeled.

Figs. 4-9 and 4-10 show similar results to those previously presented in Fig. 4-2 where the difference between the three roof technology diminishes with the number of floors in a building. When roof insulation is used, the difference is even smaller, as shown in Figs. 4-11 and 4-12 which plot the average total energy demand versus the number of floors in the building for the exact building used in Figs. 4-9 and 4-10, but with 3 m^2K/W roof insulation.

A striking difference between Boston and Lisbon, with no insulation, exists as shown in Figs. 4-9 and 4-10. In Fig. 4-9, the average annual energy consumption decreases for all three types of roof as more floors are considered. This phenomena occurs because the energy consumption of the interior floors with adiabatic ceilings

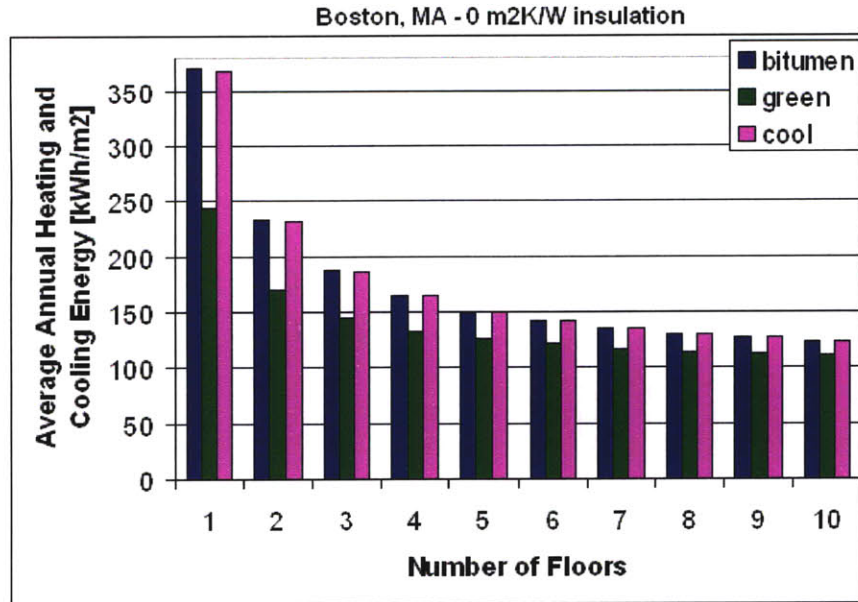


Figure 4-9: Average total annual heating and cooling load for multi-story buildings with no roof insulation as a function of number of floors in Boston, MA. See Table B.4 in Appendix B for input parameters, except for the number of floors and insulation amount, which are specified in the figure.

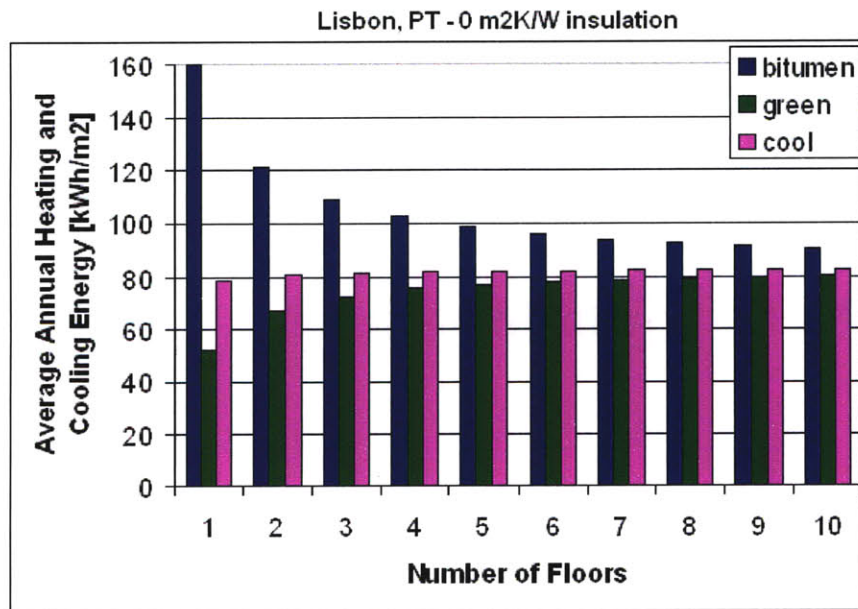


Figure 4-10: Average total annual heating and cooling load for multi-story buildings with no roof insulation as a function of number of floors in Lisbon, Portugal. See Table B.4 in Appendix B for input parameters, except for the number of floors and insulation amount, which are specified in the figure.

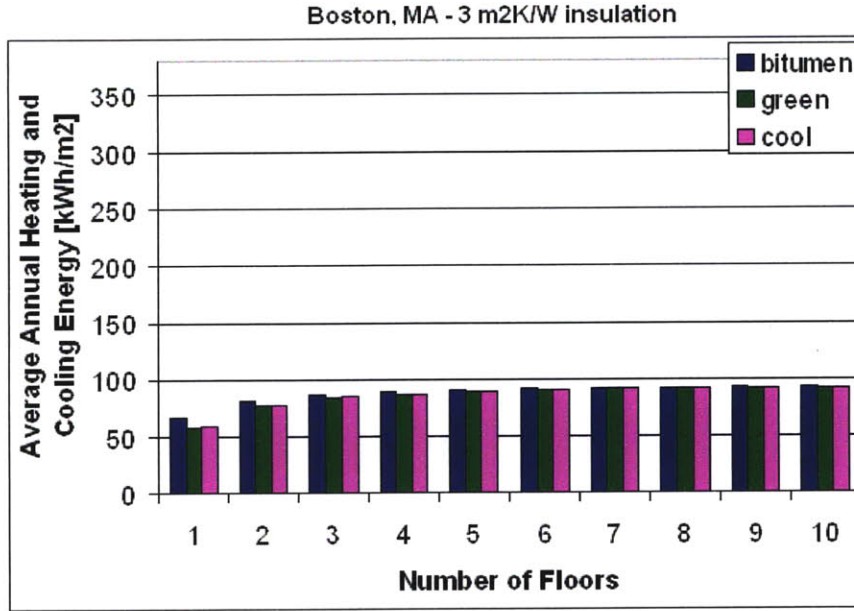


Figure 4-11: Average total annual heating and cooling load for multi-story buildings with 3 m²K/W roof insulation as a function of number of floors in Boston, MA. See Table B.4 in Appendix B for input parameters, except for the number of floors and insulation amount, which are specified in the figure.

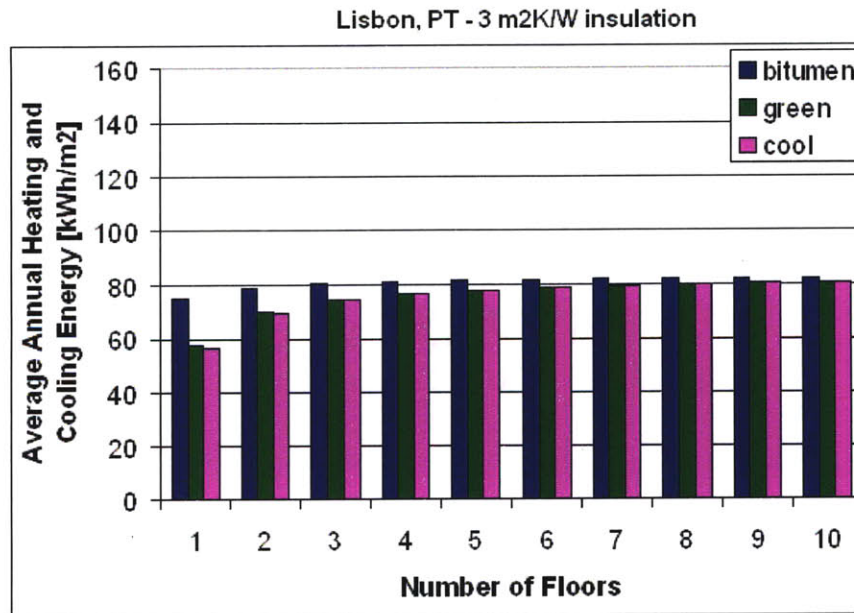


Figure 4-12: Average total annual heating and cooling load for multi-story buildings with 3 m²K/W roof insulation as a function of number of floors in Lisbon, Portugal. See Table B.4 in Appendix B for input parameters, except for the number of floors and insulation amount, which are specified in the figure.

is much less than the energy consumption of the top floor, which includes the heat flux through the roof. However, in Lisbon, only the modified bitumen roof follows this trend; the green and cool roofs actually increase in average energy consumption with the number of floors. This increase in energy consumption results from the passive cooling effect of both green and cool roofs when no roof insulation is present. When a floor has an adiabatic roof, all heat gains must be dissipated through the walls, windows, or by the cooling system. When a green or cool roof is used, though, the heat can be absorbed by the thermal mass of the roof (recall, which is 15 cm of concrete for both cases, with an additional 15 cm of soil for the green roof) and dissipated to the cooler outside environment, especially at night. Furthermore, the thermal mass will also cool at night, which in turn offsets some of the heat gains early in the day. Fig. 4-13 helps illustrate this reasoning.

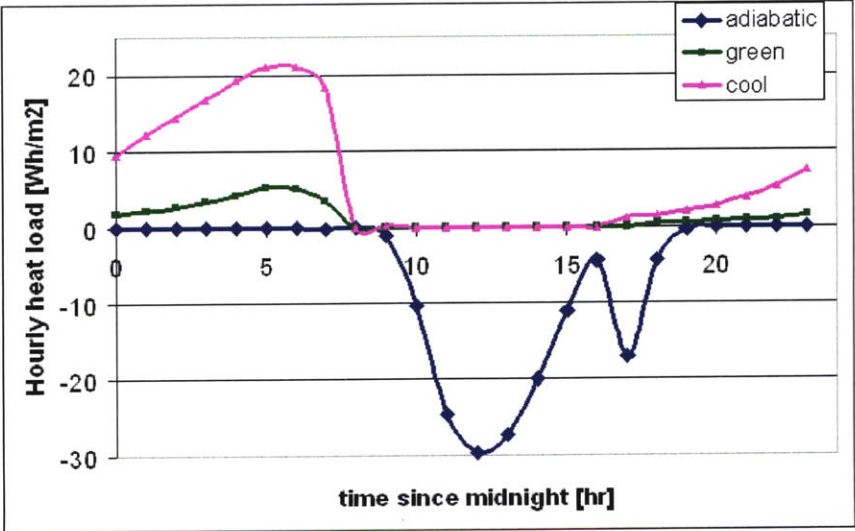


Figure 4-13: Hourly heating load for the interior floors (with adiabatic ceilings) and top floor with a green and cool roof (no roof insulation) of the building simulated in Figs. 4-9 through 4-12. The results shown are for a representative April day in Lisbon. A negative heating load indicates a cooling load is applied.

Notice in Fig. 4-13 that both green and cool roofs have no negative heat load, which corresponds to a cooling load, whereas the adiabatic case has only a cooling load. Furthermore, during the night, both green and cool roofs require a heating load because of their cooling effects, which are increased during the night. The insulative

effect and additional soil thermal mass both help the green roof perform significantly better than the cool roof when no insulation is present.

The same increase in average energy consumption with number of floors is present in both Figs. 4-11 and 4-12, where all three roofs in both locations lead to higher average energy consumption as more floors are added. In this case, the principle reason for this trend is the effect of thermal mass, as the passive cooling of the green and cool roofs is limited by the $3 \text{ m}^2\text{K}/\text{W}$ of insulation and the modified bitumen roof shows the same trend (although it does not have the same passive cooling ability). The simulated building at hand has “low” thermal mass, which consists of 2 cm of concrete on each floor. So the interior floors with adiabatic ceilings do not have much thermal mass, which leads to large interior temperature swings over short periods of time, which in turn requires more heating or cooling energy to offset the swing. However, the one-story building (or top floor of a multi-story building) with any of the three types of roof has an additional 15 cm of concrete thermal mass from the roof slab. This near sevenfold increase in thermal mass helps moderate these swings, which leads to energy savings.

Fig. 4-14 shows the moderating effect of the three types of roofs compared to the adiabatic case, with 2 cm of thermal mass, as well as the adiabatic case when 20 cm of concrete (or “heavy” thermal mass) is used. All three roofs exhibit similar behavior as they all require minimal heating during the night and minimal cooling during the day (though the modified bitumen roof requires slightly more cooling during the day and subsequently less heating at night due to its high absorptivity). The standard adiabatic case requires both more heating energy at night and more cooling energy during the day due to the lack of a moderating thermal mass. When “heavy” thermal mass is used in the adiabatic case, which is similar to the total thermal mass present when the roof slab is exposed to the room, a similar moderating effect that that of the roofs is present. However, because no heat transfers through the roof, the cold night sky does not cool the room as it does for the three types of roofs. When this night cooling effect is absent, no heating energy is required during the night, as shown in Fig. 4-14, but more cooling energy is required during the day, also shown. Therefore,

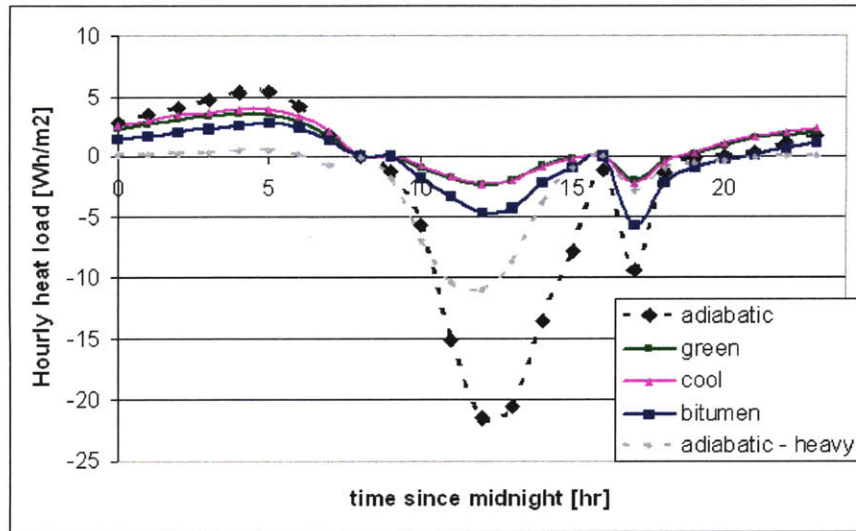


Figure 4-14: Hourly heating load for a representative April day in Boston. The interior floors (labeled “adiabatic”), top floor with a green, cool, and bitumen roof with $3 \text{ m}^2\text{K}/\text{W}$ roof insulation, and interior floors with 20 cm thermal mass (labeled “heavy”) of the building simulated in Figs. 4-9 through 4-12 are considered. A negative heating load indicates a cooling load is applied.

more thermal mass (whether in the roof assembly or on the floor) can lead to energy savings.

By comparing the two cases in Boston, Figs. 4-9 and 4-11, a drastic reduction in average total energy occurs when insulation is added to buildings with few floors. For example, a one-story building in Boston realizes an 82% drop in required energy by installing $3 \text{ m}^2\text{K}/\text{W}$ of roof insulation, whereas only a 34% drop is realized if a green roof is installed. The effect of the roof insulation also has a non-trivial impact on a ten-story building. By adding the same amount of roof insulation to a 10-story building, an average total energy savings of 24% can be realized over the un-insulated 10-story building. However, if a green roof with no insulation is installed instead, only a savings of 10% will be realized.

The roof insulation, as before, has the effect of balancing the energy demands associated with the three different kinds of roofs. For the 10-story building in Boston with roof insulation, there is less than a 1% difference between all three roofs. In the warmer climate of Lisbon, there is a slightly larger reduction of 2% for both green

and cool roofs, but it is still quite small. However, because of its more moderate climate, Lisbon differs from Boston when buildings with few floors are considered. For example, when roof insulation is added to a one-story building, the average total energy is reduced by 53%. However, if a green roof with no insulation is installed instead, the average total energy is reduced by 67%. This difference from the Boston case arises from the passive cooling capability of the green roof, which helps expell excess heat when no insulation is present. In Boston, the insulation leads to greater energy savings because it is a heating dominated climate, thus the passive cooling capability of the green roof does not lead to annual energy savings (though it does help in the spring and summer).

4.4 Considerations for Natural Ventilation

The preceeding analysis is done for a building with mechanical heating and cooling. However, the impact of a green or cool roof on a naturally ventilated building also has potential to reduce energy demand, as they both can limit heat flux through the roof. In this section, the same building used before (in Fig. 4-1) is naturally ventilated to provide cooling, but still mechanically heated. It is assumed that no energy is used to naturally ventilate the building (no fans or self-operating windows are assumed to be used), so there is no cooling energy. Instead, to evaluate the effect of installing a new roof, the number of hours in a year the building is at a certain temperature is recorded. Additionally, as before, the heating energy required is recorded. A naturally ventilated building with 0 and also 3 m^2K/W roof insulation is simulated in both Boston, MA and Lisbon, Portugal, the results of which are shown in Figs. 4-15 through 4-18. All input parameters are shown in Table B.5 in Appendix B.

A quick glance at the indoor temperatures of the buildings with both the green and cool roofs suggests they perform nearly equally as well in reducing the number of hours the building is above 28 C . However, when the heating energy is considered, the 28% increase in heating energy from switching to a cool roof must also be compared to the 18% decrease in heating energy when a green roof is used. Although both cool

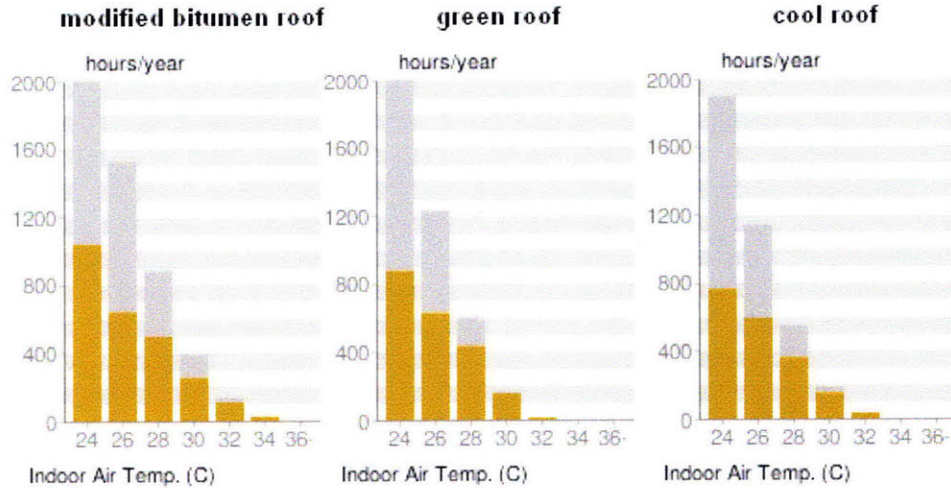


Figure 4-15: Indoor temperatures for a naturally ventilated single-story building with $0 \text{ m}^2\text{K}/\text{W}$ roof insulation in Boston, MA. The annual heating energies corresponding to the modified bitumen, green, and cool roofs are 185.2 , 151.3 , and $236.4 \text{ kWh}/\text{m}^2$ respectively. See Table B.5 in Appendix B for input parameters, except the location and insulation amount, which are specified in the figure.

and green roofs perform similarly when cooling the building with natural ventilation, the increase in heating energy associated with the cool roof makes that choice worse in terms of overall energy performance. When $3 \text{ m}^2\text{K}/\text{W}$ of insulation is added to the roof, the results are quite different, and shown in Fig. 4-16.

Little difference exists between the three types of roofs shown in Fig. 4-16. The cooling from natural ventilation for each type of roof is quite similar, as are the absolute values of the heating energy, though a 12% difference exists between the modified bitumen and cool roofs (with the modified bitumen roof performing better because of the cold climate of Boston). As before, the addition of insulation significantly evens the energy performance of the three types of roofs. The same two scenarios are now shown in Lisbon, Portugal, (Figs. 4-17 and 4-18) where cooling demand dominates.

Similar to in Boston, the cool and green roofs help reduce the number of hours the interior temperature is above 28 C . Once again, the heating energy associated with the cool roof is greatest among the three roofs, 88% higher than that for the modified bitumen roof. However, because of the more moderate climate, the absolute difference is less than in Boston. The results for the case when $3 \text{ m}^2\text{K}/\text{W}$ of roof

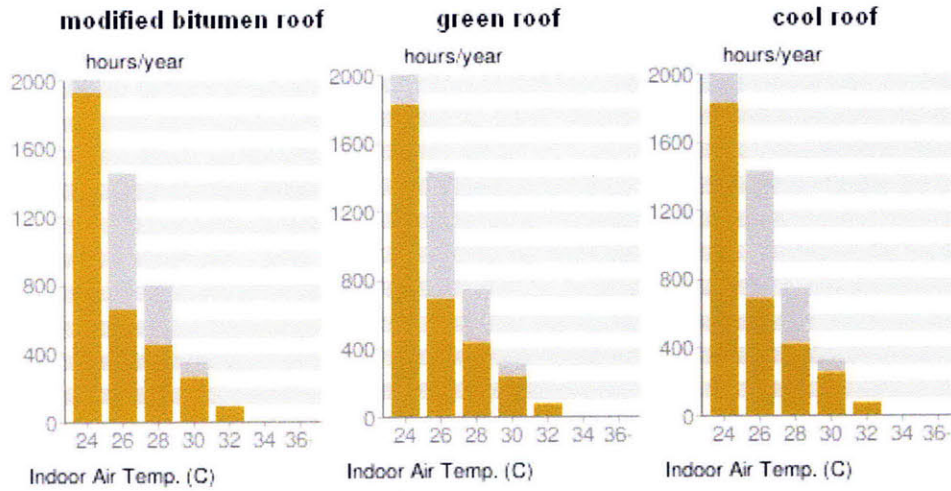


Figure 4-16: Indoor temperatures for a naturally ventilated single-story building with $3 \text{ m}^2\text{K/W}$ roof insulation in Boston, MA. The annual heating energies corresponding to the modified bitumen, green, and cool roofs are 25.3 , 27.7 , and 28.3 kWh/m^2 respectively. See Table B.5 in Appendix B for input parameters, except the location and insulation amount, which are specified in the figure.

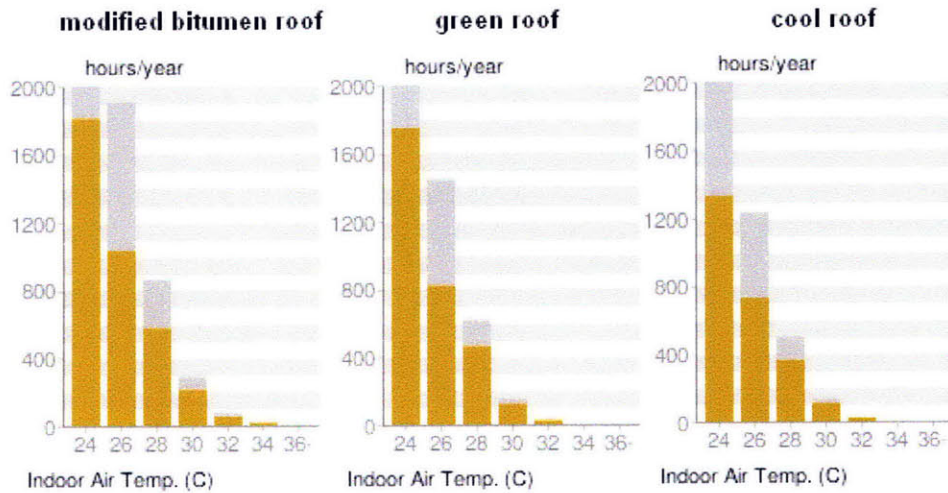


Figure 4-17: Indoor temperatures for a naturally ventilated single-story building with $0 \text{ m}^2\text{K/W}$ roof insulation in Lisbon, Portugal. The annual heating energies corresponding to the modified bitumen, green, and cool roofs are 28.5 , 25.9 , and 53.7 kWh/m^2 respectively. See Table B.5 in Appendix B for input parameters, except the location and insulation amount, which are specified in the figure.

insulation is added is shown in Fig. 4-18.

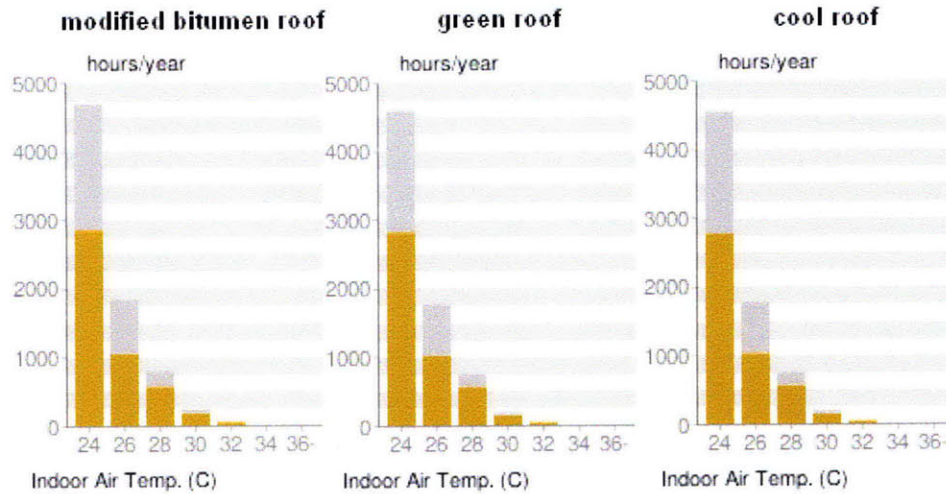


Figure 4-18: Indoor temperatures for a naturally ventilated single-story building with $3\text{ m}^2\text{K/W}$ roof insulation in Lisbon, Portugal. Note the different scale from Fig. 4-17. The annual heating energies corresponding to the modified bitumen, green, and cool roofs are 0.2 , 0 , and 0 kWh/m^2 respectively. See Table B.5 in Appendix B for input parameters, except the location and insulation amount, which are specified in the figure.

When insulation is added, the cooling performance of each roof is again nearly equal, but now, because of the warmer climate, no heating energy is required (due to the heating effect of the envelope and internal loads). This finding suggests that in moderate climates, a cool or green roof will likely not affect the energy performance of a naturally ventilated residential building with moderate roof insulation.

4.5 Conclusions

To conclude this chapter, it is again emphasized that the chief result of this thesis is the development of a tool that can quickly and easily assess the potential energy savings of various roof technologies in cities around the world (freely available online at <http://designadvisor.mit.edu>). These conclusions are based on simulations which use the input parameters available in Appendix B. Thus, any building with drastically different parameters may perform differently. The following is a list of general insights regarding roof types and construction:

- A building with no roof insulation can generally realize much higher energy savings by adding as little as $1 \text{ m}^2\text{K}/\text{W}$ roof insulation instead of installing a different kind of roof.
- Although roof insulation greatly evens the energy performance associated with different roofs, even in a heavily insulated building, a 5-10% savings can be realized if the proper roof is chosen.
- With roof insulation, cool roofs generally perform best in sunny and hot climates. Green roofs generally perform best in moderate to cold climates.
- Without roof insulation, green roofs nearly always perform best, provided they are actively growing, because of the insulative properties of the growing media and potential passive cooling. However, particularly in hot arid climates substantial water is needed to realize full passive cooling effect.
- Regardless of insulation, cool roofs nearly always decrease the cooling load while increasing the heating load.
- In most climates, with moderate to heavy plug loads, more roof insulation is not always better, especially if a green or cool roof is used.
- If a thermally massive roof structural support is used, better energy performance is realized if the roof insulation is placed on top of the support rather than beneath it.
- Multi-story buildings, especially those over 4 stories, significantly reduce the overall building energy savings associated with cool or green roofs.
- Multi-story buildings with insulation realize very little, if any at all, energy savings for the entire building by switching roofs.

- More thermal mass generally helps lower energy consumption.
- In a naturally ventilated building with no roof insulation, cool and green roofs help lower maximum indoor temperatures, though cool roofs result in significantly higher heating loads.
- In a naturally ventilated building with roof insulation, very little, if any at all, difference in maximum indoor temperature and heating load exists among the three roofs, especially in moderate climates.

4.6 Next Steps

This work completes the addition of the roof module to the MIT's Design Advisor as projected by Urban [88]. Although the roof module is complete, it can be expanded in numerous ways, including the addition of more types of roofs (specifically a ballasted roof), the inclusion of a crop coefficient in the FAO-56 Penman-Monteith equation so other vegetation types can be more specifically modeled (which can change the evapotranspiration by up to 45% [26]), the consideration of varying moisture levels in the growing media (which will affect the conductivity, heat capacity, and density of the media), and the ability to change the roof albedo for cool roofs to estimate changes in performance as roofs get dirty. Further expansion to Design Advisor might include, as suggested by Urban, "...ground thermal model, improved convection relations for systems with blinds, and additional flexibility in the user-controlled building operation decisions" [88].

Appendix A

Altered Design Advisor Java Source Files and HTML Code

To find specific changes in the Java source code, search for "steve" in the document. Nearly all changes made by Steve to incorporate the roof module are labeled with my name.

Java files altered by Steve for the roof addition:

WeatherData

- o added a new weather parameter, globalHorizontalRadiation
- o Added method getRelativeHumidity *WeatherDataReader*
- o added a new weather parameter, globalHorizontalRadiation
- o Added method getRelativeHumidity *Roof*
- o Added a new class that predicts the roof temperature given weather inputs and returns the heat flux through the roof into the top room of a building

Strategy

- o Added roof module
- o Added roof energy into runOneHour
- o Added parameter windSpeed

Sunlight

- o Added global horizontal radiation to class

Room

- o Added method setRoof() that initiates a Roof object

Scenario

- o Added 4 new parameters

Building

- o Call method setRoof to create a roof module if it is specified

SingleGlazedUnit

- o Deleted a System.out.println that printed the readymade window type

SHGCCFinder

- o Commented out three system.out.println statements

DoubleGlazedUnit

- o Commented out System.out.println

Webinterface, HTML files edited:

Setup

- o Added new field, Roof Description
- o Change getScenarioParameters to read 4 roof parameters
- o Change setScenarioParameters
- o Change the units methods

Bridge_form

- o Added 4 parameters for roof

Bridge

- o Added 4 parameters for roof

Index

- o Added lines to ensure values stored in scenario remain unchanged
- o Changed colored tabs to include roof info

Roof.html help file

- o Created help file to explain the roof addition

Energy html file

- o Changed the title and added an explanation for how the energy is calculated

Energy_monthly html file

- o Changed the title and added an explanation for how the energy is calculated

Assumptions file

- o Added assumptions associated with roof analysis

Folders changed

- Added divider to Jigsaw/WWW/design/images folder
- Added "bitumen_roof", "cool_roof", and "green_roof" to Jigsaw/WWW/design/help/help_images folder

Appendix B

Building Simulation Parameters

Table B.1: Simulation Input Parameters for Fig. 4-1

Location	<i>specified in figure</i>
Building length, side A	N/A
Building length, side B	N/A
Simulation Type	one_sided
Window Typology	dgu
Glazing Type	low-e
Window Area	40%
Blind Width	25 mm
Blind Schedule (daytime)	responds to temperature
Blind Schedule (nighttime)	always closed
Blind Angle when closed	75 degrees
Blind Color	Shiny Aluminum
Blind Emissivity	0.22
Blind Absorptivity	0.2
Wall Insulation R-Value	2 m^2K/W
Building Type	Low-rise Residential
Occupancy Load	0.025 <i>people/m²</i>
Lighting Requirements	400 lux
Equipment Load	1.00 W/m^2
Air Change Rate per Occupant	15.0 liters / sec per person
Total Air Change Rate	0.5 roomfuls per hour
Lighting Control	lights respond to sun - controlled by a one switch
Orientation	south
Room Depth	4 m
Room Width	4 m
Room Height	3 m
Thermal Mass	low
Overhang Depth	0 m
Roof Type	<i>specified in figure</i>
Roof Insulation R-Value	0 m^2-K/W
Roof Insulation Location	top of roof slab
Number of Floors	1 floor(s)

Table B.2: Simulation Input Parameters for Figs. 4-4 through 4-7

Location	<i>specified in figure</i>
Building length, side A	N/A
Building length, side B	N/A
Simulation Type	one_sided
Window Typology	dgu
Glazing Type	low-e
Window Area	40%
Blind Width	25 mm
Blind Schedule (daytime)	responds to temperature
Blind Schedule (nighttime)	always closed
Blind Angle when closed	75 degrees
Blind Color	Shiny Aluminum
Blind Emissivity	0.22
Blind Absorptivity	0.2
Wall Insulation R-Value	$2 \text{ m}^2\text{K/W}$
Building Type	Low-rise Residential
Occupancy Load	0.025 people/m^2
Lighting Requirements	750 lux
Equipment Load	5.00 W/m^2
Air Change Rate per Occupant	15.0 liters / sec per person
Total Air Change Rate	0.5 roomfuls per hour
Lighting Control	lights respond to sun - controlled by a one switch
Orientation	south
Room Depth	4 m
Room Width	4 m
Room Height	3 m
Thermal Mass	low
Overhang Depth	0 m
Roof Type	<i>specified in figure</i>
Roof Insulation R-Value	<i>specified in figure</i>
Roof Insulation Location	top of roof slab
Number of Floors	1 floor(s)

Table B.3: Simulation Input Parameters for Fig. 4-8

Location	Portugal - Lisbon
Building length, side A	N/A
Building length, side B	N/A
Simulation Type	one_sided
Window Typology	dgu_nb
Glazing Type	low-e
Window Area	50%
Wall Insulation R-Value	$2 \text{ m}^2\text{K/W}$
Building Type	Office Building
Occupancy Load	0.075 people/m^2
Lighting Requirements	500 lux
Equipment Load	5.00 W/m^2
Air Change Rate per Occupant	15.0 liters / sec per person
Total Air Change Rate	1.2 roomfuls per hour
Lighting Control	lights respond to sun - controlled by a one switch
Orientation	south
Room Depth	20 m
Room Width	5 m
Room Height	3.5 m
Thermal Mass	none
Overhang Depth	0 m
Roof Type	<i>specified in figure</i>
Roof Insulation R-Value	<i>specified in figure</i>
Roof Insulation Location	<i>specified in figure</i>
Number of Floors	1 floor(s)

Table B.4: Simulation Input Parameters for Figs. 4-9 through 4-12

Location	<i>specified in figure</i>
Building length, side A	N/A
Building length, side B	N/A
Simulation Type	one_sided
Window Typology	dgu
Glazing Type	low-e
Window Area	40%
Blind Width	25 mm
Blind Schedule (daytime)	responds to temperature
Blind Schedule (nighttime)	always closed
Blind Angle when closed	75 degrees
Blind Color	Shiny Aluminum
Blind Emissivity	0.22
Blind Absorptivity	0.2
Wall Insulation R-Value	2 m^2K/W
Building Type	Low-rise Residential
Occupancy Load	0.025 <i>people/m</i> ²
Lighting Requirements	400 lux
Equipment Load	1.00 W/m^2
Air Change Rate per Occupant	15.0 liters / sec per person
Total Air Change Rate	0.5 roomfuls per hour
Lighting Control	lights respond to sun - controlled by a one switch
Orientation	south
Room Depth	4 m
Room Width	4 m
Room Height	3 m
Thermal Mass	low
Overhang Depth	0 m
Roof Type	<i>specified in figure</i>
Roof Insulation R-Value	<i>specified in figure</i>
Roof Insulation Location	top of roof slab
Number of Floors	<i>specified in figure</i>

Table B.5: Simulation Input Parameters for naturally ventilated building in Figs. 4-15 through 4-18

Location	<i>specified in figure</i>
Building length, side A	N/A
Building length, side B	N/A
Simulation Type	one_sided
Window Typology	dgu
Glazing Type	low-e
Window Area	40%
Blind Width	25 mm
Blind Schedule (daytime)	responds to temperature
Blind Schedule (nighttime)	always closed
Blind Angle when closed	75 degrees
Blind Color	Shiny Aluminum
Blind Emissivity	0.22
Blind Absorptivity	0.2
Wall Insulation R-Value	2 m^2K/W
Building Type	Low-rise Residential
Occupancy Load	0.025 <i>people/m²</i>
Lighting Requirements	400 lux
Equipment Load	1.00 W/m^2
Air Change Rate per Occupant	15.0 liters / sec per person
Total Air Change Rate	0.5 roomfuls per hour
Lighting Control	lights respond to sun - controlled by a one switch
Orientation	south
Room Depth	4 m
Room Width	4 m
Room Height	3 m
Thermal Mass	low
Overhang Depth	0 m
Roof Type	<i>specified in figure</i>
Roof Insulation R-Value	<i>specified in figure</i>
Roof Insulation Location	top of roof slab
Number of Floors	1 floor(s)

Bibliography

- [1] Bitumen roof. http://www.mcconkeykeane.com/images/flat_roofing/images/Byron_06.jpg.
- [2] Buildings energy data book. <http://buildingsdatabook.eren.doe.gov/>.
- [3] The cool colors project. <http://coolcolors.lbl.gov/>.
- [4] Cool roof rating council. <http://www.coolroofs.org/index.html>.
- [5] Decibel (Loudness) comparison chart. <http://www.gcaudio.com/resources/howtos/loudness.html>.
- [6] Energy information administration search : Us energy consumption sector. <http://usasearch.gov/search?input-form=simple-firstgov&v%3Aproject=firstgov&query=us+energy+consumption+sector&affiliate=eia.doe.gov&x=0&y=0>.
- [7] EPS molders. <http://www.epsmolders.org/5E.html>.
- [8] Google maps. <http://maps.google.com/>.
- [9] Green roofs for healthy cities. <http://www.greenroofs.org/>.
- [10] greenroof1.jpg. <http://greentheaters.org/wp-content/themes/mimbo2.2/images/2009/03/greenroof1.jpg>.
- [11] Modified bitumen roofing - beacon commercial roofing. <http://www.beaconroofingsupply.com/commercial-roofing/modified-bitumen/default.html>.

- [12] Modified bitumen roofing : ROOF FACTS.
<http://www.roofingtechnology.net/membrane.php/modified-bituminous>.
- [13] neprohodniKR.png (PNG image, 340x255 pixels).
http://www.knaufinsulation.gr/files/ki_gr/upload/neprohodniKR.png.
- [14] NYC green roof pic. <http://www.hallenterprises1.com/gr03.html>.
- [15] OECD glossary of statistical terms - bitumen definition.
<http://stats.oecd.org/glossary/detail.asp?ID=4587>.
- [16] spf6.JPG (JPEG image, 1296x972 pixels) - scaled (26%).
<http://home.att.net/~wavetrader/spf6.JPG>.
- [17] Welcome to weather underground : Weather underground.
<http://www.wunderground.com/>.
- [18] Wind10m.gif (gif image, 855x511 pixels) - scaled (50%).
<http://www.windatlas.dk/AuxiliaryFiles/images/Wind10m.gif>, July 2005.
- [19] H. Akbari, M. Pomerantz, and H. Taha. Cool surfaces and shade trees to reduce energy use and improve air quality in urban areas. *Solar Energy*, 70(3):295–310, 2001.
- [20] Hashem Akbari. Energy saving potentials and air quality benefits of urban heat island mitigation. Technical report, Lawrence Berkeley National Laboratory.
- [21] Hashem Akbari, Sarah Bretz, Dan M. Kurn, and James Hanford. Peak power and cooling energy savings of high-albedo roofs. *Energy and Buildings*, 25(2):117–126, 1997.
- [22] Hashem Akbari and Steven Konopacki. The impact of reflectivity and emissivity of roofs on building cooling and heating energy use. In *Thermal VII Thermal Performance of the Exterior Envelopes of Buildings VII*, 1998, Miami, FL.
- [23] Hashem Akbari and Ronnen Levinson. Evolution of Cool-Roof standards in the US. *Advances in Building Energy Research*, 2:1–32, 2008.

- [24] Sami A. Al-Sanea. Thermal performance of building roof elements. *Building and Environment*, 37(7):665–675, July 2002.
- [25] R. G Allen, , and Water Resources Institute (U.S.) Environmental. *The ASCE Standardized Reference Evapotranspiration Equation*. American Society of Civil Engineers, Reston, Va, 2005.
- [26] Richard Allen, Luis Pereira, Dirk Raes, and Martin Smith. Crop evapotranspiration - guidelines for computing crop water requirements. Technical Report FAO Irrigation and drainage paper 56, FAO - Food and Agriculture Organization of the United Nations, Rome, 1998.
- [27] ASHRAE. *ASHRAE Handbook - Fundamentals*. Atlanta: American Society of Heating, Refrigeration, and Air-Conditioning Engineers, Inc., 2005.
- [28] Bas Baskaran, David van Reenen, Judy Overton, and Karen Liu. Engineering performance of garden roofs in north (Canadian) climate - 5 years of field data. Technical report, National Research Council Canada.
- [29] Brad Bass and Bas Baskaran. Evaluating rooftop and vertical gardens as an adaptation strategy for urban areas. Technical Report NRCC-46737, National Research Council Canada, March 1999.
- [30] Sarah E. Bretz and Hashem Akbari. Long-term performance of high-albedo roof coatings. *Energy and Buildings*, 25(2):159–167, 1997.
- [31] George Burba, Daniel Robert Taub, and Judith S. Weis. Evapotranspiration. <http://www.eoearth.org/article/Evapotranspiration>, November 2006.
- [32] Timothy Carter and Todd Rasmussen. Use of green roofs for ultra-urban stream restoration in the georgia piedmont (USA). The University of Georgia, April 2005. Kathryn J. Hatcher, Editor, Institute of Ecology, The University of Georgia, Athens GA 30602.
- [33] Francis X. Clines. Up on the roof. *The New York Times*, June 2009.

- [34] California Energy Commission. California title 24, 2010.
- [35] James Cummings, Chuck Withers, Jeff Sonne, Danny Parker, and Robin Vieira. Ucf recommissioning, green roofing technology, and building science training; final report. Technical Report FSEC-CR-1718-07 and FSEC# 20127036, Florida Solar Energy Center, Florida, May 2007.
- [36] Barbara Deutsch, Heather Whitlow, Michael Sullivan, and Anouk Savineau. Re-Greening washington, DC: a green roof vision based on quantifying storm water and air quality benefits. Technical report.
- [37] Peter Droogers and Richard G. Allen. Estimating reference evapotranspiration under inaccurate data conditions. *Irrigation and Drainage Systems*, 16(1):33–45, February 2002.
- [38] EPA. Green roof terrace. http://www.epa.gov/region8/images/green-roof_terrace.jpg.
- [39] Green Roofs for Healthy Cities. Green roof industry posts greater than 80% growth, April 2006.
- [40] FSEC. Experiment database management system. <http://www.logger.fsec.ucf.edu/cgi-bin/wg40.exe?user=baihppsp>.
- [41] J.A. Goff and S Gratch. Low-pressure properties of water from -160 to 212 f. pages 95–122, New York, 1946.
- [42] R.U. Halwatura and M.T.R. Jayasinghe. Thermal performance of insulated roof slabs in tropical climates. *Energy and Buildings*, 40(7):1153–1160, 2008.
- [43] Mark Henderson. Professor Steven Chu: paint the world white to fight global warming. *The London Times*, May 2009.
- [44] Roger Norris Hilten, Thomas Mark Lawrence, and Earnest William Tollner. Modeling stormwater runoff from green roofs with HYDRUS-1D. *Journal of Hydrology*, 358(3-4):288–293, September 2008.

- [45] Terry Howell and Evett Steven. The penman-monteith method. Technical report, USDA-Agricultural Research Service, Conservation & Production Research Laboratory, Bushland, Texas.
- [46] Frank P. Incropera, David P. DeWitt, Theodore L. Bergman, and Adrienne S. Lavine. *Fundamentals of Heat and Mass Transfer*. Wiley, 6 edition, March 2006.
- [47] John Lienhard IV and John Lienhard V. *A Heat Transfer Textbook*. Phlogiston Press, Cambridge, MA, 3rd edition, 2006.
- [48] Mark Z Jacobson. *Fundamentals of Atmospheric Modeling*. Cambridge University Press, Cambridge, UK, 2nd edition, 2005.
- [49] H. G. Jones. *Plants and Microclimate*. Cambridge University Press, Cambridge, UK, 1992.
- [50] G. W. Kite and P. Droogers. Comparing evapotranspiration estimates from satellites, hydrological models and field data. *Journal of Hydrology*, 229(1-2):3–18, March 2000.
- [51] S. Konopacki and H. Akbari. Measured energy savings and demand reduction from a reflective roof membrane on a large retail store in austin. Technical Report LBNL-47149, Heat Island Group, Lawrence Berkeley National Laboratory, Berkeley, CA 94720, June 2001.
- [52] Lisa Kosareo and Robert Ries. Comparative environmental life cycle assessment of green roofs. *Building and Environment*, 42(7):2606–2613, July 2007.
- [53] Monica Kuhn and Steven Peck. Design guidelines for green roofs. http://egov.cityofchicago.org/webportal/COCWebPortal/COC_ATTACH/design_guidelines_for_green_roofs.pdf.
- [54] Renato M. Lazzarin, Francesco Castellotti, and Filippo Busato. Experimental measurements and numerical modelling of a green roof. *Energy and Buildings*, 37(12):1260–1267, December 2005.

- [55] Ronnen Levinson. Cool colors for summer: Characterizing the radiative properties of pigments for cool roofs. In *Lawrence Berkley National Lab*, Berkeley, CA, April 2004. <http://coolcolors.lbl.gov/assets/docs/OtherTalks/Pigment-Talk-2004-04-22a.pdf>.
- [56] Ronnen Levinson, Hashem Akbari, and Joseph C. Reilly. Cooler tile-roofed buildings with near-infrared-reflective non-white coatings. *Building and Environment*, 42(7):2591–2605, July 2007.
- [57] Marlo Martin and Paul Berdahl. Characteristics of infrared sky radiation in the united states. *Solar Energy*, 33:321–336, 1984.
- [58] Gregory McPherson, David Nowak, and Rowan Rowntree. Chicago’s urban forest ecosystem: results of the chicago urban forest climate project. Technical Report General technical report NE-186, United States Department of Agriculture, Forest Service, Northeastern Forest Experimental Station, Randnor, PA, 1994.
- [59] C. Miller, D. Narejo, Robert M. Koerner, George R. Koerner, Y. Grace Hsuan, and Marilyn V. Ashley. State of the green roof industry in the united states. In *Geosynthetics Research and Development in Progress (GRI 18)*, volume 161, page 22, Austin, Texas, USA, 2005. ASCE.
- [60] W Miller and et al. Special infrared refelective pigments make dark roofs reflect almost like white roofs, December 2004.
- [61] Anthony Mills. *Heat Transfer*. CRC, 1st edition, 1991.
- [62] J. L. Monteith. Evaporation and surface temperature. *Quarterly Journal of the Royal Meteorological Society*, 107(451):1–27, 1981.
- [63] A. Niachou, K. Papakonstantinou, M. Santamouris, A. Tsangrassoulis, and G. Mihalakakou. Analysis of the green roof thermal properties and investigation of its energy performance. *Energy and Buildings*, 33(7):719–729, September 2001.

- [64] University of Wisconsin-Milwaukee. Great lakes WATER institute green roof project. <http://www.glwi.uwm.edu/research/genomics/ecoli/greenroof/roofinstall.php#purpose>.
- [65] S. Onmura, M. Matsumoto, and S. Hokoi. Study on evaporative cooling effect of roof lawn gardens. *Energy and Buildings*, 33(7):653–666, September 2001.
- [66] M. Ozel and K. Pihtili. Investigation of the most suitable location of insulation applying on building roof from maximum load levelling point of view. *Building and Environment*, 42(6):2360–2368, June 2007.
- [67] Danny Parker, Yu Joe Huang, Steven Konopacki, Lisa Gartland, John Sherwin, and Lixing Gu. Measured and simulated performance of reflective roofing systems in residential buildings. *ASHRAE Transactions*, 104, Pt. 1, 1998.
- [68] H. L. Penman. Natural evaporation from open water, bare soil and grass. *Proceedings of the Royal Society of London. Series A, Mathematical and Physical Sciences*, 193(1032):120–145, April 1948.
- [69] T. Van Renterghem and D. Botteldooren. Numerical evaluation of sound propagating over green roofs. *Journal of Sound and Vibration*, 317(3-5):781–799, November 2008.
- [70] Graham Russell, Bruce Marshall, and Paul Gordon Jarvis. *Plant Canopies: Their Growth, Form and Function*. Cambridge University Press, 1990.
- [71] M. Santamouris, C. Pavlou, P. Doukas, G. Mihalakakou, A. Synnefa, A. Hatzibiros, and P. Patargias. Investigating and analysing the energy and environmental performance of an experimental green roof system installed in a nursery school building in athens, greece. *Energy*, 32(9):1781–1788, September 2007.
- [72] Federico Sau, Kenneth J. Boote, W. McNair Bostick, James W. Jones, and M. Ines Minguez. Testing and improving evapotranspiration and soil water balance of the dssat crop models. *Agron J*, 96(5):1243–1257, September 2004.

- [73] Campbell Scientific. Am25t solid state multiplexer for thermocouples. http://www.campbellsci.com/documents/product-brochures/b_am25t.pdf.
- [74] National Weather Service. Arizona precipitation page. [http :
//www.wrh.noaa.gov/psr/DroughtPage.php?wfo = psr&data = ALLDATA](http://www.wrh.noaa.gov/psr/DroughtPage.php?wfo=psr&data=ALLDATA), 2009.
- [75] Jonathan Smith. *Building Energy Calculator: A Design Tool for Energy Analysis of Residential Buildings in Developing Countries*. Mechanical engineering SM thesis, Massachusetts Institute of Technology, June 2004.
- [76] Jeff Sonne. Evaluating green roof energy performance. *ASHRAE Journal*, (48):59–61, 2006.
- [77] Jeff Sonne. Fsec web site message from steve ray. Email, December 2008.
- [78] Gilbert Strang. *Computational Science and Engineering*. Wellesley-Cambridge Press, November 2007.
- [79] Ayman A. Suleiman and Gerrit Hoogenboom. Comparison of priestley-taylor and fao-56 penman-monteith for daily reference evapotranspiration estimation in georgia. *Journal of Irrigation and Drainage Engineering*, 133(2):175–182, April 2007.
- [80] Haider Taha, Hashem Akbari, Arthur Rosenfeld, and Joe Huang. Residential cooling loads and the urban heat island—the effects of albedo. *Building and Environment*, 23(4):271–283, 1988.
- [81] Hideki Takebayashi. Re: Surface heat budget data. email, November 11, 2008.
- [82] Hideki Takebayashi and Masakazu Moriyama. Surface heat budget on green roof and high reflection roof for mitigation of urban heat island. *Building and Environment*, 42(8):2971–2979, August 2007.

- [83] Hideki Takebayashi and Masakazu Moriyama. Surface heat budget for green roof and high reflection roof for urban heat island mitigation. In *6th International Conference on Urban Climate*, Goteborg, Sweden, June 2006.
- [84] Alar Teemusk and Ulo Mander. Rainwater runoff quantity and quality performance from a greenroof: The effects of short-term events. *Ecological Engineering*, 30(3):271–277, July 2007.
- [85] Christopher Teh. *Introduction to mathematical modeling of crop growth*. Brown Walker Press, April 2006.
- [86] N. C. Turner, C. J. Thomson, and H. M. Rawson. Effect of temperature on germination and early growth of subterranean clover, capeweed and wimmera ryegrass. *Grass and Forage Science*, (56):97–104, 2001.
- [87] Mississippi State University. Giles roofing project. <https://ssl2.msstate.edu/vpfa/admin/fm/conprojects/conprojimages/00000441.jpg>, May 2006.
- [88] Bryan Urban. *The MIT Design Advisor: Simple and rapid energy simulation of early stage building designs*. Mechanical engineering SM thesis, Massachusetts Institute of Technology, June 2007.
- [89] Watlow. Sensors catalog. <http://www.watlow.com/literature/catalogs/files/sensors.pdf>. Page 199.
- [90] Eva Wong. Reducing urban heat islands: Compendium of strategies - cool roofs. Technical report, EPA. <http://www.epa.gov/hiri/resources/pdf/CoolRoofsCompendium.pdf>.
- [91] N. H. Wong, D. K. W. Cheong, H. Yan, J. Soh, C. L. Ong, and A. Sia. The effects of rooftop garden on energy consumption of a commercial building in singapore. *Energy and Buildings*, 35(4):353–364, May 2003.

- [92] Nyuk Hien Wong, Yu Chen, Chui Leng Ong, and Angelia Sia. Investigation of thermal benefits of rooftop garden in the tropical environment. *Building and Environment*, 38(2):261–270, February 2003.
- [93] Nyuk Hien Wong, Su Fen Tay, Raymond Wong, Chui Leng Ong, and Angelia Sia. Life cycle cost analysis of rooftop gardens in singapore. *Building and Environment*, 38(3):499–509, March 2003.
- [94] Jun Yang, Qian Yu, and Peng Gong. Quantifying air pollution removal by green roofs in chicago. *Atmospheric Environment*, 42(31):7266–7273, October 2008.
- [95] Tan Puay Yok and A Sia. A pilot green roof research project in singapore. In *Third Annual Greening Rooftops for Sustainable Communities Conference, Awards and Trade Show*, Washington, DC, May 2005.
- [96] Robert R. Zarr. Analytical study of residential buildings with reflective roofs. *NIST Publication*, (NISTIR 6228), October 1998.
- [97] Willa Zhu and David Schultz. National severe storms laboratory (nssl) historical weather data archive. <http://data.nssl.noaa.gov/credits.html>.